UC Berkeley
UC Berkeley Electronic Theses and Dissertations

Title
Actomyosin mediated tension orchestrates thermogenic programs in adipocytes

Permalink
https://escholarship.org/uc/item/1g26d365

Author
Tharp, Kevin Menard

Publication Date
2017

Peer reviewed|Thesis/dissertation

eScholarship.org Powered by the California Digital Library
University of California

Actomyosin mediated tension orchestrates thermogenic programs in adipocytes

By

Kevin Menard Tharp

A dissertation submitted in partial satisfaction of the
Requirements for the degree of
Doctor of Philosophy
In
Metabolic Biology
in the
Graduate Division
of the
University of California, Berkeley

Committee in Charge:
Professor Andreas Stahl, Chair
Professor Kevin Healy
Professor Hei Sook Sul
Professor James Olzmann

Summer 2017

Abstract

Actomyosin mediated tension orchestrates thermogenic programs in adipocytes

By

Kevin Menard Tharp

Doctor of Philosophy in Metabolic Biology

University of California, Berkeley

Professor Andreas Stahl, Chair

Innovative approaches to shift energy balance are urgently needed to combat metabolic disorders such as obesity and diabetes. One promising approach has been the expansion or activation of thermogenic adipose tissues to improve metabolic homeostasis. My doctoral studies presented in the following text have identified novel approaches to translate adipose based metabolic therapeutics and the underlying mechanisms by which thermogenic adipocytes establish their therapeutically applicable metabolic capacity.

In chapter I, I present a novel biomaterial technology optimized to expand metabolically beneficial thermogenic adipose depots in vivo. This system enabled me to determine the degree of metabolic enhancement possible with the exogenous expansion of thermogenic adipose depots. To generate therapeutic adipose implants I modified hyaluronic acid-based hydrogels to support the differentiation of white fat derived multipotent stem cells (ADMSCs) into lipid accumulating, uncoupling protein 1 (UCP1) expressing thermogenic adipocytes. Subcutaneous implantation of the synthetic tissues successfully attracted host vasculature and persisted for several weeks and the implant recipients demonstrated elevated core body temperature during cold challenges, enhanced respiration rates, improved glucose homeostasis, and reduced weight gain demonstrating the therapeutic merit of this highly translatable approach.

In chapter II, I outline the experimentation leading to the discoveries presented in chapter III as well as thoroughly review pertinent tissue engineering strategies. Specifically, I sought to define the mechanism by which synthetic ECM components identified in chapter I could alter differentiation outcomes of preadipocytes to yield greater thermogenic capacity.

In chapter III, I demonstrate that actomyosin based mechanical responses provide a critical differentiation cue for the development of thermogenic adipocytes. Since I had determined that the hydrogel optimization techniques described in chapter I were likely acting through cytoskeletal-mediated processes I examined the role of cytoskeletal structure and tension in thermogenic adipose development. I identified that the muscle-like gene expression patterns of UCP1+ adipocytes are critical for the acute induction of oxidative metabolism and uncoupled respiration and regulate mechanosensitive transcriptional co-activators, YAP/TAZ, that control thermogenic gene expression.

This dissertation establishes the role of physical mechanics in the development and function of thermogenic adipocytes which may engender future metabolic therapeutics.

Table of Contents

Abstract 1
Table of contents i
Dedication Page ii
Acknowledgements iii
Curriculum Vitae iv
Chapter I: Matrix assisted transplantation of functional beige adipose tissue 1
Summary 1
Introduction 1
Results 2
Discussion 4
Figures 6
Methods 19
Chapter II: Synthetic ECM promotes thermogenic adipogenesis through actin cytoskeleton dynamics 22
Summary 22
Introduction 22
Results 26
Discussion 27
Figures 28
Methods 33
Chapter III: Actomyosin-mediated tension orchestrates uncoupled respiration in adipose tissues 34
Summary 34
Introduction 34
Results 35
Discussion 39
Figures 41
Methods 53
Conclusion 56
References 57

Dedication page

In loving memory of Boseph and Brooke, who we will love eternally.



Acknowledgements

I would like to specifically thank Dr. Andreas Stahl for supporting my scientific career and mentoring me toward my ‘license to uncouple’.

Curriculum Vitae

Kevin M. Tharp
344 Morgan Hall, UC Berkeley, Berkeley, CA 94720
510.982.6292 ktharp@berkeley.edu

Education

Ph.D., 2017 (Aug), Metabolic Biology, University of California, Berkeley, CA

B.S., 2009 (Dec), Biochemistry and Molecular Biology, Honors in Major, University of California, Santa Cruz, CA

Awards

2017 Keystone Symposia Future of Science Fund Award, NIDDK - 1R13DK104611-03 Scholarship

2016 Ellsworth C. Dougherty Memorial Fund Award, Nutrition Sciences and Toxicology, University of California, Berkeley, CA

2016 Angela Little Memorial Fund Award, College of Natural Resources, University of California, Berkeley, CA

2016 École de Technologie Supérieure Trainee Award, World Bioengineering Congress 2016

2009 Graduated with honors in the major, Chemistry and Biochemistry, University of California, Santa Cruz, CA

2009 Recipient of the UC Santa Cruz Dean's Award for Outstanding Achievement in Chemistry, University of California, Santa Cruz, CA

Research Experience

2013-Present Graduate Student Researcher, Metabolic Biology, University of California, Berkeley, CA

2011-2013 Research Specialist, Nutritional Science and Toxicology, University of California, Berkeley, CA

2009-2011 Laboratory Manager, Physiology and Pharmacology, Oregon Health and Sciences University Portland, OR

2009 Laboratory Assistant, Exelixis, Plant Sciences Division, Tigard, OR

2008-2009 Undergraduate Researcher, Molecular, Cell and Developmental Biology, University of California, Santa Cruz, CA

2006-2009 Undergraduate Researcher, Microbial and Environmental Toxicology, University of California, Santa Cruz, CA

Publications

Tharp K.M., Kang M. S., Timblin G.A., Zushin P.H, Benavides J., Choi c., Li C.X., Kajimura S., Healy K.E., Saijo K., Kumar S., and Stahl A. (2017). Actomyosin-mediated tension orchestrates uncoupled respiration in adipose tissue. Some journal… whatever.

Riera, C. E., Follett, P., Halloran, J., **Tharp, K.M.**, Anderson, C. M., Stahl, A., & Dillin, A. (2017). The sense of smell impacts metabolic health and obesity. Cell Metabolism.

Loskill P., Sezhian T., **Tharp K.M.**, Lee-Montiel F.T., Jeeawoody S., Reese W.M., Zushin P.H., Stahl A., Healy K. (2017). WAT-on-a-chip: A physiologically relevant microfluidic system incorporating white adipose tissue. Lab Chip

Secco B., Camiré É., Brière M., Caron A., Billong A., Gélinas Y., Lemay A., **Tharp K.M.**, Lee P. L., Gobeil S., Guimond J. V., Patey N., Guertin D. A., Stahl A., Haddad É., Marsolais D., Bossé Y., Birsoy K., Laplante, M. (2017). Amplification of Adipogenic Commitment by VSTM2A. Cell Reports 18 (1), 93-106.

Sambeat, A., Gulyaeva, O., Dempersmier, J.; **Tharp, K.M.**, Stahl, A.; Paul, S.M. Sul, Hei Sook. (2016). LSD1 Interacts with Zfp516 to Promote UCP1 Transcription and Brown Fat Program. Cell Reports 15 (11)

Tharp, K.M., Khalifeh-Soltani, A., Park, H.M., Yurek, D.A., Falcon, A., Wong, L., Feng, R., Atabai, K., and Stahl, A. (2016). Prevention of gallbladder hypomotility via FATP2 inhibition protects from lithogenic diet-induced cholelithiasis. American journal of physiology gastrointestinal and liver physiology, ajpgi.00316.02015.

Jha, A.K., **Tharp, K.M.**, Browne, S., Ye, J., Stahl, A., Yeghiazarians, Y., and Healy, K.E. (2016). Matrix metalloproteinase-13 mediated degradation of hyaluronic acid-based matrices orchestrates stem cell engraftment through vascular integration. Biomaterials *89*, 136-147.

Khalifeh-Soltani, A., Ha, A., Podolsky, M.J., McCarthy, D.A., McKleroy, W., Azary, S., Sakuma, S., **Tharp, K.M.**, Wu, N., Yokosaki, Y.*, et al.* (2016). alpha8beta1 integrin regulates nutrient absorption through an Mfge8-PTEN dependent mechanism. eLife *5*.

Li, L., Che, L., **Tharp, K.M.**, Park, H.M., Pilo, M.G., Cao, D., Cigliano, A., Latte, G., Xu, Z., Ribback, S.*, et al.* (2016). Differential Requirement for de novo Lipogenesis in Cholangiocarcinoma and Hepatocellular Carcinoma of Mice and Humans. Hepatology.

Tharp, K.M., Jha, A.K., Kraiczy, J., Yesian, A., Karateev, G., Sinisi, R., Dubikovskaya, E.A., Healy, K.E., and Stahl, A. (2015). Matrix-Assisted Transplantation of Functional Beige Adipose Tissue. Diabetes *64*, 3713-3724.

Tharp, K.M., and Stahl, A. (2015). Bioengineering Beige Adipose Tissue Therapeutics. Frontiers in endocrinology *6*, 164.

Jha, A.K., **Tharp, K.M.**, Ye, J., Santiago-Ortiz, J.L., Jackson, W.M., Stahl, A., Schaffer, D.V., Yeghiazarians, Y., and Healy, K.E. (2015). Enhanced survival and engraftment of transplanted stem cells using growth factor sequestering hydrogels. Biomaterials *47*, 1-12.

Chudnovskiy, R., Thompson, A., **Tharp, K.**, Hellerstein, M., Napoli, J.L., and Stahl, A. (2014). Consumption of clarified grapefruit juice ameliorates high-fat diet induced insulin resistance and weight gain in mice. PLoS One *9*, e108408.

Khalifeh-Soltani, A., McKleroy, W., Sakuma, S., Cheung, Y.Y., **Tharp, K.**, Qiu, Y., Turner, S.M., Chawla, A., Stahl, A., and Atabai, K. (2014). Mfge8 promotes obesity by mediating the uptake of dietary fats and serum fatty acids. Nat Med *20*, 175-183.

Alston, E.N., Parrish, D.C., Hasan, W., **Tharp, K.**, Pahlmeyer, L., and Habecker, B.A. (2011). Cardiac ischemia-reperfusion regulates sympathetic neuropeptide expression through gp130-dependent and independent mechanisms. Neuropeptides *45*, 33-42.

Lorentz, C.U., Woodward, W.R., **Tharp, K.**, and Habecker, B.A. (2011). Altered norepinephrine content and ventricular function in p75NTR-/- mice after myocardial infarction. Autonomic neuroscience : basic & clinical *164*, 13-19.

Patents
Patent Application No. PCT/US2014/069612: Compositions and Methods for Producing and Administering Brown Adipocytes

Presentations
Tharp, K.M., et. al. (May 2017). Mechanosensitive YAP/TAZ transcriptional program enables the thermogenic capacity of adipose tissue. Oral presentation, NST Departmental Seminar, UC Berkeley.

Tharp, K.M., et. al. (April 2017). Mechanosensitive YAP/TAZ transcriptional program enables the thermogenic capacity of adipose tissue. Poster presentation*, UCSF-UCB-UCSC Stem Cell Center Retreat. *Best poster award

Tharp, K.M., et. al. (September 2016). Mechanosensitive YAP/TAZ transcriptional program enables the thermogenic capacity of adipose tissue. Oral presentation, UCSF Diabetes Center annual retreat.

Tharp, K.M., et. al. (May 2016). Synthetic Beige Adipose Tissue. Oral presentation, World Bioengineering Congress.

Tharp, K.M., et. al. (April 2016). Synthetic Beige Adipose Tissue. Oral presentation, The Berkeley Stem Cell Center annual retreat.

Tharp, K.M., et. al.(February 2016). Matrix assisted transplantation of functional beige fat. Poster presentation, Keystone Symposia: Obesity and Adipose Tissue Biology.

Tharp, K.M., et. al. (September 2015). Matrix assisted transplantation of functional beige fat. Oral presentation, UCSF Diabetes Center annual retreat.

Tharp, K.M., et. al.(June 2015). Matrix assisted transplantation of functional beige fat. Oral presentation, UC Systemwide Bioengineering Symposia.

Tharp, K.M., et. al.(December 2014). Matrix assisted transplantation of functional beige fat. Poster presentation, Cell Symposia: Stem Cell Energetics

Tharp, K.M., et al. (October 2014). Prevention of gallbladder hypomotility via FATP2 inhibition protects from lithogenic diet-induced cholelithiasis. Invited speaker, UCSF Liver Center Symposia: Biliary Development and Disease.

Research Support
2014-2018 NIDDK: 1R01DK101293-01A1, Stahl (PI) *Matrix Assisted Cell Transplantation of Brown Fat*
2014-2016 ADA Basic Science Award 1-14-BS-191, Stahl (PI) *Matrix Assisted Cell Transplantation of Brown Fat*

Chapter I: Matrix assisted transplantation of functional beige adipose tissue

Summary

Novel, clinically relevant, approaches to shift energy balance are urgently needed to combat metabolic disorders such as obesity and diabetes. One promising approach has been the expansion of brown adipose tissues that express uncoupling protein 1 (UCP1) and thus can uncouple mitochondrial respiration from ATP synthesis. While expansion of UCP1 expressing adipose depots may be achieved in rodents via genetic and pharmacological manipulations or the transplantation of brown fat depots, these methods are difficult to employ for human clinical intervention. We present a novel cell scaffold technology optimized to establish functional brown fat-like depots in vivo. We adapted the biophysical properties of hyaluronic acid-based hydrogels to support the differentiation of white fat derived multipotent stem cells (ADMSCs) into lipid accumulating, UCP1 expressing beige adipose tissue. Subcutaneous implantation of ADMSCs within optimized hydrogels resulted in the establishment of distinct UCP1-expressing implants that successfully attracted host vasculature and persisted for several weeks. Importantly, implant recipients demonstrated elevated core body temperature during cold challenges, enhanced respiration rates, improved glucose homeostasis, and reduced weight gain demonstrating the therapeutic merit of this highly translatable approach. This novel approach is the first truly clinically translatable system to unlock the therapeutic potential of brown fat-like tissue expansion.

Introduction

The unabated growth of the obesity epidemic and associated diseases such as type-2 diabetes reflect the current lack of effective strategies for intervention and treatment. Since obesity results from an imbalance in the ratio of energy intake to energy expenditure, it can be treated with reduced caloric uptake and/or increasing energy expenditure. Brown adipose tissue (BAT) as well as inducible brown-like cells in white adipose tissue (WAT), currently referred to as beige or bright adipocytes (*1*), possess the innate ability to dissipate metabolic energy as heat through non-shivering thermogenesis. This is possible due to the presence of the uncoupling protein UCP1 (*2*), a long-chain fatty acid anion/proton symporter (*3*), in the inner mitochondrial matrix, which allows the return of protons after they have been pumped across the mitochondrial inner membrane by the electron transport chain, thereby bypassing ATP synthase. While the importance of BAT for thermogenesis in smaller mammals and human infants has been well documented(*4*), only recent observations have demonstrated the presence of BAT in adult humans(*5, 6*). These observations have reversed the dogma that BAT is absent in adult humans and have presented a new route for the treatment of obesity-related disorders. Over 90% of the metabolic energy consumed by activated BAT will be derived from the β-oxidation of free fatty acids (FFA) (*7*). Furthermore, many studies have suggested that the amount of BAT correlates inversely with body mass index (BMI), raising the possibility that variations in the amount of BAT may drive alterations in body weight(*8*). Thus, increasing BAT mass may serve as a novel approach to combat obesity and related disorders such as type-2 diabetes. This concept is supported by recent studies that found evidence for metabolic enhancement, including the reversal of type-1 diabetes(*9*) and resistance to diet-induced obesity, in mouse models of BAT expansion(*10*) via transplantation of existing brown adipose tissues.

Strategies for expanding BAT can be grouped into two general categories: pharmaceutical/genetic intervention to trigger endogenous BAT/beige differentiation pathways, and the *ex vivo* generation of brown fat for implantation (*11-15*). Gene therapy approaches, for example the ectopic overexpression of the transcriptional regulator PRDM16(*14, 16*), are powerful tools to investigate BAT biology but are difficult to apply clinically due to the risks associated with

current gene therapy regiments(*17*). Pharmacological activation of differentiation pathways that drive a white adipose tissue (WAT) to BAT transition ("browning"), run the risk of affecting the function of other tissues and offer little control over the location and temporal extent of BAT expansion. Similarly, heterologous transplantation of existing BAT into immune-compromised recipients has demonstrated the metabolic impact of BAT expansion(*10*), but this approach has no clinical translatability due to a paucity of donor tissues and the expected host-vs.-graft rejection. Thus, we propose an alternative approach that takes advantage of current progress in the field of bio-inspired hyaluronic acid (HyA) hydrogels to engineer a Matrix-Assisted Cell Transplantation (MACT) system for Beige Adipose Tissue (BAT-MACT) derived from the readily available, multipotent stem cell (MSC) containing, stromal-vascular fraction of WAT(*18*).

Results

The importance of cell adhesion and matrix interactions has significant effects on MSC differentiation(*19*), however, no screens have examined how these interactions affect the browning of white adipose tissue derived MSCs (ADMSCs). To this end, ADMSCs were extracted from WAT (*20*) and cultured on tissue culture polystyrene (TCPS) plates coated with specific peptides found to be ligands for integrins and syndecans (Fig. 1A and Sup. Tab. 1). Differentiation was induced, lipid droplet accumulation (Fig. 1B) and UCP1 expression was assessed (Fig.1c). Our initial screens identified non-RGD peptide sequences such as AG73 (CGGRKRLQVQLSIRT), an adhesion ligand for α_6 integrins and syndecan-1(*21, 22*), as particularly efficient in driving UCP1 expression of ADMSCs, while C16 (CGGKAFDITYVRLKF), an $\alpha_{5/v}\beta_{1/3}$ integrin-engaging ligand(*23*), induced lipid accumulation. Interestingly, while all peptide-coated substrates outperformed uncoated TCPS in UCP1 expression assays, a combination of AG73 with C16 (1:3 molar ratio) had significant effects on UCP1 expression (Fig. 1D-E). Combining varied concentrations of AG73 with AG32 (CGGTWYKIAFQRNRK), another $\alpha_6\beta_1$ integrin-engaging ligand(*22*), we observed attenuated UCP1 expression (Fig. 1F). The impressive enhancement of UCP1 expression achieved by optimizing adhesion ligands is highlighted by the fact that previous attempts to differentiate WAT-derived MSCs into BAT yielded UCP1 levels significantly lower than BAT-derived MSCs(*11*). In contrast, we find UCP1 expression by WAT-derived ADMSCs differentiated on optimized adhesion ligands at comparable levels to differentiated BAT-derived ADMSCs *in vitro* (Sup. Fig. 1).

Optimized hydrogel provides instructive microenvironment for beige fat

Engagement with the extracellular matrix provides a crucial factor in driving MSC differentiation through biophysical properties and composition(*24-26*). Using our expertise in biomaterials(*27-30*), we synthesized acrylated HyA (AcHyA) macromers (Fig.2A) conjugated with the bioactive peptides. These functionalized AcHyA macromers (AcHyA-Ag73 and AcHyA-C16) were combined with specific matrix metalloprotease (MMP) sensitive peptide crosslinkers at defined concentrations to form hydrogels with precise physical characteristics and degradation kinetics (Fig. 2B). The synthesis of hydrogel networks takes advantage of the Michael-type addition reaction (i.e., attack of the acrylate group by available cysteine thiols to form a covalent bond)(*31, 32*), which forms a defined hydrogel scaffold within 5 minutes (Fig. 2C-D).

We verified that the ADMSCs embedded in the optimized matrix were forming functional cell adhesions with the hydrogel. By suspending ADMSCs in uncrosslinked AcHyA-Ag73:C16 or unmodified AcHyA, we found that the inclusion of adhesion peptides resulted in a significant increase in the storage modulus of uncrosslinked hydrogels seeded with ADMSCs, indicating that the adhesion peptides enable cells to mechanically integrate the synthetic ECM (Fig. 2E). The optimized hydrogel scaffold allowed the ADMSCs to evenly distribute and differentiate into UCP1 positive adipocytes *in vitro* without direct cell-cell contact (Fig. 2F and Sup. Fig. 2). Importantly, culturing cells in AcHyA-Ag73:C16 hydrogels significantly improved UCP1

expression of differentiated ADMSCs *in vitro* compared to monolayers exposed to adsorbed Ag73:C16 (Fig. 2G). Notably, unconjugated hyaluronan or RGD (CGGNGEPRGDTYRAY) conjugated hydrogels were not capable of inducing UCP1 expression independent of Ag73 and C16 (Fig. 2H)

To produce a functional BAT-MACT, we isolated ADMSCs from donor WAT, initiated differentiation *in vitro*, and suspended the cells in Ag73 and C16 presenting AcHyA macromers. BAT-MACTs were formed by mixing cells ($3*10^6$/ml) with AcHyA macromers (3 wt%) and a MMP-13 sensitive crosslinker. The cell suspension was immediately injected with a 22.5 gauge needle into the subcutaneous inguinal fat pad (or as noted) of recipient animals. The viability of the implanted BAT-MACT was monitored via bioluminescence using luciferase expressing donor cells delivered in a hydrogel or suspended in PBS. Subcutaneous injections of luciferin adjacent to implant demonstrate luminescence for both conditions after implantation. Importantly, the PBS delivered ADMSCs produce little luminescence when the bioluminescent substrate is introduced into general circulation. By delivering luciferin with IP injections distant from the BAT-MACT implant site, we observed massive signal expansion during the first week, which declines to undetectable levels 4 weeks post implantation (Fig. 3A).

Due to the rapid crosslinking kinetics, BAT-MACTs form a distinct subcutaneous lobe upon injection that is clearly brown/beige in appearance (Fig. 3B). BAT-MACTs were highly vascularized on a macroscopic level and thin sections of implants demonstrated an extensive and consistent vascular network throughout the implants (Fig. 3C). Likewise, UCP1 positive and lipid droplet accumulating cells were evenly spread throughout the BAT-MACT (Fig. 3D). Interestingly, regions of the implant showed positive staining for tyrosine hydroxylase (TH), the rate-limiting enzyme in the synthesis of catecholamines (Sup. Fig. 3). TH is essential for the production of norepinephrine by sympathetic neurons and macrophages to not only activate respiration, but also to maintain differentiation status and function(*33*). UCP1 mRNA expression of the implanted MACT was >10 fold higher than that of comparable *in vitro* cultured MACTs (Fig. 3E) and reached 7-17% of the levels found in endogenous BAT (Sup. Fig. 4). Importantly, PRDM16 and PPARγ expression in BAT-MACTs were comparable to endogenous BAT (Fig. 3F), highlighting the potential of the -MACT.

Immense differences of UCP1 induction within white fat depots have been shown to be under genetic control (*34*). We confirmed these differences by generating BAT-MACTs from FVB/NJ and C57BL6/J mice. Similar to previously published findings, C57BL6/J visceral fat depots produce significantly less UCP1 protein than FVB/NJ or subcutaneously sourced C57BL6/J ADMSCs within our BAT-MACT system (Fig. 3G). To assess the effect of implant location, we analyzed two different implant sites in the thoracic and inguinal regions for lipid droplets and UCP1 expression. In BAT-MACTs from both implantation sites, we observed multilocular lipid droplets, UCP1 positive cells, and blood vessels with no apparent difference between the implantation sites. Impressively, UCP1 protein levels in both BAT-MACT sites reached ~ 30% of BAT from the same animals (Fig. 3H). Importantly, inflammatory cytokines measured in serum were not upregulated whatsoever by the BAT-MACT system, in fact IL-2 was dissipated (Fig. 3I). Therefore, the BAT-MACT system allows for the measurement of metabolic effects independent of inflammatory artifacts.

To determine the metabolic impact of BAT-MACTs, we examined the respiratory capacity of animals augmented with a BAT-MACT or white adipocytes scaffolded by unmodified hyaluronic acid (WAT-MACT). Hyaluronic acid matrixes have been shown to aid in the development and persistence of WAT(*35, 36*) and WAT-MACTs formed fatty implants that were well vascularized, contained extensive lipid stores, and undetectable UCP1 expression (Sup. Fig. 5). The BAT-MACT implanted animals displayed significantly enhanced oxygen consumption rate ($V0_2$) and reduced respiratory exchange ratio (RER), recapitulating the elevated fatty acid utilization and respiration following classical BAT activation (Fig. 4A-B). Furthermore, BAT-MACT augmented animals were significantly more responsive to CL-

316,243, a β3-specific adrenergic agonist (Fig. 4C). To verify that free fatty acids would be taken up by BAT-MACTs, we utilized a recently developed optical probe for fatty acid uptake(*37*) and observed that an intraperitoneal injection of the probe was robustly taken up by BAT-MACTs. Importantly, as previously shown for endogenous BAT(*38*), injection of a β3-adrenergic agonist significantly enhanced fatty acid uptake rates by the BAT-MACTs (Fig. 4D).

To test the impact of BAT-MACTs on thermogenesis we examined core body temperature at room temperature (21 ^{0}C) and over 24 hours of 4 ^{0}C. Body temperatures of BAT-MACT recipients were higher throughout the cold challenge as well as at room temperature (Fig. 4E). Thermography revealed that the implant is distinctly thermogenic (Sup. Fig. 6). Importantly, this thermogenic effect was dependent on the amount of cells implanted (Fig. 4F) and the environmental temperature (Fig. 4G). Using C57Bl/6 mice as a model for diet induced obesity, we measured the BAT-MACT's impact on weight gain and glucose homeostasis. Animals implanted with BAT-MACTs and housed at 21°C for 2 weeks gain significantly less weight when fed a 60% fat diet compared to PBS delivered ADMSCs, cell-free matrix, or WAT-MACTs (Fig. 5A) in spite of slightly higher food consumption (Fig. 5B). Extended monitoring of weight gain identified the reduction of weight gain was significant within 2 weeks post BAT-MACT implantation and concomitant high-fat feeding. The difference in weight gain was sustained over a time period coinciding with the lifetime of the BAT-MACT cells as measured by bioluminescence (Fig. 5C).

After two weeks, serum triglyceride levels were found to trend lower and serum free fatty acids were reduced in animals augmented with BAT-MACTs (Fig. 5D, Sup. Fig. 7). Accompanying the reduced weight gain and serum FFAs, resting blood glucose levels (Fig. 5E) and glucose tolerance (Fig. 5F) were improved in BAT- but not WAT-MACTs, cell-free implants, or matrix-free implants of BAT-like cells.

Discussion

Expansion of UCP1 positive tissue holds exciting potential to combat obesity and related disorders (41). However, few practicable approaches for clinical deployment have been presented thus far. This novel strategy to integrate WAT derived MSCs with bioactive hydrogels bespoke to enhance differentiation, support tissue formation, and survival upon implantation provides the required core technology for autologous expansion of BAT mass in patients. ADMSCs are easily extractable and abundant, and are already utilized in regenerative medicine(18). ADMSCs used in this study were only partially purified, further gains in differentiation effectiveness could be anticipated by sorting for UCP1 enriching markers such as Sca-1(13), CD24, CD29(15, 42), and CD137(43).

Hydrogel based therapies are minimally invasive therapeutic options that will complement pharmacological and cell based approaches(44). We selected HyA as the core scaffold of our matrix for its biocompatibility, biodegradability, non-immunogenic properties, and its role in tissue development and repair(30). Recently, hyaluronic acid has been shown to augment integrin-mediated mechanotransductive signaling(45) and likely plays an essential role in the overall effect that our matrix has on the differentiation of ADMSCs. Similar hydrogel systems have been proposed for clinical use that employed crosslinkers and adhesion ligands that directly compete for attachment to the available functional groups on core polymeric chains within the hydrogel. These systems have struggled with compromised crosslinking efficiencies, unbound adhesion ligands preventing cell association with the matrix, and low molecular weight core structures that degrade too rapidly to be useful(46).

Matrix stiffness plays an important role in cell fate determination and should be a critical design feature of cell transplantation systems(27). We have developed a modular hydrogel system that allows for modulus and biological properties of the hydrogel to be tuned independently. This modular approach to tissue engineering may be essential to target an optimal

net modulus for development and maintenance of our BAT-MACT by allowing us to integrate and independently tune the crosslinking modulus and modulus that cells produce through ligand specific mechanotransduction observed in Figure 2E.

We have already shown that some ADMSCs spontaneously differentiate into UCP1 expressing cells in vitro using our bioinspired hydrogel (Fig. 2F). In our future studies, generation of UCP-1 positive adipocytes could be enhanced with matrices presenting heparin binding growth factors, specifically BMP7 and FGF21, which have been implicated in BAT differentiation(47). This objective is feasible, as heparin-binding growth factors can be associated with the matrix through the addition of thiolated heparin to the AcHyA(20). Ultimately, there is potential to generate a cell-free matrix that would orchestrate WAT transdifferentiation.

Our current generation of BAT-MACTs were viable for ~30 days in vivo following ~10 days in vitro culture. Duration of the implants is likely determined by a combination of the matrix susceptibility to biodegradation, through the MMP sensitive crosslinker and HyA backbone, and the lifespan of brite/beige cells (~50 days)(48). Importantly, we developed MMP sensitive crosslinkers(30) to enable tissue remodeling and recruitment of host vasculature (Fig. 3C). MMP13 has been shown to be essential for vascularization processes(49) and its expression is one of the most significantly upregulated MMPs during the differentiation of adipocytes(50). Additionally, crosslinkers designed to be sensitive to other MMPs appear to degrade too rapidly in vivo to be employed for these applications.

In vivo experiments with BAT-MACTs validated prior notions about the metabolic impact of BAT expansion. Recipients exposed to cold demonstrated that a 100 µl BAT-MACT implant had a significant effect on thermogenesis in a cell-number dependent manner. BAT-MACTs increased respiration rates, fatty acid utilization, reduced weight gain, and improved glucose homeostasis. These results are in line with recent reports demonstrating that transplantation of primary BAT fragments into mice can prevent diet-induced obesity(10). It remains to be determined if these beneficial effects are solely due to the increased caloric expenditure afforded by the implant or in addition also rely on an endocrine component such as IL-6(10) or other factors secreted by UCP1-positive adipose.

In summary, beige adipose tissue can be engineered using an optimized bioinspred HyA hydrogel system in conjunction with WAT derived stem cells and can persist under defined spatio-temporal conditions to affect body temperature, energy homeostasis, weight gain, and insulin sensitivity. These data from our preclinical model demonstrate the feasibility of a novel autologous transplantation based anti-obesity approach with a clear path for ultimate translation into clinical practice. Importantly, the BAT-MACT approach will facilitate systematic evaluation of the metabolic effects of BAT expansion and the underlying biological mechanisms.

Figures

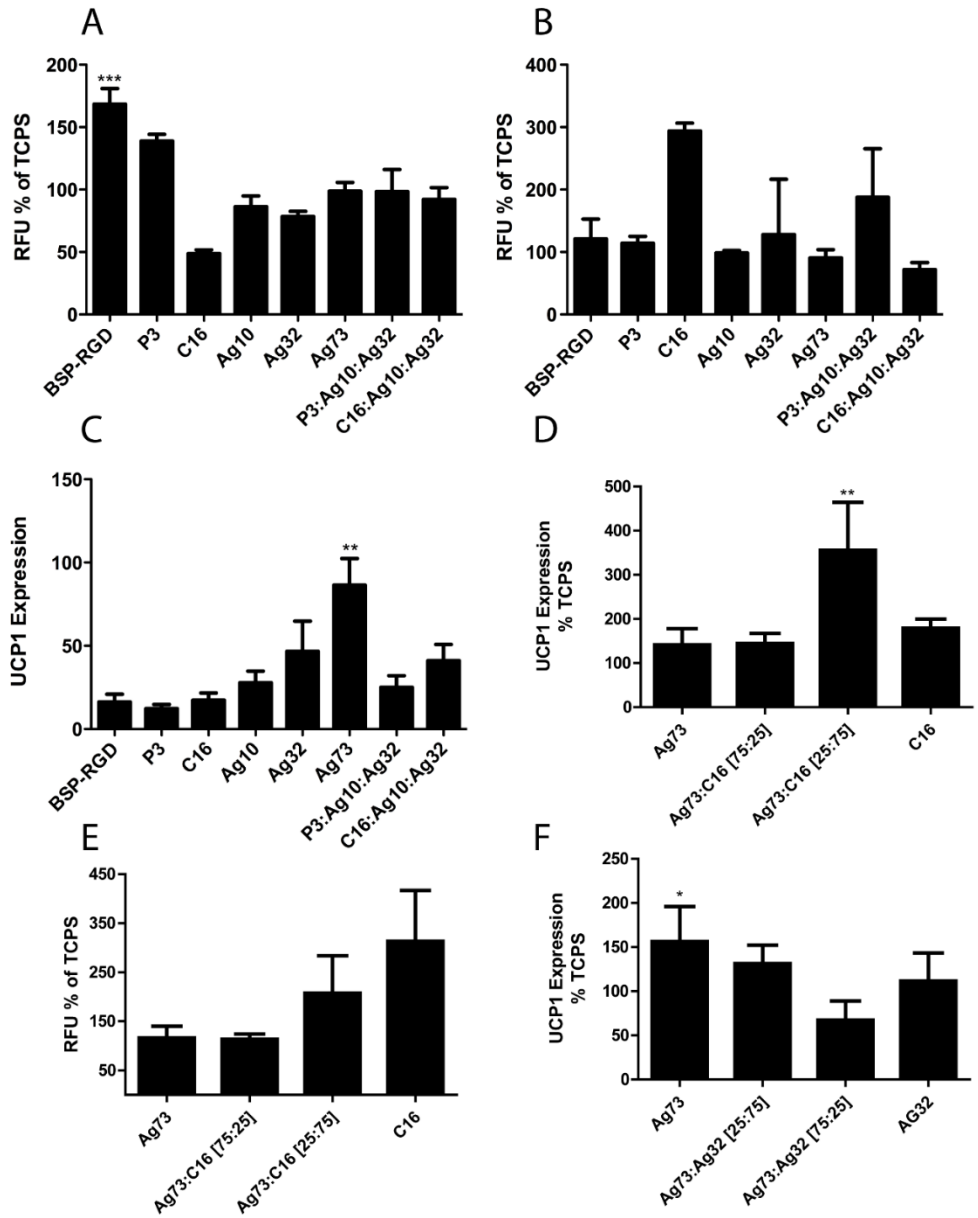


Figure 1: Effects of adhesion ligands on ADMSC differentiation. A) Adhesion of ADMSCs to adsorbed peptides following 4hr incubation, relative fluorescent units of adherent cells (n=3). B) Neutral lipid staining of ADMSCs after differentiation on indicated adhesion ligands (n=3). C) UCP1 mRNA expression of WAT derived murine ADMSCs that were differentiated on indicated adhesion substrate coated TCPS relative to undifferentiated ADMSCs (n=3). D) UCP1 mRNA expression of WAT derived ADMSCs differentiated on mixtures of Ag73 and C16 relative to differentiated ADMSCs on TCPS (n=6). E) Neutral lipid staining of WAT derived ADMSCs on varied mixtures of Ag73 and C16 relative to differentiated ADMSCs on TCPS (n=6). F) UCP1 mRNA expression of WAT derived ADMSCs differentiated on mixtures of Ag73 and Ag32 relative to differentiated ADMSCs on TCPS (n=6).

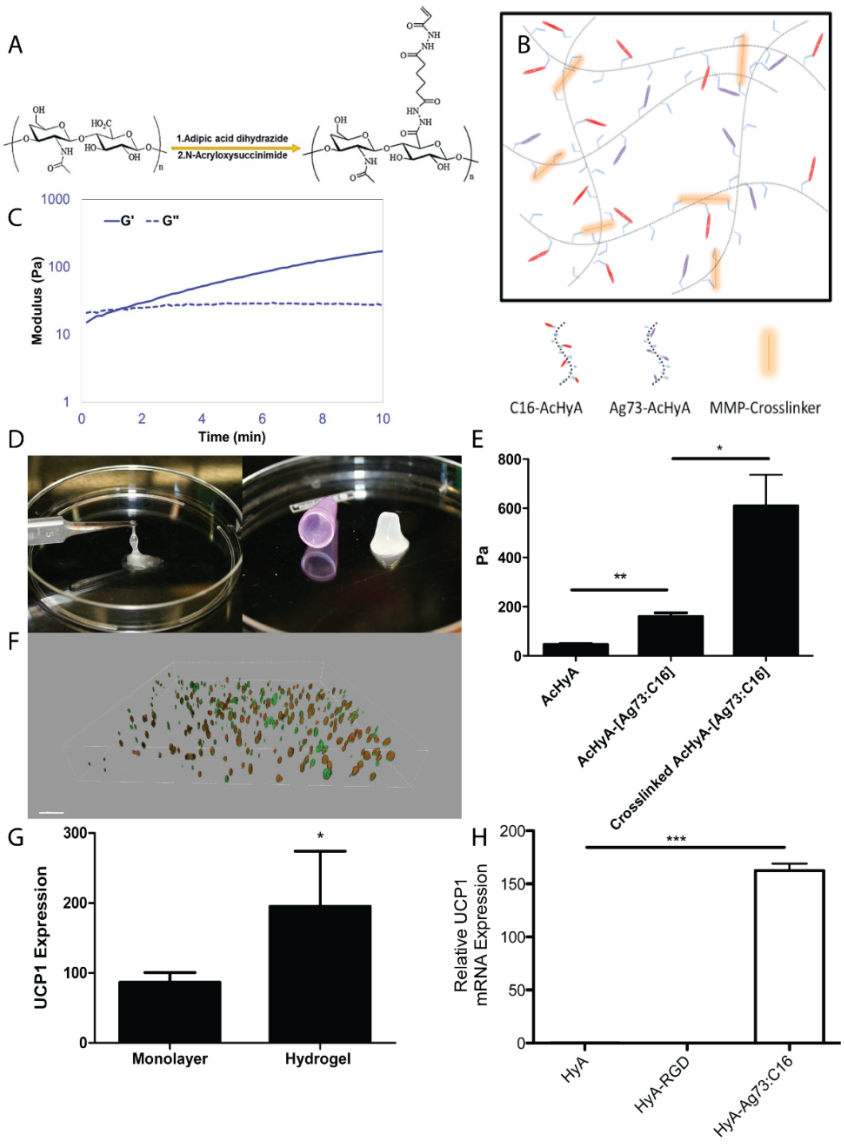


Figure 2: Bio-inspired HyA hydrogels. A) Schematic of the synthesis of acrylated hyaluronic acid (AcHyA) by sequential conjugation of adipic acid dihydrazide and N-acryloxysuccinimide. B) Representation of the assembly of optimized hydrogel through crosslinking of C16-AcHyA to Ag73-AcHyA macromers with an MMP-degradable crosslinker (not to scale). C) Timeline of HyA hydrogel gelation, gelation was considered complete when the storage modulus (G') exceeded the loss modulus (G'') (measured in Pascals). D) Photographs of AcHyA before (left) and 5 min after the addition of the crosslinker (Right). E) Storage modulus of ADMSC suspended in uncrosslinked and crosslinked hydrogels cultured *in vitro* after 72hr (n=3). F) 3D reconstruction of *in vitro* ADMSCs in optimized hydrogel (red: UCP1, green: mitotracker) after completion of differentiation. G) UCP1 expression of differentiated ADMSCs with the optimized peptide mixture in monolayer and comparable hydrogel (n=4). H) ADMSCs differentiated in unconjugated HyA hydrogels, RGD conjugated hydrogels, and Ag73:C16 conjugated hydrogels, GAPDH normalized UCP1 mRNA expression relative to WAT (n=5).

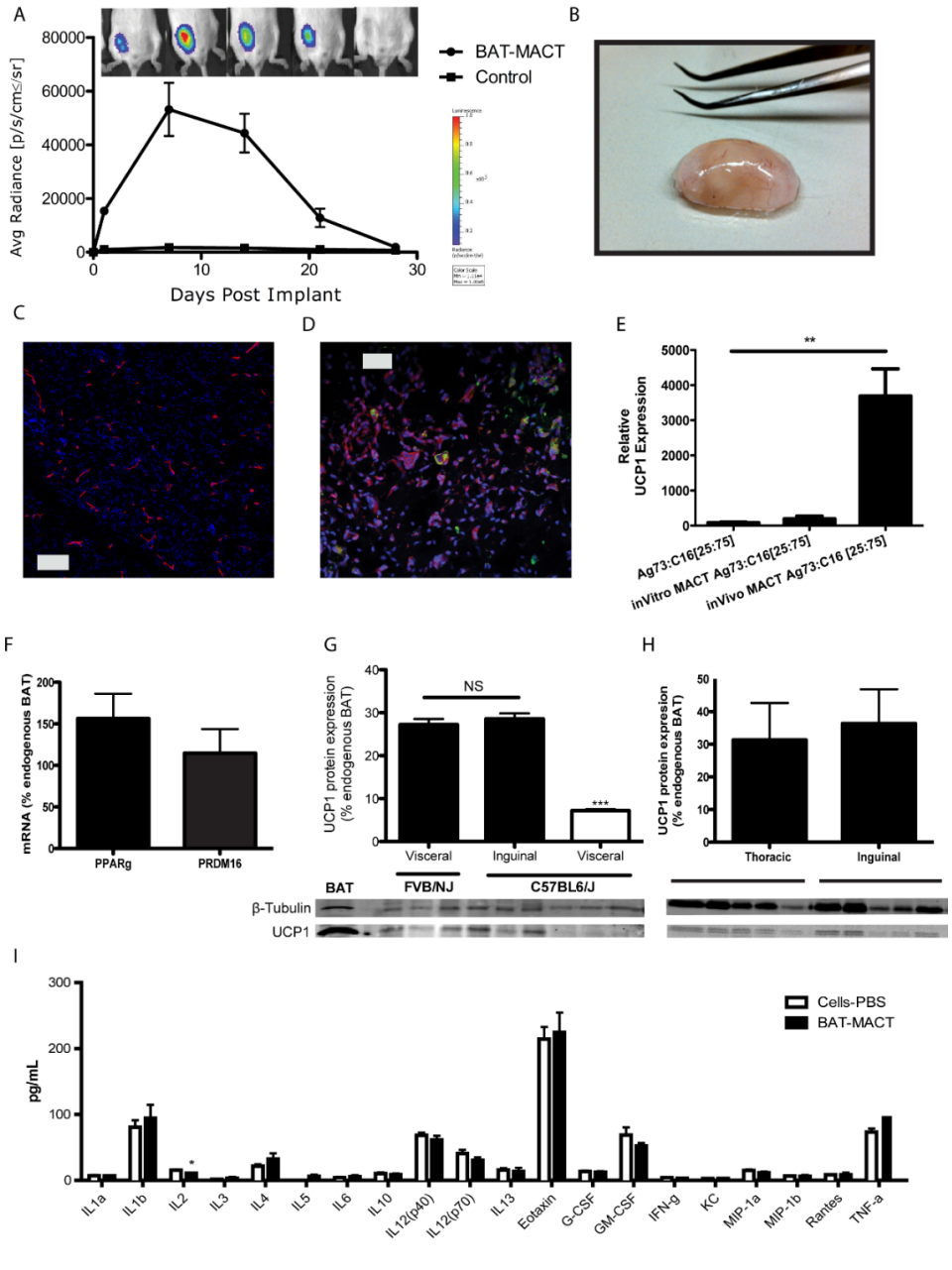


Figure 3: BAT-MACT *in vivo* characteristics. A) Persistence of BAT-MACT over time monitored by luciferase activity in live animals (FVB/NJ n=5), false color heat-scale image indicting average photon radiance. B) Macroscopic morphology of implants after 2 weeks. BAT-MACTs were removed after 14 days, fixed, cryosectioned, and stained with DAPI and stained for the vascularization marker endomucin (C), or (D) neutral lipids (green) and UCP1 (red). E) mRNA expression of UCP1 relative to WAT using samples from differentiated ADMSCs plated on Ag73 and C16 peptide coated TCPS, or in a Ag73 and C16 conjugated AcHyA hydrogels cultured *in vitro*, or implanted into recipient animals (FVB/NJ n=4, 3, or 6 respectively). F) PRDM16 and PPARγ mRNA expression normalized to GAPDH of BAT-MACTs after two weeks *in vivo*, relative to endogenous BAT (FVB/NJ n=9). G) UCP1 protein expression of BAT-MACTs generated with ADMSCs from visceral or subcutaneous FVB/NJ or C57BL6/J mice two weeks post implantation into a syngenic recipient relative to endogenous BAT (n=3) H) UCP1 protein expressed in BAT-MACTs of different implant sites after two weeks *in vivo* relative to endogenous BAT (FVB/NJ n=5). I) Serum cytokine levels measured two weeks post implantation of BAT-MACT or the same ADMSCs delivered via PBS. Animals were administered the 60% fat diet for the duration of this study (C57BL6/J n=6).

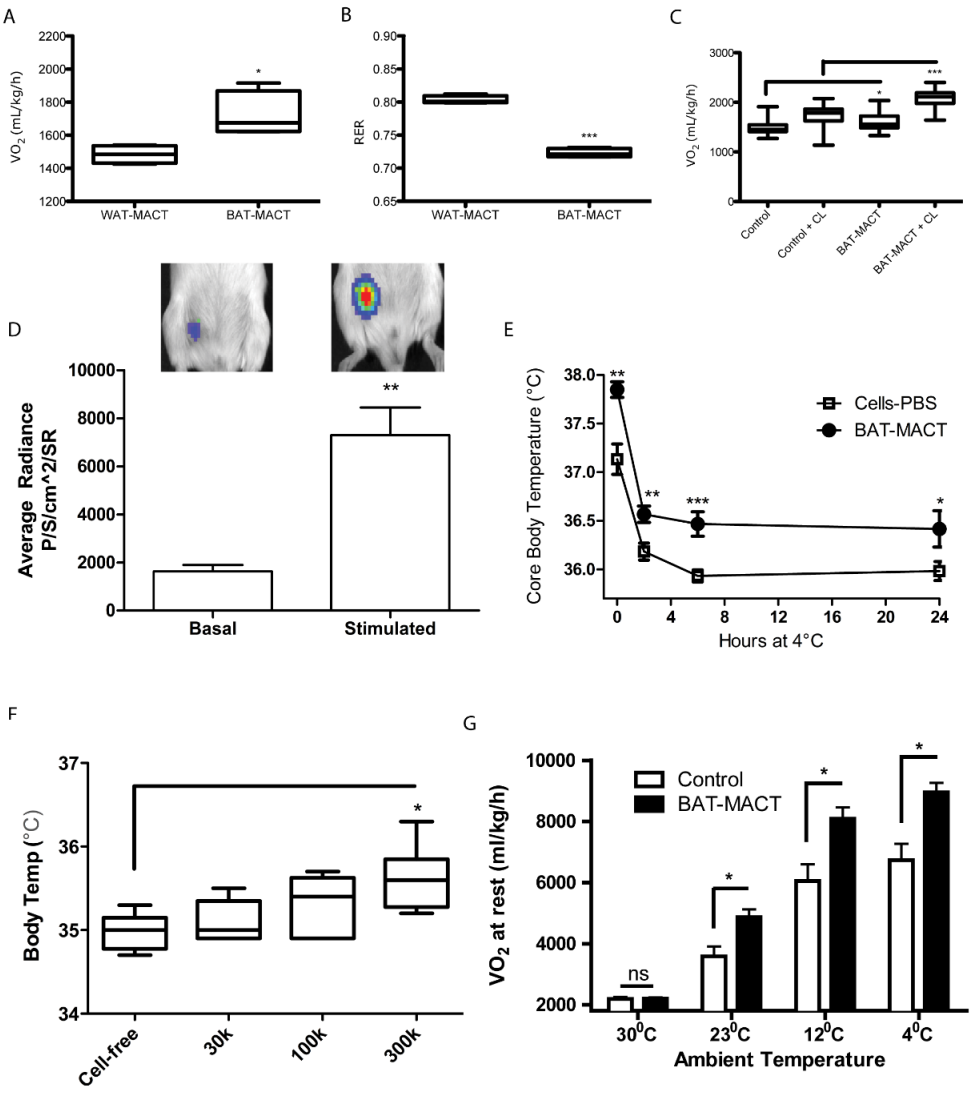


Figure 4: Metabolic effects of BAT-MACTs two weeks post implantation. A) Average oxygen consumption (VO_2) rate over 24 hours (FVB/NJ n=4). B) Average respiratory exchange ratio over 24 hours (FVB/NJ n=4). C) Average oxygen consumption rate 4 h before and after ß-adrenergic agonist CI-316,243 was administered (FVB/NJ n=4). D) Fatty acid uptake of BAT-MACTs under basal and CI-316,243 stimulated conditions (FFA-SS-Luc) (FVB/NJ n=3). E) Core body temperature during a 24 hour cold challenge (4 °C) (FVB/NJ n=6). F) Core body temperature after a 6 hours cold challenge (4 °C) of animals implanted with the indicated number of ADMSC in 100 μL of optimized hydrogels on a normal chow diet (FVB/NJ n=6). G) Average oxygen consumption rate of mice implanted with BAT-MACT or comparable cells delivered in PBS during the 10-14 days post implantation in temperature controlled CLAMS unit (C57BL6/J n=4). Explanation of controls: WAT-MACT: ADMSCs differentiated without T3 embedded in a peptide less hyaluronic acid hydrogel and Cells-PBS: equivalent number of differentiated ADMSCs delivered in 100 μL PBS.

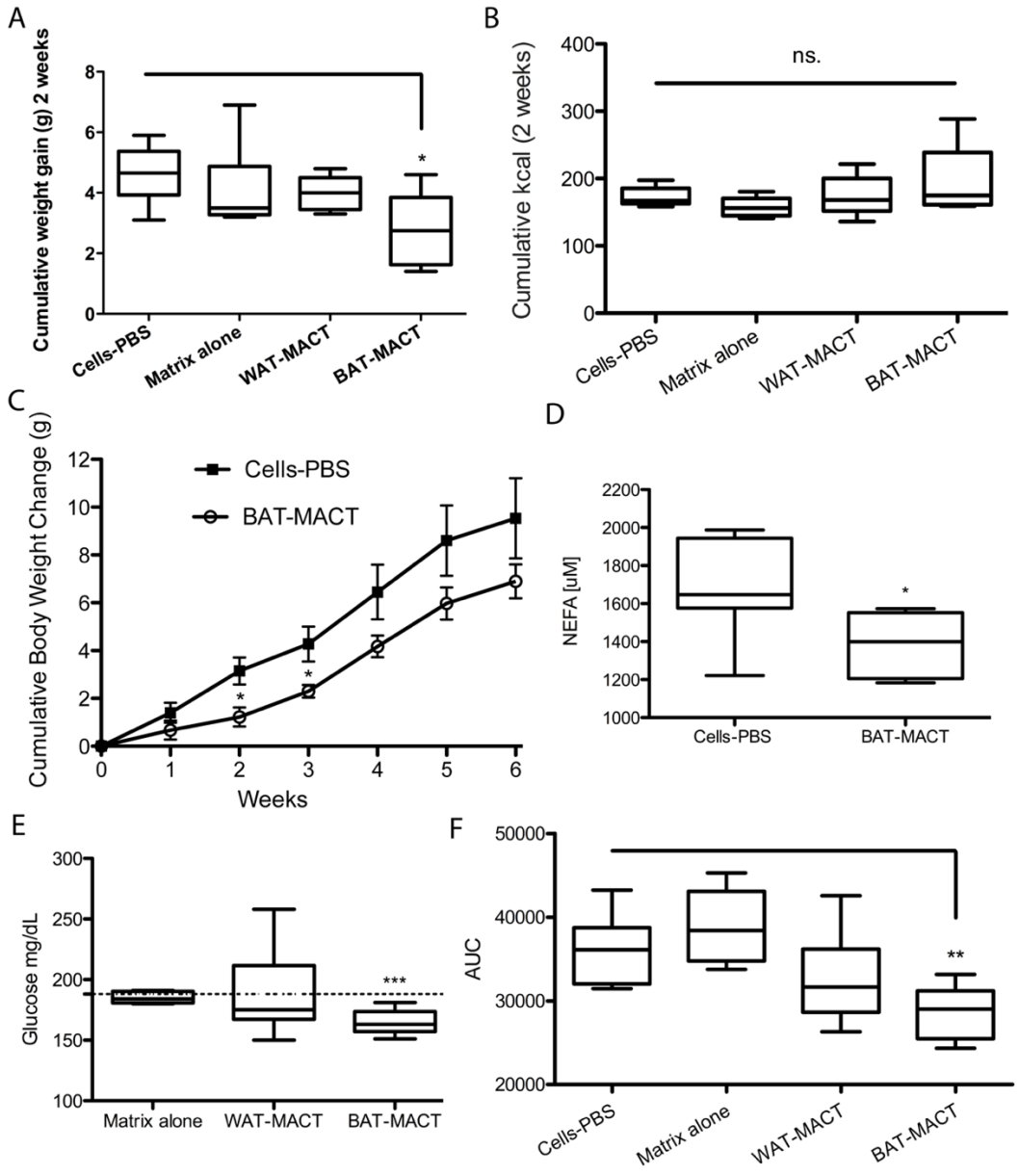
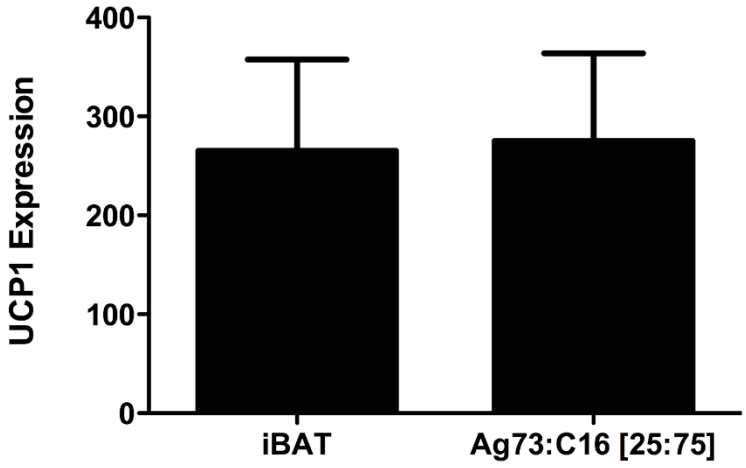
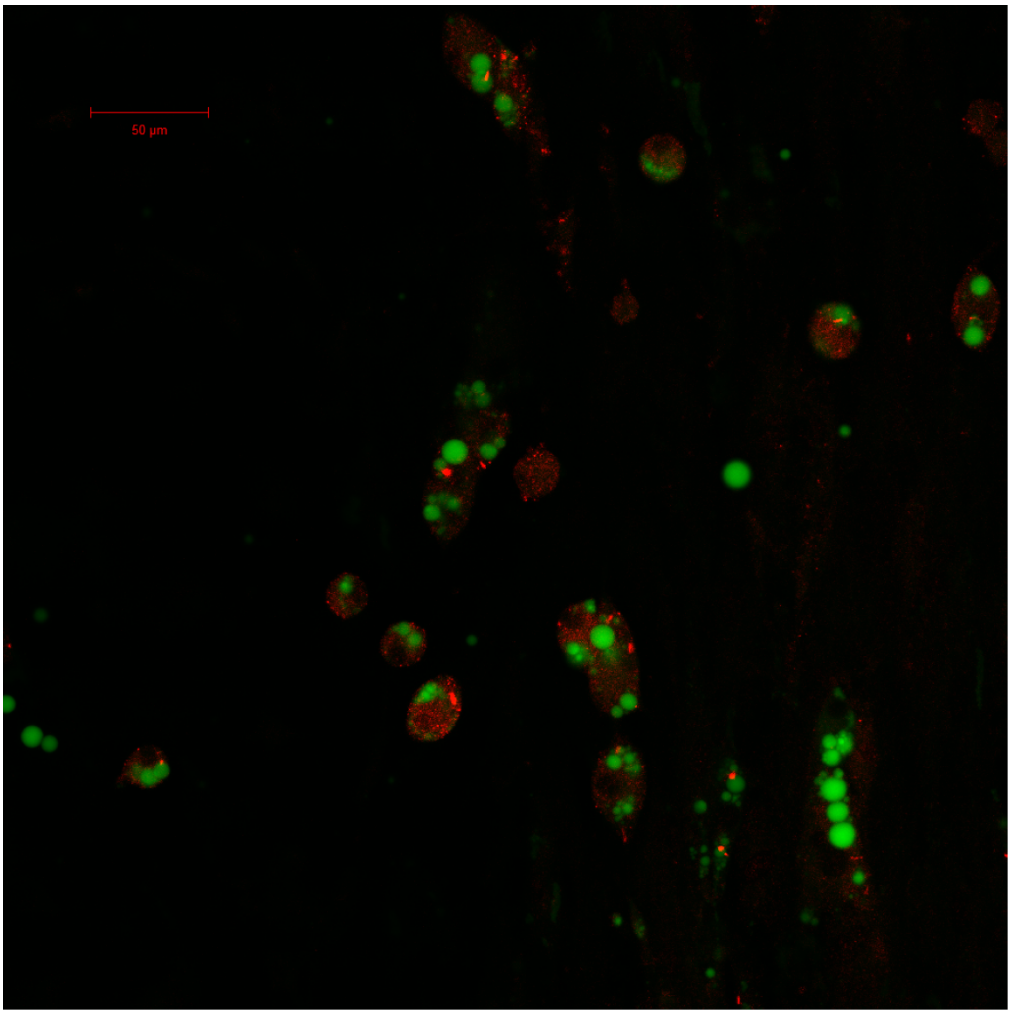


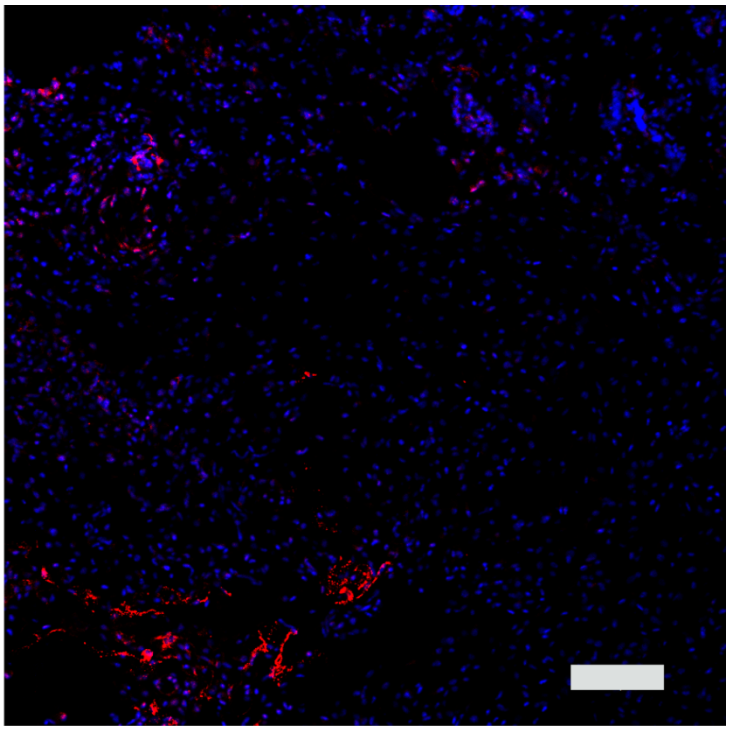
Figure 5: Beige Fat expansion promotes improved metabolic profiles in C57BL6/J mice. A) Weight gain of mice after two weeks of consuming 60% fat diet and being implanted with BAT-MACT or controls receiving either cells with no matrix, cell-free matrix, or WAT-MACTs (n=6). B) Cumulative kcal consumed by the animals over two weeks. C) Body weight of animals injected with matrix-free cells or BAT-MACTs consuming a 60% fat diet over the course of 6 weeks (n=4). D) Serum non-esterified fatty acid concentration, E) Resting blood glucose concentrations, and F) glucose tolerance test area under curve (time points: 0, 20,30,60,and 120 minutes) with an identical dose of glucose given to animals after two weeks of consuming 60% fat diet and being implanted with either BAT-MACT or matrix-free control (n=6).



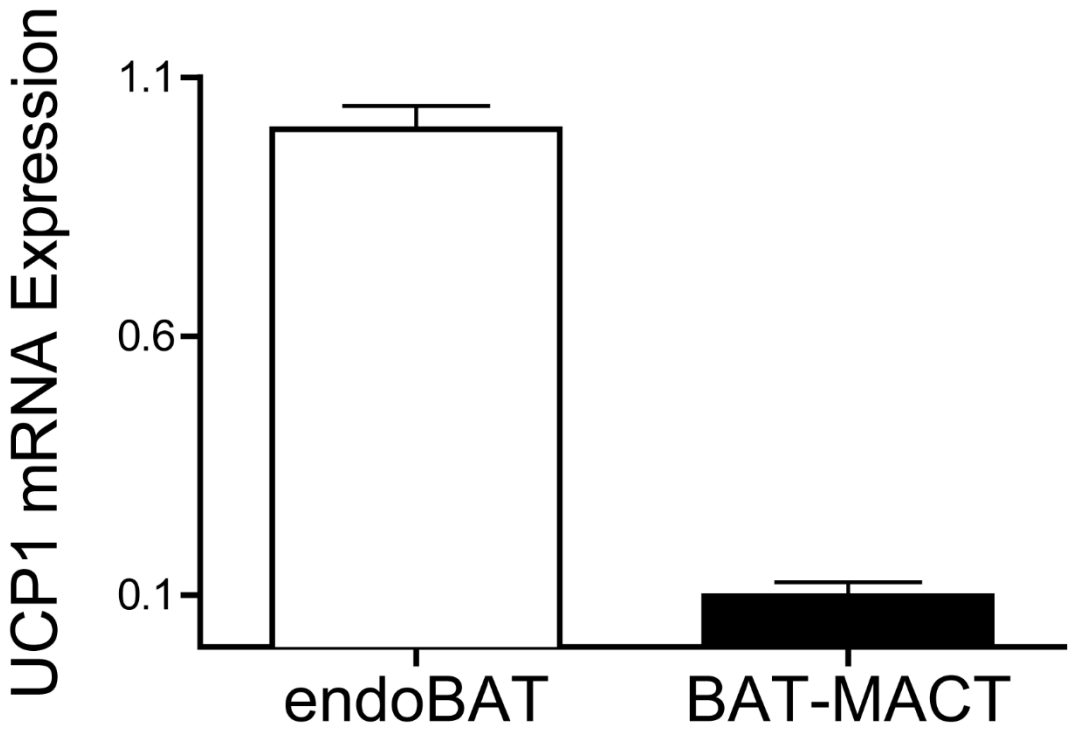
Supporting Figure 1: UCP1 expression of WAT and BAT derived ADMSCs. Differentiated ADMSCs derived from interscapular BAT plated on TCPS or perigonadal WAT derived ADMSCs plated on the Ag73 and C-16 (25:75 molar ratio) coated plates, GAPDH normalized UCP1 mRNA expression relative to WAT (n=5).



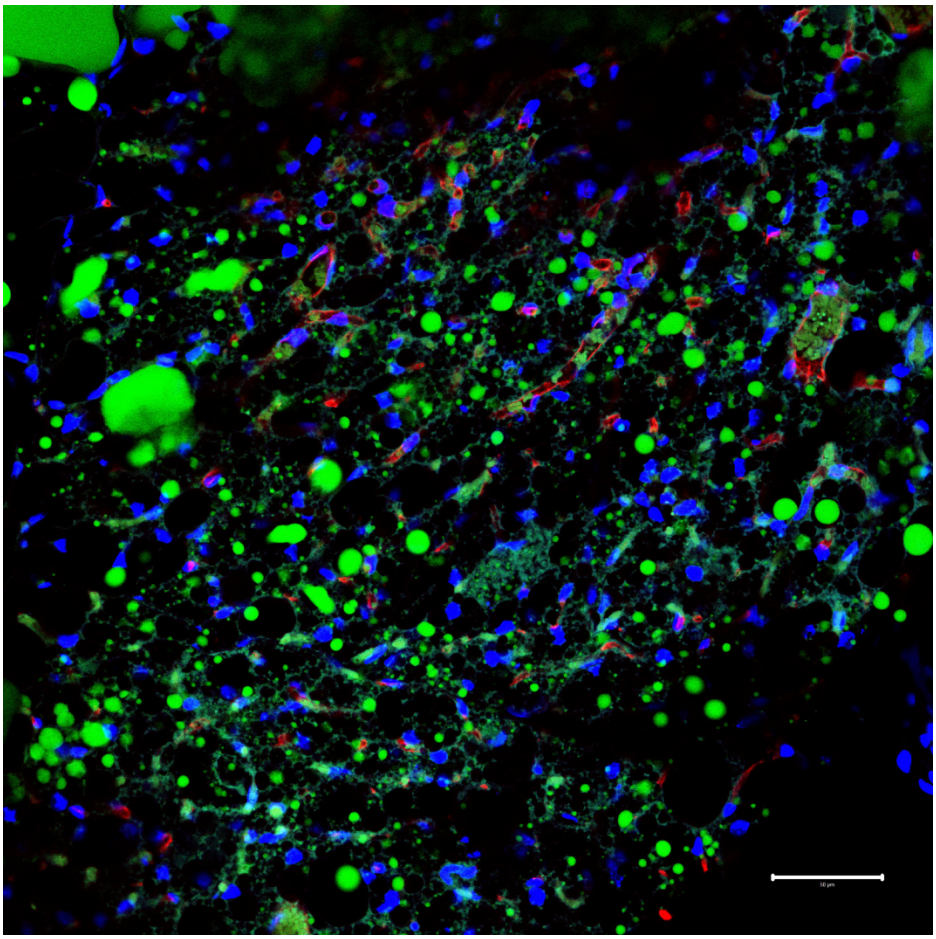
Supporting Figure 2: UCP1 and neutral lipid staining of *in vitro* hydrogel. IHC of differentiated ADMSCs in Ag73:C16 hydrogel with UCP1 (red) and Bodipy3922 (green).



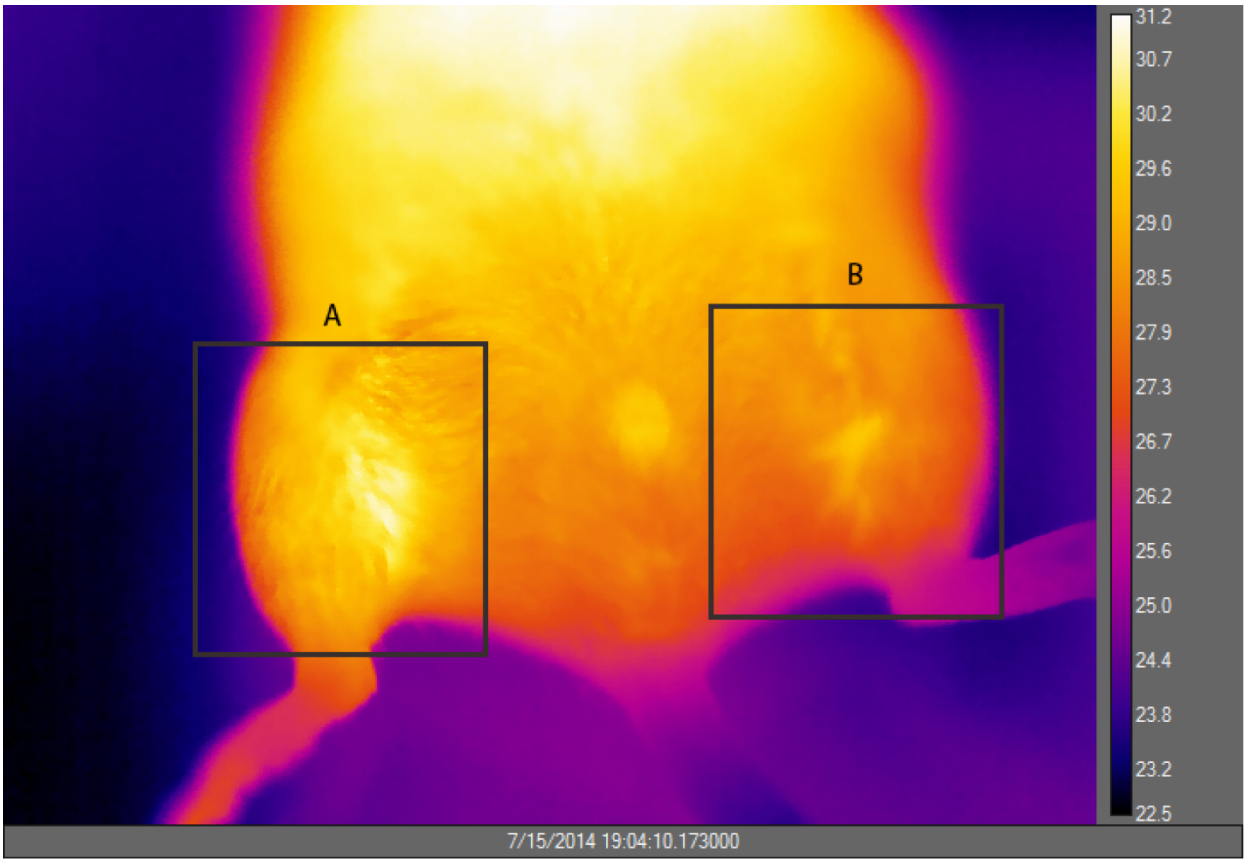
Supporting Figure 3: Tyrosine hydroxylase expression in BAT-MACT. Two weeks post implantation BAT-MACT were stained with DAPI (blue) and tyrosine hydroxylase specific antibodies (red).



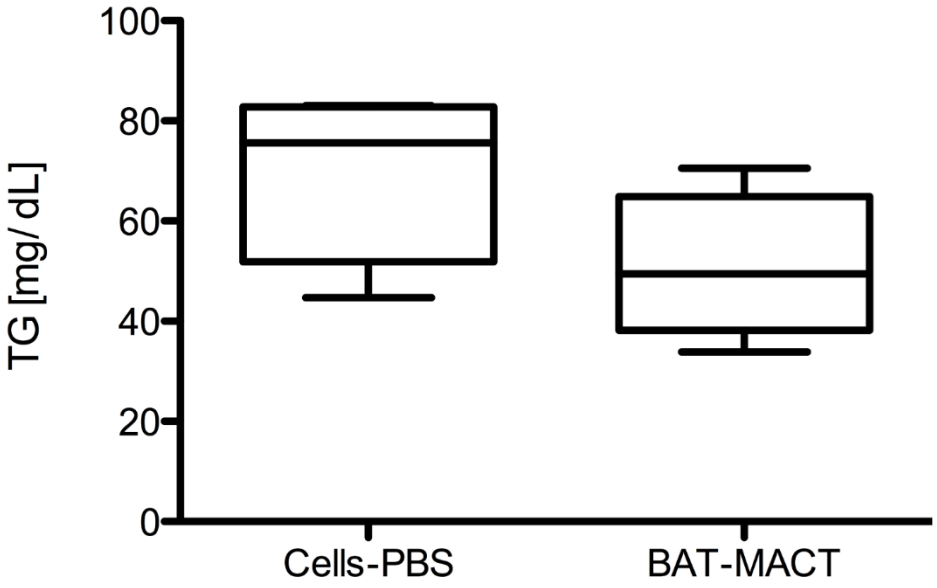
Supporting Figure 4: UCP1 expression of BAT-MACT compared to endogenous BAT. GAPDH normalized UCP1 mRNA expression relative to average endogenous BAT expression (n=5).



Supporting Figure 5: WAT-MACT morphology. Two weeks post implantation WAT-MACT were stained with DAPI (blue) and endomucin specific antibodies (red) to highlight the vasculature.



Supporting Figure 6: Thermograph of BAT-MACT implanted animal. BAT-MACT in area A compared to unaltered inguinal region in area B, 5 days post implantation at room temperature. Max temperature for area: A) 30.86°C B) 29.43°C.



Supporting Figure 7: Serum triglyceride concentrations of control and BAT-MACT implanted animals. Serum triglycerides concentrations of animals from Fig. 5D.

Methods

Animals and diets
Experiments were performed according to AAALAC guidelines and approved by the University of California, Berkeley Animal Care and Use Committee. 8 week old male C57BL/6J or FVB/NJ Mice (Jackson Labs) were group housed for a one-week acclimation period (temperature: 21 ± 2°C, humidity: 30-70 %) in Tecniplast cages filled with sani-chip bedding (Harlan). Then individually housed one-week prior to implantation and administration of high 60% fat diet (Teklad TD.06414). Luciferase expressing L2G85 (FVB/NJ) mice were utilized as cell source for experiments using bioluminescent monitoring of implant viability and function.
ADMSC Isolation: Fat depots from L2G85 (FVB/NJ) or C57BL6/J mice, perigonadal (visceral) or inguinal (subcutaneous) respectively, were isolated from 3 month old mice as previously described (*20*).

In-vitro differentiation of ADMSCs**:** ADMSCs [initial density ~100 k/cm²] were cultured to post confluence on TCPS or adsorbed peptide surfaces. Differentiation was induced for 3 days with [0.85 µM Insulin, 10 nM Triiodothyronine (T3), 1 µM Dexamethasone, 500 µM Isobutylmethylxanthine (IBMX)] in high glucose DMEM (Invitrogen) with 10% FCS (Gibco) and penicillin/streptomycin (P/S) (Gibco). The induced cells were then treated with 0.85 µM Insulin and 100 nM Rosiglitizone in high glucose DMEM (Invitrogen) with 10% FCS and penicillin/streptomycin for 12 subsequent days. Before harvest with Trizol, cultures were treated with 5 µg/mL CL316,243 for 4 hours. The initial peptide screening differentiation experiments were carried with the goal of determining the differentiation outcome of an adhesion selected cell fraction, a process referred to as “panning”. To this end, primary ADMSCs were given 4 hours to adhere onto the surface coating, cultures were then PBS washed twice to remove less adherent cells within the ADMSC population and differentiation was induced as described above (Fig. 1a-c). Experiments to determine optimal proportions of selected peptides were carried out without washing off poorly adherent cells (Fig. 1d-f).

Immunohistochemistry
IHC was performed as previously described (*27*). Whole in vitro hydrogels were fixed with 4% PFA for 30 minutes at RT and imaged within their MilliCell insert (Milipore) placed on coverslips.
mRNA

Tissue samples suspended in RNALater ICE (Ambion) and stored at -20°C. mRNA was isolated from RNALater ICE stabilized tissues or directly from in vitro cultures of monolayers or cell laden hydrogels with Trizol reagent (Ambion). Tissue samples were homogenized with a Polytron PT2100. Assays were carried out on an ABI 7500 RT PCR System with TaqMan universal mastermix II and validated PrimeTime primer probe sets (IDT). First strand cDNA synthesis kit (Fisher) was employed to transcribe 5 µg of RNA per 20 µL. 100ng of cDNA was used per rtPCR reaction in triplicates. The delta-delta-CT method was employed to comparatively assess mRNA quantity. All data is represented as sample’s value normalized to GAPDH relative to source tissue derived ADMSCs, source tissue, or endogenous BAT.

Protein quantification and western blotting
Pierce BCA kit and Li-Cor Oddessy with anti UCP1 (Invitrogen) and anti β-tubulin E7 clone (DSHB). Data presented as UCP1 normalized to β-tubulin relative to endogenous BAT.

Synthesis of HyA hydrogels
Modified HyA (500 kDa) was synthesized using previously established methods(*39*). The AcHyA-C16 or AcHyA–Ag73 was synthesized by reacting peptides (CGGKAFDITYVRLKF, 10

mg) or (CGGRKRLQVQLSIRT, 10 mg) with AcHyA (25 mg, 10 ml DI water) at room temperature. To synthesize hydrogels, AcHyA (2 mg), AcHyA-C16 (6 mg), and AcHyA-Ag73 (2 mg) were dissolved in 0.3 mL of triethanolamine-buffer (TEOA; 0.3 M, pH 8), and incubated for 30 minutes at 37 oC, and subsequentely MMP-13-cleavable peptide (CQPQGLAKC, 3 mg in 50 µL TEOA buffer) was added to HyA-peptide solution. The crosslinker concentration was varied to achieve complete crosslinking of available acrylate functionalities on the HyA macromers, ~200 mM. The initial storage modulus of all hydrogels (in vitro and in vivo) were measured to be consistently ~850 Pa.

BAT-MACT generation

ADMSCs were cultured in vitro in DMEM with 10% FBS and 1% P/S on TCPS. 2 days post confluency differentiation was induced with 0.85 µM insulin, 10 nM triiodothyronine, 1 µM dexamethasone, and 500 µM isobutylmethylxanthine (for WAT-MACT, triiodothyronine was omitted from the cocktail). 3 million cells per mL were suspended in AcHyA-Ag73:C16 [1:3 molar ratio] just before implantation (for WAT-MACT cells were suspended in AcHyA). The cell suspension was mixed with the MMP13 cleavable crosslinker at a final concentration of ~200 mM (sufficient to achieve a modulus of ~850 Pa) and 100 µL of the forming BAT-MACT was immediately injected to recipient mice.

Experiments where BLI imaging was used to monitor the viability and function of the BAT-MACTs, in conjunction with metabolic measures, were preformed in FVB/NJ mice with ADMSCs isolated from perigonadal fat depots of syngenic L2G85 donor mice. Experiments where metabolic parameters were assessed without BLI monitoring were preformed with C57BL6/J mice implanted with BAT-MACTs generated with ADMSCs isolated from the inguinal adipose depot.

In Vitro BAT-MACT

ADMSCs were cultured in vitro in DMEM with 10% FBS and 1% P/S on TCPS. 3 million subconfluent cells per mL were suspended in the specific hydrogel and injected into a Milicell transwell chanber (Millipore) in a 24 well tissue culture plate (Falcon). After two days of culture in DMEM with 10% FBS and 1% P/S, the differentiation protocol described for the in vitro differentiation of ADMSCs was implemented.

Bioluminescent Imaging (BLI)

Imaging was accomplished with an IVIS Spectrum. 45 µL luciferin (4mg/mL) in PBS was injected into animals IP. FFA-SS-LUC 100 µl of (1.4 µg/µl) compound injected IP into mice. Once the BLI signal dropped off (~40 minutes) the animals were removed to recover. 4 hours later, once all original BLI signal was extinguished, 1 µg CL316,243 per gram body weight was injected IP followed by another dose of the FFA-SS-LUC.

Respirometry

Respirometry was performed with the Comprehensive Laboratory Animal Monitoring System (Columbus Instruments). Measurements were taken over 24 hour periods and average values were assessed (*40*). CL-316,243 was administered to animals and the 4 hour pre- were compared to the 4 hour post- injection time periods. Activity was monitored in 1 min intervals of infrared beam breaks in X, Y and Z-axis and found to be not significantly different for any of the groups.

Serum cytokine measurements

BioRad Bio-Plex Pro Mouse Cytokine 23-Plex immunoassay kit was utilized as per manufacturer's instructions with a BioRad MAGPIX system.

Rheology

Viscoelastic properties of the hydrogel were determined using an oscillatory rheometer with parallel plates geometry (8 mm) and a gap height of 0.2 mm under 10% constant strain and frequency ranging from 0.1 Hz to 10 Hz at 37 °C in a humidity-controlled chamber.

Cell adhesion assays

Purified peptides were suspended at 20 μM in ultrapure water with 1% P/S. 20 μM peptide suspensions were allowed to adsorb to the 24-well TCPS plates (BD Falcon) overnight at 4 °C. Plates were then washed 2 times with PBS. 20,000 primary ADMSCs suspended in DMEM with 10% FBS and 1% P/S were added to each well and incubated at 37 °C for 4 hours. Media and non-adherent cells were removed and centrifuged to separate the cells from media. The adherent and non-adherent cells were then counted with the CyQuant kit (Invitrogen).

Cold challenge and core body temperature

Physitemp Model BAT-12 microprobe was employed to measure core body temperature of mice rectally. Cold challenges took place in a 4 °C walk-in refrigerator approved for use in accordance with AAALAC guidelines.

Serum glucose and glucose tolerance tests

Blood glucose was measured with a NovaMax blood glucometer and NovaMax glucose test strips (Sanvita). Mice were injected with an equivalent dose of glucose (167 μL of 300 g/L glucose). This dose was selected as a dose that the median mouse weight would warrant to achieve the standard glucose dose of 2 mg/g body weight generally used for a GTT.

Statistical Analysis

All data is presented as SEM analyzed using Prism (Graphpad). Statistical significance was determined by either one-way ANOVA followed by Tukey post-test or unpaired two-tailed student's t-test. Significance presented at *$P<0.05$, **$P<0.01$, and ***$P<0.001$.

Chapter II: Synthetic ECM promotes thermogenic adipogenesis through actin cytoskeleton dynamics

Summary

Unlocking the therapeutic potential of brown/beige adipose tissue requires technological advancements that enable the controlled expansion of this uniquely thermogenic tissue. Transplantation of brown fat in small animal model systems has confirmed the expectation that brown fat expansion could possibly provide a novel therapeutic to combat obesity and related disorders. Expansion and/or stimulation of UCP1-positive adipose tissues have repeatedly demonstrated physiologically beneficial reductions in circulating glucose and lipids. Unfortunately, there are no sources of transplantable brown adipose tissues for human therapeutic purposes at this time. Chapter I demonstrates that hyaluronic acid based hydrogels can be used to generate large quantities of UCP1-positive adipose tissue with the potential to be used as a metabolic therapy. To further advance this approach, mechanistic explanations for how biomaterial derived cues govern stem cell differentiation will be required to develop the BAT-MACT system as a therapeutic tool. In this chapter, we identified the actin cytoskeleton as a putative regulator of thermogenic adipose differentiation via pharmacological perturbations during differentiation of brown adipocytes. Since ECM mediated responses are known to directly alter actomyosin dynamics, these finding will facilitate further study of synthetic ECM based control of adipogenesis.

Introduction

Proposing brown adipose tissue (BAT) expansion as a therapeutic treatment for obesity and obesity-related disorders has recently gained significant traction (*41, 42*). BAT, as well as beige adipocytes (*1, 43*) have high metabolic capacity due to high mitochondrial content and expression of uncoupling protein-1 (UCP1) (*2*), a long-chain fatty acid anion/proton-symporter (*3*), found in the inner mitochondrial membrane. UCP1 decouples the action of ATP-synthase and dissipates the proton gradient produced by the electron transport chain, thus generating heat. BAT mass inversely correlates with body mass index (BMI), which supports the notion that BAT may regulate overall bodyweight and metabolic health (*44*). The benefits of expanded UCP1-expressing adipose may not be limited to their metabolic characteristics, as brown adipose has been shown to possess a potent secretome (*45*). Notably, implanted BAT has been shown to produce secretions of IGF-1, which was reported to enable the insulin independent reversal of type-1 diabetes (*46*). BAT also appears to exert significant effects on the lipid metabolism in the liver (*47*) and bone mineral density (*48, 49*). Overall, the generation of functional beige or brown adipocytes for therapeutic purposes appears to hold significant merit for a number of possible treatments.

The current strategies to clinically deploy BAT fall into two main categories: pharmaceutical or genetic interventions to induce endogenous BAT/beige differentiation pathways, and the *ex vivo* generation of autologous cell/tissue transplants (*11-15*). Current gene-therapy approaches still have challenges to overcome before they are applied as anti-obesity therapeutics (*17*), but have proven to be significant instruments for investigating BAT biology (*14, 16*). Pharmacological activation of the pathways that drive a white adipose tissue (WAT) to beige/brite transition, a process known as “browning”, offer little control over the location and temporal extent of the effects. Transplantation of autologous BAT in small animal models has shown clear metabolic enhancements (*9, 10, 50*) but approaches are unlikely to be suitable for human therapies since there are few sources of transplantable mature human BAT and immune-rejection would need to be overcome. To successfully harness the therapeutic

potential of BAT, a readily available source of transplantable cells with the potential to robustly generate UCP1-positive (UCP1+) adipocytes must first be identified or created. Secondly, the basis to form a functional, non-immunogenic, highly localized, and metabolically active brown/beige tissue must be defined.

The use of small molecules or growth factors to induce the browning of WAT is a promising area of research, but systemic dosing has the potential to produce off target effects with undesirable consequences. One notable browning agent, rosiglitazone, was widely used to treat diabetes but has disconcerting side effects that included heart failure (*51*). Browning factors (*20, 40, 52-65*) generally target conserved signaling pathways, making specificity a concern. By using biomaterials to localize and control release kinetics of browning factors to desired anatomical locations, an acceptable level of specificity may be achieved (*66-72*). When increasing the number of brown-adipocytes, other supporting cell types are required for producing a functional tissue. For BAT, this includes interactions between the nervous, vascular, and immune systems, with UCP1+adipocytes. Efforts to understand how brown or beige fat responds to cold temperature have uncovered evidence that classical brown fat relies on the sympathetic nervous system (*73-75*) and immune system (*33, 76*) to initiate and maintain the thermogenic response. While immune (*40, 60*) and nervous systems (*77*) also play a major role in beige fat development and activation, beige adipocytes have the innate ability to sense temperature and independently respond by either differentiating into UCP1+adipose and/or by inducing uncoupled respiration (*78*). Thus, classical brown, but not beige, tissue therapeutics will likely require sympathetic innervation for thermogenic function and persistence. The vascular system enables access to metabolic substrates, as well as the oxygen required for the metabolic activity of brown/beige fat (*47*). Additionally, vascular networks circulate activating or browning signals (*53, 58, 61, 79-81*). In addition to innervation and vascularization, tissue-based therapies facilitate important cell-cell and cell-extracellular matrix (ECM) interactions that provide function altering chemical and physical inputs (*82-87*).

Natural ECM is comprised of collagens, elastins, fibronectin, laminins, proteoglycans, and glycosaminoglycans (*88*). The ECM is a highly organized network of physical signals that dynamically interact with the cells it supports. The topology and composition of the ECM is heavily remodeled, especially during differentiation. Remodeling of the ECM is a balance of specific degradation by matrix metalloproteinases (MMPs), new matrix component deposition, unmasking of cryptic binding sites in response to cleavage or tension, crosslinking or bonding of ECM components, and inside-out signaling from adhesion receptors on cellular surfaces. Growth factor signaling is regulated through the ECM by controlling their capture or exclusion, rate of delivery to the cell surface receptor, and molecular presentation (*89*). The ECM establishes a biological framework that provides physical support to cells, but also regulates signaling through adhesion receptors and alters endocrine, paracrine, autocrine, and juxtacrine signals (*87*). To date, many groups have remade “synthetic” tissues by decellularizing the desired tissue, then reseeding the remaining native ECM with cell populations (*90, 91*). However, given the inaccessibility of mature BAT, this approach will be difficult to translate to artificial UCP1+ tissues.

Tissue architecture has been known to exert strong effects on cell behavior, and *in vitro* hydrogels, meant to mimic natural ECMs, appear to be a successful option to improve cell culture models (*92*). These 3-dimensional (3D) hydrogels, which are water swollen polymer networks, have been utilized to enhance hepatocyte (*93*) and pancreatic islet function (*94*). Not only does 3D-organization affect the function and viability of cells (*95*), but it mediates the differentiation of many cell types (*96*), especially adipocytes. Adipogenesis is highly dependent on cytoskeletal rearrangements where cell shape is altered to accommodate the intracellular accumulation and organization of lipids. This was discovered when preadipocytes could not differentiate when cultured on a surface of fibronectin (*97*); this phenotype was rescued by disrupting the cytoskeletal response to the supraphysiological abundance of fibronectin. Laminin

also has been found to play a role in white adipose tissue expansion (*98*). Another adipose ECM component, Collagen VI, was found to be an essential microenvironmental signal for adipocytes to regulate the amount TAG they accumulate (*99*). When Collagen VI is removed from the adipose ECM, adipocytes develop a hypertrophic state in which the adipocytes are capable of sequestering significantly more lipids than normal. Specific ECM degradation is also a critical feature of WAT development (*100*). These phenomenal findings support the notion that the adipose ECM is an integral signal for adipocyte behavior and overall condition and function of the organ. When working with *in vitro* models of white adipocytes, it is also evident that the prototypical unilocular lipid droplets observed *in vivo* are not present unless cultured in 3D-matrices (*101, 102*).

Comparatively little is known about the ECMs of WAT, BAT, and the changes in adipose-matrix during browning. As this area of research is explored further, ECM-derived signals will hopefully be identified to build our understanding of adipocyte-ECM interactions and provide applicable systems to induce the formation of UCP1+adipocytes. Biomaterials have utilized the incorporation of whole ECM components, such as laminin (*103*) or collagen (*104*), to improve their biocompatibility and effectiveness as cell scaffolds. Whether or not specific mixtures of ECM components can be combined with preadipocytes to form functional brown fat has yet to be determined, but this approach has already been applied to WAT (*91, 105, 106*). ECM molecules could theoretically be derived from the same tissues used to isolate the primary precursor cell populations for the generation of an adipose allograft (*91*) but thermogenic fat may have a distinct structural niche capable of engaging specific integrin (*107*) and syndecan (*108*) populations. Integrin expression is known to be highly dynamic during adipogenisis (*109*) and the beta-1 integrin has been extensively used to purify preadipocytes (*110*). Therefore, targeting integrin signaling appears to be a logical method to alter adipogenesis and it is likely that UCP1+ tissue function is dependent on specific 3D interactions and organization. This has now been demonstrated via integrin-ligands, in the form of matrix-derived peptide sequences and secreted molecules, on both UCP1-expression and lipid accumulation (*111, 112*).

Decellularized tissue based tissue-engineering is not the only method to produce synthetic tissues (*106, 113, 114*). Polymeric biomaterials with bioactive modifications have been employed to generate many tissue-types (*32, 86, 115, 116*). Tissue-engineering is a sophisticated endeavor that requires significant tuning, therefore modular approaches should be considered for the construction of functional synthetic tissues. Specifically, the physical properties, degradation kinetics, and biologically interactive components should be able to be altered independently. Bioengineered tissues can be generated through the selection of a core polymer, a crosslinking system, bioactive modifications, and the incorporated cell populations (figure 1). The core material of the biomaterial determines the method of deployment (injectable-vs-implantable), macrostructure, and the behavior of the cellular payload.

While many biocompatible materials have been proposed to engineer beige/brown-adipose tissue (*117*), HyA based hydrogels show particular promise for the engineering of adipose tissue for therapeutic purposes (*118, 119*) and is the only material that has been successfully used to establish brown/beige fat implants *in vivo* (*111*). HyA is a naturally occurring glycosaminoglycan, consisting of β-1,4-D-glucuronic acid – β-1,3-N-acetyl-D-glucosamine, that is highly tractable for tissue-engineering for biomedical purposes (*118, 119*). Endogenous HyA is synthesized by hyaluronic acid synthase and extruded into the extracellular microenvironment, where it functions as an essential component of the native extracellular matrix and interacts with cell surface receptors such as CD44 or RHAMM (*120*). HyA is highly variable in length, spanning lengths up to 10 μM and ranging from 100 kDa to 8 mDa. Hyaluronic acid plays a pivotal role in extracellular matrix organization through its interactions with the other major components of the ECM (*88*).

HyA scaffolds enhance survival of autologous adipose stem cell implants (*35, 36, 121, 122*) and possibly promote adipose expansion (*123*). Not only are HyA based hydrogels

naturally occurring, biocompatible, modifiable, injectable, biodegradable, non-immunogenic, and anti-thrombogenic (*118, 124*), but also HyA has already been FDA approved for a number of clinical applications such as correction of facial lipoatrophy, wrinkle and scar removal, amelioration of osteoarthritic joint pain, dietary supplementation, ulcers, and cataract surgery. HyA has also showed clinical success for the temporary aesthetic augmentation of lips, breasts, and buttocks (*125*), and achieved impressive results as a replacement of traditional dressings of epidermal burns and lesions (*126*). Importantly, utilizing HyA avoids fibrotic encapsulation of implants, a problem that has plagued the early literature of bioengineering (*127*). In general, avoiding encapsulation requires the use of non-immunogenic materials and cells, biodegradable materials, nearly anisotropic physical properties to the surrounding tissues, and possibly growth factors to induce recruitment of host-derived cells into the implant. HyA has been shown to have significant effects on tissue remodeling and cell signaling, and is naturally degraded by hyaluronidase or oxidizing agents (*128*)

Generation of bioengineered-BAT will rely on an easily accessible and ample source of progenitor cells. A key discovery in this regard came from the observation that UCP1+adipocytes can be generated by certain WAT depots (*129*). These distinct adipocytes are described as beige/brite, and they express unique surface markers (*43*). While genetic factors play a major role in the ability to generate beige-adipocytes (*130, 131*), the expansion of beige-adipose mass has been linked to improved metabolic health. Therefore, the isolation of adipose derived multipotent stem cells from undesirable WAT-depots and subsequent reintroduction as autologous-BAT shows therapeutic promise. One of the most abundant sources of pre-adipocytes is WAT, and the implantation of WAT derived stem cells is an FDA accepted procedure (*132*).

The most common source of WAT-derived stem cells is the stromal vascular fraction (SVF), which contains T cells, B cells, mast cells, adipose-tissue macrophages, and multipotent stem cells (MSC) such as preadipocytes and endothelial progenitor cells. This cellular fraction can be further purified to enrich preadipocytes by selecting for cell surface markers such as Pref-1+, Lin−,CD29+,CD34+,Sca-1+,CD24+,CD45 -,Mac1-, PDGFRα+ (*13, 15, 133*). Additionally, preadipocyte sorting can be used to enrich for populations that are known to readily transdifferentiate into beige/brite fat such as CD137, TMEM26, ASC-1, PAT2, and P2RX5 (*134*). Alternatively, as stem cell therapies become more accepted, induced pluripotent cells might be a suitable option since iPSC derived brown adipocytes have also been generated and transplants of these cells shows promising metabolic effects (*14, 135*).

While a purified population of preadipocytes or adipocytes may provide more conclusive insights for biological experiments it may not be optimal for building a functional tissue. As previously mentioned, the immune system and vascular systems are essential for supporting the function and formation of beige adipose tissue and other SVF components could contribute to these tissue types. For example, macrophages and T-cells have been shown to be an important part of beige/brown-adipose function and development (*60, 76, 136*) and interactions between the adipocytes and the vascular niche may also be important for browning (*137-140*) particularly through cell-cell interactions, cytokines, and growth factors such as Il-33 (*61*) or VEGF-A (*141*). Thus, the use of multiple purified cell population or utilization of non-purified-SVF, as recently demonstrated for the generation of bioengineered-BAT (*111*), may offer distinct advantages.

Degradation and remodeling ability of the synthetic ECM is just as important as the initial structure itself. If the synthetic tissues are not biodegradable through mechanisms that cells naturally use for movement and reorganization, integrating with the host will be jeopardized. Specifically, to facilitate effective remodeling and reorganization of the tissue by the immune and vascular systems, biodegradable and biologically interactive biomaterials should be utilized. The simplest way to imbue a biomaterial with biodegradability is to use MMP sensitive crosslinking agents. Most of the available core materials can be easily modified to

accommodate the current MMP-sensitive crosslinkers, which are short peptides containing an MMP-specific cleavage site (*28, 30, 86, 142*). Most of these core materials will be modified to facilitate efficient crosslinking by spontaneous aqueous phase reactions, such as the Michael addition where a thiol and acrylate form a thio-ether bond (*31, 32*). These types of biodegradable crosslinkers have been shown to be essential for the recruitment of host cells for the successful *in vivo* integration of biomaterial implants (*28, 143*).

Additionally, the elastic modulus of biomaterials has been shown to be highly instructive for the differentiation of MSCs into adipocytes (*24, 144, 145*). This mechanotransductive control of differentiation can be accomplished without applying direct physical forces to cells. By presenting a cell with an adhesion-promoting environment, matrix-associated adhesions form and produce an intrinsic mechanotransductive signal for the cell, as well as adjacent cells in the microenvironment. Therefore, a soft biomaterial optimized with specific adhesion-promoting-ligands may be capable of inducing the same mechanotransductive signals as a much stiffer material. Numerous biological processes are affected by mechanical signals; notably, nuclear envelope plasticity and permeability (*146, 147*), splicing (*148*), and signal transduction (*149*). The prominent browning factor, BMP7, is known to alter cytoskeletal dynamics in adipocytes and other cell types, which supports the notion that physical cues may be important for bioengineered-BAT (*59, 150-152*). Interestingly, our group found that the storage modulus of WAT seems to differ from that of BAT (WAT ~ 3 kPa, BAT ~ 4 kPa). How important this difference in modulus is for brown fat development and function remains to be explored more systematically.

Bioactive modifications, such as integrin-binding domains conjugated to hydrogels, have become commonplace to enhance the bioactivity of biomaterials (*86, 115, 116*) and HyA-hydrogels augment integrin signaling (*153*). These materials provide some degree of ECM-mimicry without replicating the entire complexity of the native-ECM. For example, alginate conjugated with RGD-containing ligands is supportive to cardiomyocytes and also promotes adipogenisis (*154, 155*). However, alginate's effects on adipogenisis may be due to the rounded morphology, shown to be strongly instructive to adipogenesis (*97*), cells undergo when encapsulated in alginate-based materials (*156*). Other peptide-modified hydrogels promote the formation of bone via collagen mimetic peptides (*157*). ADMSC-spheroids entrapped in Poly(ethylene glycol)-hydrogels have been proposed to form beige-adipocytes *in vitro* (*158*) and have been modified to drive MSCs toward adipogenic or osteogenic fates (*159*) . Interestingly, Vaicik et al. find UCP1-expression highest when the storage modulus of the hydrogel is BAT-equivalent.

Results

To define the mechanism by which peptide surfaces tested in chapter I affected MSC differentiation, we chose to examine the actin cytoskeleton. The morphological differences of preadipocytes cultured on surface coatings that contained AG73 were grossly obvious with f-actin staining (Figure 2). Since AG73 promoted the remodeling of the actin cytoskeleton and facilitated the induction of UCP1 in adipocytes we opted to perturb the actin cytoskeleton during differentiation of a clonal brown adipose cell line (*160*). Strikingly, any disruption of actomyosin dynamics during the differentiation of brown adipocytes downregulated UCP1 expression, and generally promoted FABP4 expression (Figure 3) [Blebbistatin inhibits type-II myosin, Y27632 inhibits ROCK, Latrunculin B promotes actin depolymerization, cytochalasin D promotes actin depolymerization, CK-666 inhibits the ARP2/3 complex, and ML-141 inhibits CDC42].

Since the effects of actomyosin inhibition were so robust during differentiation of brown adipocytes, we applied said inhibitors to fully differentiated brown adipocytes (figure 4) [along with ML7, an MYLK inhibitor, and Swinholide A, another actin depolymerization agent]. We identified that unlike the during differentiation treatments, Y27632, cytochalasin D and

latrunculin B induced UCP1 expression in fully differentiated brown adipocytes but Swinholide A treatment did not. At this time, a number of publications implicated Myocardin Related Transcription Factor-A (MRTFA) as a critical regulator of adipogenic fate and UCP1 expression (*59, 161*). Interestingly, the breakdown of actin filaments (f-actin) into monomeric actin (g-actin) promoted by Y27632, latrunculin B, and cytochalasin D will directly alter MRTFA mediated transcriptional responses. Swinholide A, is an actin depolymerization agent that yields actin dimers, rather than monomers. Actin dimers have not been found capable to interact with MRTFA, thereby breaking down actin filaments without altering MRTFA-mediated transcriptional responses.

To verify that latruculin B affected UCP1 expression levels via MRTFA-actin interactions that reduce the amount of nuclear MRTFA present, we utilized an inhibitor of nuclear export in conjunction with latrunculin B treatment. Application of Leptomycin B in conjunction with latrunculin B dramatically reduced UCP1 expression while also increasing the expression of MRTFA target gene, CTGF, in fully differentiated brown adipocytes. In effect, this demonstrates that MRTFA nuclear exclusion in mature adipocytes does promote UCP1 expression. However, the fact that during the differentiation process latrunculin B treatment yields a loss of UCP1 expression we hypothesized that the structural role of actin may be critical to UCP1 expression in an unknown fashion.

Discussion

Adipocyte differentiation encompasses significant changes in cell morphology and anchorage to the surrounding ECM. Traction forces generated within cells have been identified to affect cell fate decisions of mesenchymal stem cells which are generally generated by the actomyosin network. Alterations of the actin cytoskeleton branched network during differentiation with ARP2/3 inhibition during differentiation and inhibition of force generation type-II myosin both perturb the ability of cells to generate intrinsic physical forces. Since type-II myosin inhibition during differentiation and in fully differentiated adipocytes reduced UCP1 expression, and myosin based tension requires actin networks to scaffold their functions, we opted to further explore the mechanisms by which actomyosin-based tension affects thermogenic adipose development and function (see chapter III).

Figures

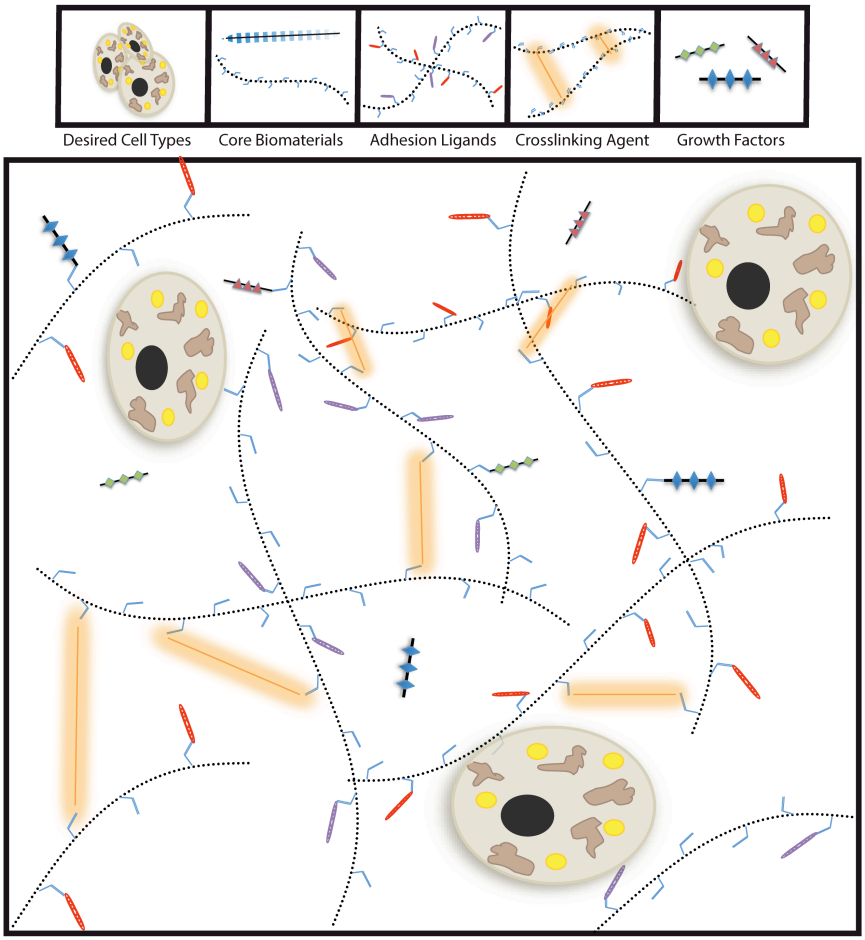


Figure 1: Modular tissue-engineering
Here we visually depict the five bioengineering variables discussed throughout this review. By tailoring the properties biochemical and physical properties of the biomaterial, synthetic tissues for therapeutic purposes can be successfully generated.

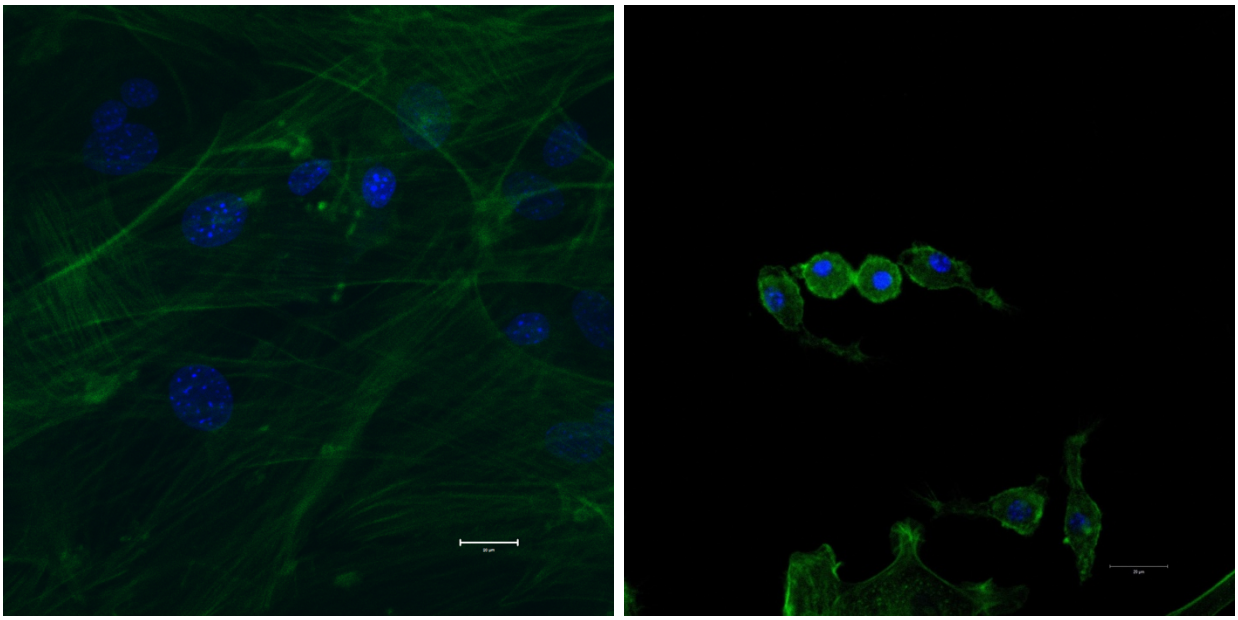


Figure 1: Representitive immunofluorescece of primary SVF on TCPS surface (left) or 200 μM AG73 (Right) 48h after seeding. (scale bar = 20 μm)

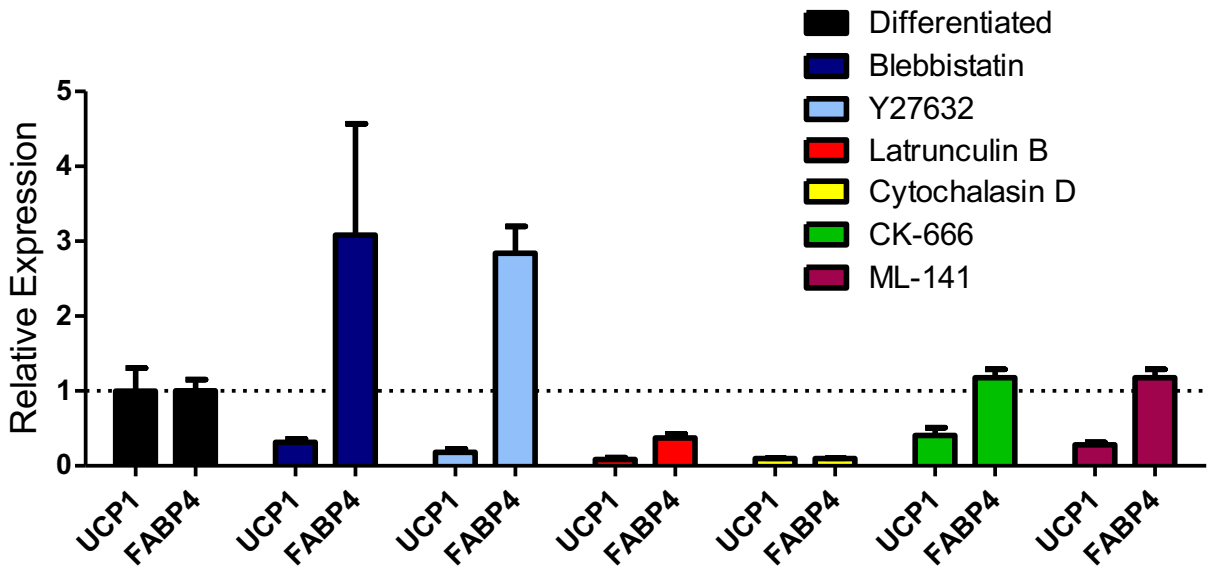


Figure 2: Relative gene expression of clonal brown adipose cell line treated with vehicle, 100 μM bebbistain, 20 μM Y27632, 20 μM latrunculin, 2 μM cytochalasin D, 8 μM CK-666, or 4 μM ML-141 durring the course of 8 days of differentiation.

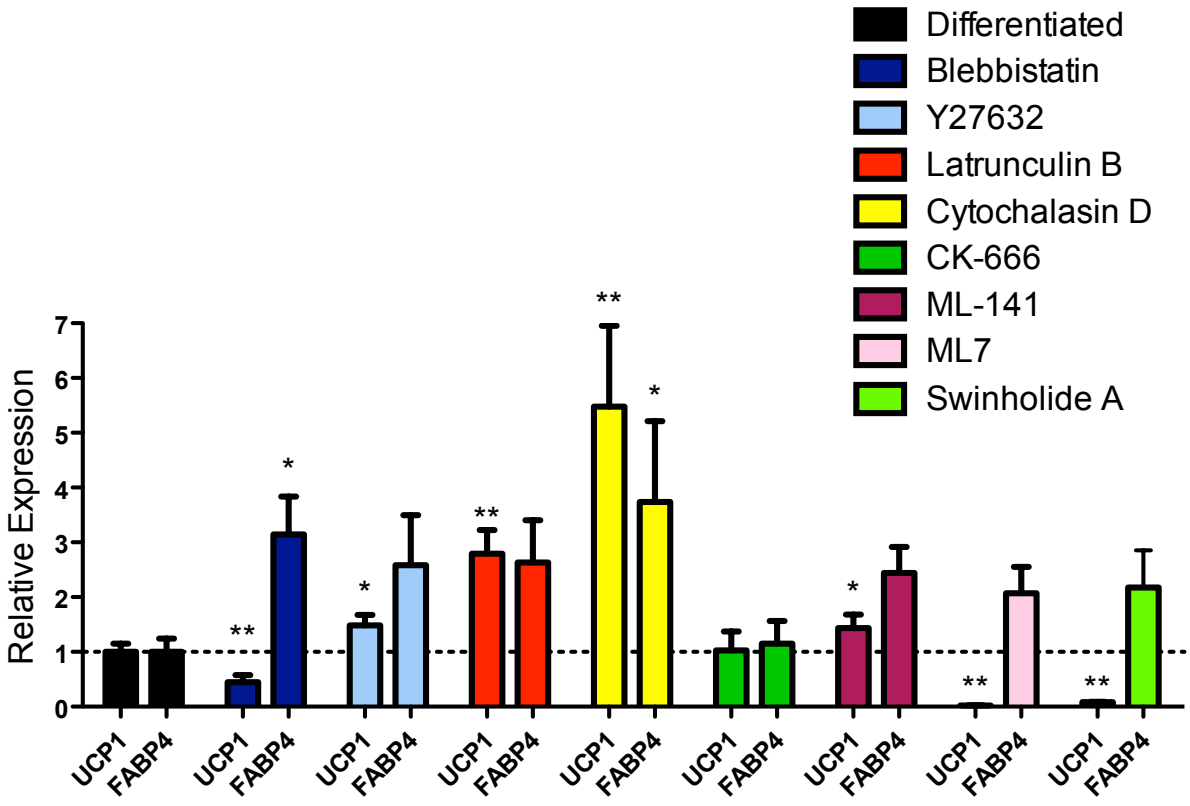


Figure 3: Relative gene expression of clonal brown adipose cell line treated with vehicle, 100 μM bebbistain, 20 μM Y27632, 20 μM latrunculin, 2 μM cytochalasin D, 8 μM CK-666, 4 μM ML-141, 20 μM ML7, or 0.2 nM Swinholide A for 24 h on day 7 of differentiation

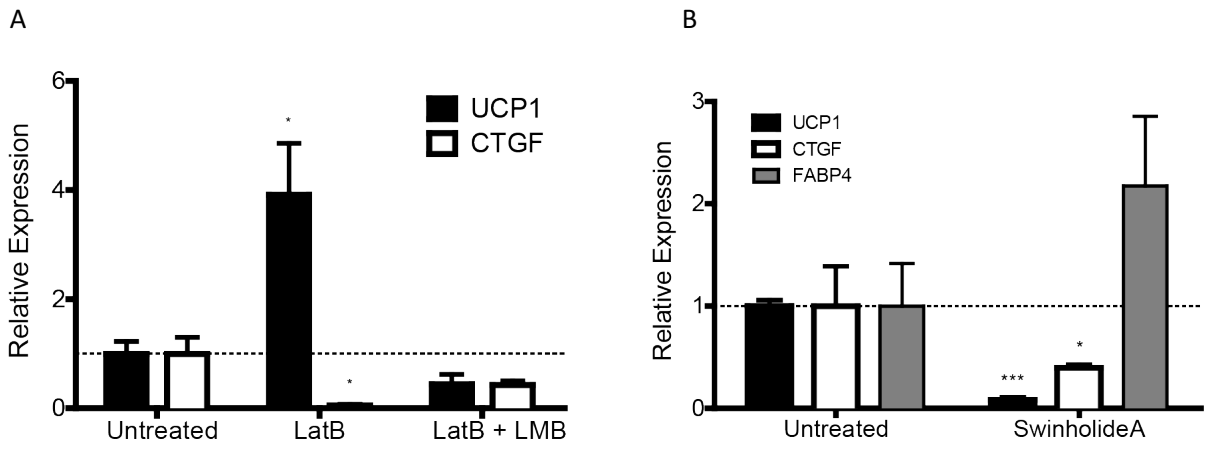


Figure 4: A. Relative gene expression of clonal brown adipose cell line treated with vehicle and 20 μM latrunculin with or without 20 μg/mL Leptomycin B for 24 h on day 7 of differentiation. B. Relative gene expression of clonal brown adipose cell line treated with vehicle or 2 nM Swinholide A for 24 h on day 7 of differentiation.

Methods

ADMSC Isolation
Fat depots from L2G85 (FVB/NJ) or C57BL6/J mice, perigonadal (visceral) or inguinal (subcutaneous) respectively, were isolated from 3 month old mice as previously described (*20*).

Brown adipocyte and beige adipocyte cell lines
Cells were maintained in DMEM with 10% serum and 1% penicillin/streptomycin (p/s) (Gibco), and induced to differentiate with the maintenance media fortified with 5 µg/ml Insulin, 1 nM T3, 2 µg/ml Dexamethasone, and 500 µM IBMX (Sigma), and 100nM rosiglitazone (beige cells). After 3 days of differentiation media cells were maintained in DMEM with 10% serum, 1% p/s. Cells were considered fully differentiated on day 6 of differentiation as they stably expressed BAT comparable levels of UCP1, (UCP1-GAPDH with a ΔCT of ~2-3).

rtPCR
mRNA was isolated from tissues or in vitro cultures with TRIzol reagent (Ambion). Tissue samples were homogenized with a Polytron PT 2100. Assays were carried out on an ABI 7500 RT-PCR system with TaqMan Universal Master Mix II and validated PrimeTime primer probe sets that detect all splice variants (Integrated DNA Technologies). A first-strand cDNA synthesis kit (Fisher) was used to transcribe 5 µg RNA/20 µL. cDNA (100 ng) was used per RT-PCR reaction in triplicates. The ΔΔCT method was used to comparatively assess mRNA quantity.

Immunofluorescence Microscopy
Cells or tissues were fixed in 4% paraformaldehyde for 30 min at room temperature, washed and blocked with a blocking buffer (HBSS fortified with: 10% FBS, 0.1% BSA, 0.05% saponin, and 0.1% Tween20) and ThermoFisher Phalloidin A12379. Samples were imaged with a Zeiss 710 confocal microscope and Zeiss Zen software.

Chapter III: Actomyosin-mediated tension orchestrates uncoupled respiration in adipose tissues

Summary

The activation of brown/beige adipose tissue (BAT) metabolism and the induction of uncoupling protein-1 (UCP1) expression are essential for BAT-based strategies to improve metabolic homeostasis. Adrenergic signaling is viewed as a key regulator of thermogenesis and UCP1-expression in BAT, while also operating as a potent contractile stimulator in muscle. The muscle-like gene expression patterns of UCP1+ adipocytes have previously been utilized as tissue specific markers, but have not been attributed with any functional role. Here, we demonstrate that BAT utilizes key components of muscular contractile machinery to generate tensional responses following adrenergic stimulation. We show that activation of muscle-like actomyosin mechanics are critical for the acute induction of oxidative metabolism and uncoupled respiration in UCP1+ adipocytes. Additionally, actomyosin-mediated tension regulates mechanosensitive transcriptional co-activators, YAP/TAZ, that regulate the thermogenic capacity of adipose. These unappreciated signaling and mechanical mechanisms may inform future strategies to promote the expansion and activation of brown/beige adipocytes.

Introduction

Brown and beige adipose tissues (BAT) are critical for thermoregulation by uncoupling oxidative phosphorylation through the action of uncoupling protein 1 (UCP1). Brown adipose is innate, whereas beige adipose is adaptive and arises from the trans-differentiation of white adipocytes or de novo from mesenchymal stem cells (MSCs) residing in white adipose tissues (WAT) (*162-164*). The process of adipogenesis encompasses transformative cytoskeletal rearrangements thought to facilitate intracellular accumulation of lipids (*165*). However, these cytoskeletal rearrangements are now recognized as critical components of the adipogenic program that facilitate Myocardin Related Transcription Factor-A (MRTFA) nuclear exclusion (*59, 161*). MRTFA binds G-actin during cytoskeletal remodeling thereby preventing its function as a Serum Response Factor (SRF) co-factor (*166-168*) thereby promoting adipogenic gene expression necessary for differentiation of preadipocytes into adipocytes. Interestingly, tension of the actin cytoskeleton also plays a major role in the development and function of mesenchymal-origin tissues (*24, 169, 170*). Transcriptional co-activators, Yes Associated Protein-1/WW domain-containing transcription regulator protein 1 (YAP/TAZ), regulate growth and differentiation based on sensing the cytoskeletal tensional homeostasis (*171-175*).
The cytoskeletal dissimilarity between WAT and BAT are implied by their morphological differences with white adipocytes consisting of a unilocular lipid droplet with a predominantly cortical cytoskeleton whereas brown/beige adipocytes maintain an extensive cytoskeletal network that supports and organizes multilocular lipid droplets and numerous mitochondria. However, the functional differences of these BAT vs WAT cytoskeletal structures and organizations have yet to be characterized. Previous tissue engineering efforts by us, led us to measure the mechanical properties of adipose depots where we noticed that brown adipose possesses muscle-like stiffness (*176*). Brown/beige adipose are known to display noticeably muscle-like gene expression patterns and due to the observations that physical mechanics regulates MSC fate determinations, we hypothesized that the muscle-like actomyosin structures enable brown/beige adipose to generate intracellular tension necessary to promote or maintain its function and differentiation status. Muscular actomyosin tension is dynamically regulated by adrenergic signaling (*177*), but serves as the key cold-inducible signaling pathway in BAT leading to UCP1 expression (*163, 178*). Signaling by β-adrenergic receptors (β-AR) has been

intensively studied in adipose tissues (*4*), and the associated induction of UCP1-expression has been thought to lie downstream of the canonical cAMP/PKA/p38MAPK axis (*179, 180*). However, here we show that stiffening of brown adipocytes following β-AR activation is a required component of metabolic activation and uncoupled respiration that additionally mediates the induction of UCP1 expression through tension sensing mechanisms that promote YAP/TAZ transcriptional activity.

Results

Adrenergic stimulation promotes actomyosin-mediated tension via muscle-like signaling in BAT
To characterize tissue-scale physical differences between BAT and WAT, we performed parallel plate rheometery on intact/live tissues and decellularized tissues. Intact WAT has a storage modulus of ~3 kPa, whereas BAT is ~4.5 kPa (Figure 1A). When the tissues are decellularized (Young et al., 2011), the remaining cell-free tissue has a significantly reduced storage modulus. We then estimated the cellular contribution to modulus by subtracting the decellularized tissue modulus from the intact tissue modulus (Figure 1B). Based on this (intact - decelluarlized) assessment, brown adipocytes collectively generate and/or experience significantly more tension than their white adipose counterparts. Strikingly, a 24 h cold exposure (4°C) induces elevated stiffness in BAT when compared to BAT from mice exclusively housed at room temperature (23°C) (Figure 1C).

An interesting, but largely ignored, aspect of the muscle-like characteristics of BAT is the expression of muscle-specific type II myosin heavy chains (MyH) which are known to facilitate intrinsic physical forces in cells. In adipose tissues, MyH expression is distinct between the subcutaneous depots (Figure S1A and S1B) with the “cardiac-specific” type-II myosin heavy chain 7 (MyH7) enriched in BAT. Importantly, cardiac muscle contraction and muscle system process genes are not lost when mice are fed a prolonged high fat diet (*181*), a human lifestyle factor thought to impair BAT function and induce WAT-like expression patterns (Figure 1D). To investigate whether these myosin species are a product of the differentiation program in UCP1+ adipocytes and not a product of contaminating stromal vascular fraction (SVF), we examined their expression in a clonal brown adipose cell line (brown adipocytes) that the Kajimura lab developed previously (*160*). In these clonal brown adipocytes, we found that MyH7 expression is induced during differentiation while expression of other MyH species such as MyH9 (NMIIa) and MyH10 (NMIIb) remained constant (Figure 1E).

Due to the fact that adrenergic stimulation in MyH7+ cells has been found to induce increased beat rate and contractile velocity (*177*), both of which require cytoskeletal stiffening, we utilized atomic force microscopy (AFM) to directly measure if differentiated brown adipocytes analogously stiffen when challenged with isoproterenol. Surprisingly, isoproterenol administration induces a contractile-like response that initially stiffens the cell cortex followed by transduction of tension to the interior of the cell depicted in AFM force maps of single cells (Figure 1F and E). In these conditions, this does not appear to mimic an authentic muscle-like contraction as the cell borders do not migrate. On a tissue level, BAT explants also respond acutely to isoproterenol with elevated cellular tension reaching its peak thirty minutes after stimulation (Figure 1H). Immunofluorescence microscopy of MyH7 in endogenous BAT demonstrates localization to the most F-actin dense regions of the cell cortex (Figure 1I) and western blots confirm MyH7 protein expression in BAT (Figure S1B).

Actomyosin-mediated tension is critical for thermogenic capacity of adipocytes
Due to the fact that adrenergic stimulation promotes actomyosin-mediated tension (Figure 1) and thermogenic responses in BAT, we decided to test if cytoskeletal tension affects the thermogenic capacity of BAT. We tested two different type-II myosin-ATPase inhibitors, blebbistatin and 2,3-butanedione monoxime (2,3-BDM) (*182-188*) and found that they both significantly reduced the expression of UCP1 in BAT explants (Figure 2A). We then applied

these inhibitors to fully differentiated brown adipocytes already expressing levels of UCP1 comparable to BAT, and found that myosin ATPase inhibition reduced UCP1-expression within 24 h of treatment (Figure S2A). To determine if tension is a critical regulator of UCP1 in beige adipose we used a white adipose derived cell line (beige adipocytes) analogous to the brown adipocyte cell line, that express high levels of UCP1 upon treatment with rosiglitazone. When UCP1+ beige adipocytes are subjected to 24 h of actomyosin inhibition, we found a nearly ~70% reduction of UCP1 mRNA expression (Figure S2B). AFM revealed that tension in the cytoplasmic regions of brown adipocytes is significantly reduced by blebbistatin, and increased by 24 h of isoproterenol treatment (Figure S2C) whereas 2,3-BDM only affected tension in the stiffest regions of brown adipocytes (Figure S2D). This regional specificity may be due to the fact that 2,3-BDM has been proposed to preferentially inhibit muscle-specific type-II myosin, such as MyH7, that we find to localize only to the most F-actin dense cortical regions (Figure 1I).

To determine the upstream regulators of actomyosin-mediated tension in adipose, we examined the expression levels of myosin light chain kinases (MYLKs), serene/threonine kinases which promote type-II myosin-mediated contractions (*189*), and found the predominant MYLK expressed in brown adipocytes was the calcium-sensitive smooth muscle isoform (Figure S2E). Interestingly, Ca2+ release from the ER and extracellular medium are known responses to adrenergic stimulation in brown adipocytes which could promote MYLK activity (*190, 191*). To determine the if MYLK activity plays a role in actomyosin-based tensional regulation of UCP1, we applied treatments of ML7 (MYLK inhibitor) and blebbistatin (type-II myosin inhibitor) to brown adipocytes with/without isoproterenol for 24 h and found that while UCP1 is still induced by isoproterenol, UCP1 expression is dramatically reduced relative to vehicle controls (Figure 2B). To verify the role of MYLK, we utilized genetic manipulations MYLK expression during differentiation of brown adipocytes that resulted in the loss of UCP1-expression while PRDM16, PPARG, and FABP4 were all significantly upregulated (Figure 2C). While ML7 or blebbistatin treatments did result in the loss of the majority of UCP1 expressed in brown adipocytes, isoproterenol induction of UCP1 expression did occur (Figure 2B). It is well established that cAMP Response Element Binding protein (CREB) is phosphorylated by PKA in response to adrenergic stimulation, and phosphorylated-CREB (pCREB) activates UCP1 expression (*192*). We therefore examined whether blebbistatin interferes with CREB:pCREB in response to isoproterenol and found that blebbistatin had no effect on pCREB levels in response to adrenergic stimulation (Figure 2E). Which suggests that actomoyosin-mediated regulation of UCP1 expression is orthogonal to the known mechanisms of UCP1 regulation and explains why isoproterenol induction of UCP1 expression remains intact during treatments of ML7 or blebbistatin.

To verify that the loss of UCP1-expression in response to actomyosin inhibition had functional ramifications, we examined cellular respiration rates of brown adipocytes treated for 24 h with blebbistatin with/or isoproterenol prior to respirometery (Figure 2E). Isoproterenol-induced basal and uncoupled respiration was significantly impaired by 24 h actomyosin inhibition in brown adipocytes due to the loss of UCP1-expression (Figure 2B). However, we noticed that UCP1-independent maximal uncoupling (FCCP) was also reduced by blebbistatin treatment. Previous reports have specifically identified blebbistatin as not perturbing mitochondrial respiration in cardiomyocytes in vitro (*188*) leading us to postulate that brown adipocytes utilize actomyosin dynamics to support mitochondrial number/mass or mitochondrial structure/function.

In cardiomyocytes, one of the mechanisms by which type-II myosin mediated contractile responses are generated in response to adrenergic stimulation is through PKA mediated activation of L-type Ca2+ channels (CACNA1a-CACNA2d4) (Bers, 2002; Kamp and Hell, 2000), which we found be expressed in BAT from tissue/clonal cell line level RNAseq (Figure 1D and Figure 5A). The L-type Ca2+ channel-mediated influx of calcium stimulates MYLKs which

phosphorylate type-II myosin hexamers, promoting their assembly into think filaments, myosin association with actin, and ATPase activity which enhances actomyosin-based tension. Impressively, expression of a constitutively active form of MYLK during differentiation elevates UCP1 expression (Figure 3A) in brown adipocytes. Since MyH7 appears to be uniquely expressed in brown rather than white or beige adipocytes, we knocked down expression of MyH7 during differentiation of brown adipocytes and found significant reduction of UCP1 expression (Figure 3B). This observation, coupled with the expression profile of a muscle-like contractile program led us test if altering component abundance/activity of this signaling pathway altered the metabolic capacity of brown adipocytes (schematic of pathway (Figure 3C) and associated metabolic responses (figure 3D-G)).

To examine the dynamic role of type-II myosin mechanics and the upstream signaling during β-AR induced activation of brown adipose metabolism, we treated differentiated brown adipocytes with: blebbistatin (type-II myosin inhibitor) and MyH7 RNAi (2 days prior to respirometry); MYLK RNAi (2 days prior to respirometry), ML7 (MYLK inhibitor), and verapamil (L-type Ca2+ channel inhibitor); Omecamtiv mecarbil (OM) (MyH7 activator), EMD57003 (MyH7 Activator), and lentiviral mediated expression of constitutively active (CA-) MYLK (2 days prior to respirometry); latrunculin B (actin depolymerization) and jasplakinolide (actin polymerization) concomitant with/without isoproterenol for 45 min prior to respirometery (Figure 3D-G). It should be noted that the pharmacological treatments applied in figure 3, had no effect on UCP1 mRNA expression levels with this length of treatment (Figure 5C, and data not shown). Strikingly, inhibition/knockdown of type-II myosins, myosin light chain kinase, or PKA-activated L-type Ca2+ channels dramatically reduced the metabolic rates of brown adipocytes, especially their uncoupled respiratory capacity (Figure 3D and E). The effect of blebbistatin relative to MYH7 knockdown is highly suggestive that other type-II myosin species may play a role in metabolic flux, notably MyH9 which has recently been described as critical for lipid droplet dissociation (*193*), which would explain the acute reduction in maximal respiration observed with blebbistatin treatment but not MyH7 knockdown. It should be noted that unlike 45 min of blebbistatin treatment, MyH7 knockdown (48 h post treatment with RNAi) reduced UCP1 expression at the time of respirometry (Figure 3B), so it is not surprising that there are significant differences in uncoupled respiration between MyH7 RNAI and blebbistastin treatment. Importantly, verapamil had no effect on the metabolic rates of white adipocytes, as they do not express functional levels of “cardiac-specific” L-type Ca2+ channels (Figure S3A). OM and EMD57003 (*194*), MyH7 potentiators, enhanced the isoproterenol-induced uncoupled and maximal respiratory capacity of brown adipocytes as did the expression of a CA-MYLK (*195*), which also induced UCP1 expression Figure 3A). Interestingly, perturbations to actin polymerization with latrunculin B or jasplakinolide had limited effects (Figure 3F), suggesting that cellular tension is a critical component of brown adipocyte’s metabolic response to adrenergic stimulation.

To test if the pharmacological enhancement of MyH7 function had effects on BAT activity in vivo, mice were treated with a subcutaneous injection of OM directly into the interscapular BAT, which markedly enhanced oxygen consumption 48 h post treatment both at room temperature (23°C) as well as in the cold (4°C) (Figure 4A). This enhanced respiratory rate is a striking phenotype since OM and other myosin activators (EMD 57003) that bind to this region of MyH7 have been found to not significantly alter oxygen consumption of cardiomyocytes while increasing actomyosin based tension (*196-199*), suggesting that the metabolic enhancement observed in (Figure 4A) is largely due to the brown adipocyte mediated uncoupled respiration (Figure 3E) . Interestingly, treatment with OM alone for 24 h did not induce UCP1-expression in brown adipocytes, but pharmacologically relevant concentrations of OM co-treatment with isoproterenol did significantly enhance UCP1-expression relative to isoproterenol treatment alone (Figure S4). Conversely, acute treatment with clinically relevant concentrations of verapamil, the L-type Ca2+ Channel inhibitor widely used treatment for hypertension, significantly impaired oxygen consumption (Figure 4B) and also decreased core

body temperature (Figure 4C), similar to the effects observed when brown adipocytes were treated in vitro (Figure 3E).

To verify that the downregulation of UCP1-expression in response to actomyosin-inhibition was not due to de-differentiation and loss of the adipocyte phenotype, we profiled the expression of FABP4, ZFP423, CIDEA, PRDM16, PPARA, PPARG, PGC1a, and TFAM during 24 h treatments (Figure S5A). We found that these adipogenic mediators were largely induced by blebbistatin, which is surprising due to the fact that ectopic expression of PRDM16 or PGC1a are sufficient to enhance UCP1-expression. To determine in an unbiased fashion what mediated the loss of UCP1-expression, we utilized RNAseq to evaluate transcriptomic changes following actomyosin inhibition. KEGG patway analysis identified the hippo signaling pathway (Figure 5A). Specifically, motif analysis revealed robust reductions of genes with promoters under the control of TEAD1, TEAD2, and TEAD4 (Figure 4B). YAP/TAZ are co-factors that associate with varied TEADs to function as the canonical effectors of the hippo signaling network and mechanosensing pathways to affect cell fate decisions and organ development (*171, 172*). Since genes regulated by the hippo signaling pathway were strongly suppressed by actomyosin inhibition in brown adipocytes, we examined whether or not the canonical YAP/TAZ target gene, CTGF, was also regulated by blebbistatin or 2,3-BDM (Figure 5C and D). Over the course of 24 h of treatment, CTGF levels trend with UCP1-expression for both blebbistatin and 2,3-BDM. Additionally, during the course of brown adipocyte differentiation, CTGF expression increases along with UCP1 (Figure S5B). Being that CTGF expression is a product of YAP/TAZ-associated transcriptional regulation, we used immunofluorescence to determine whether these actomyosin dysregulating treatments affected YAP nuclear localization in brown adipocytes. Analysis of nuclear YAP localization in regions twenty times larger than what is pictured in (Figure 4E) for brown adipocytes treated with 2,3-BDM or blebbistatin demonstrated impaired nuclear localization while isoproterenol treatment enhanced nuclear traffic (Figure S5C). Surprisingly, blebbistatin did not significantly alter MRTFA localization (Figure S5D) which validates the minimal SRF-MRTFA associated transcriptional changes we observed (Figure 5B).

To verify that endogenous YAP/TAZ transcriptional activity was associated with UCP1-expression in vivo following a 24 h 4°C cold challenge, we analyzed BAT, inguinal WAT, and perigonadal WAT and found CTGF and UCP1 significantly upregulated in all of these adipose tissues (figure S6A) as well as brown adipocytes in vitro treated with isoproterenol (Figure S6B).). Impressively, overexpression of YAP in mature beige adipocytes enhanced UCP1 and CTGF expression with no significant changes to adipogenic gene expression (Figure 6A) with transfection efficiency around ~15%. Overexpression of YAP in mature brown adipocytes, with ~15% transfection efficiency, results in significant induction of UCP1 and CTGF mRNA expression 24 h after transfection (Figure 6C). Overexpression of YAP did not result in any alteration of the expression of ZFP423, FABP4, PRDM16, PGC-1a, PPARA, or PPARG. To further test if YAP/TAZ is required for UCP1-expression in differentiated brown adipocytes, we knocked down expression of YAP with siRNA which resulted in a ~60% reduction of UCP1-expression while important adipogenic genes were unaffected (Figure 6A), analogous to what was observed with YAP overexpression. Which likely reflects the critical function of the three YAP/TAZ-TEAD binding motifs approximately 1.1kb, 1.05kb and 0.4kb upstream of the TSS for UCP1. To determine if the YAP paralog, TAZ, functions equivalently and if a specific TEAD is associated with this program, we used siRNA to knockdown expression of TAZ and TEAD1-4. We found that TAZ knockdown also resulted in decreased UCP1-expression, and that YAP/TAZ likely coordinates with TEAD1 to mediate effects on UCP1-expression in brown adipocytes (Figure S6C).

To characterize the role of YAP/TAZ in BAT function in vivo, we generated heterozygous YAPfl/+Tazfl/+UCP1-Cre mice (YTU). The reduction in YAP/TAZ expression significantly impairs BAT depot size and visibly whitened the BAT depot in heterozygous YTU mice (Figure 7A). Whitening of the BAT depots was also apparent on the gene expression level with leptin

expression comparable to white adipose tissues along with reduced UCP1 expression (Figure 7B). The reduced size and UCP1 expression of the BAT from heterozygous YTU mice resulted in impaired metabolic activity of these male and female mice at 4 weeks of age (Figure 7C and S7). At 20 weeks of age YTU mice have significantly lower core body temperatures (Figure 7D) and weigh significantly more than control animals on normal chow (Figure 7E). This difference in weight is exclusively due to increased fat mass, making these mice ~28% fat compared to the ~11% fat mass of control animals.

Discussion

Here, we have identified that β-adrenergic stimulation of BAT induces cellular tension that facilitates uncoupled respiration and concomitantly promotes thermogenic gene expression. Our findings suggest that the muscle-like expression patterns observed in brown/beige adipose tissues enables internally generated mechanical stimuli that activates YAP/TAZ to promote thermogenic gene expression. We propose that YAP/TAZ-mediated regulation of UCP1-expression uncovered here is basally required but operates in concert with the previously described regulators of UCP1-expression in adipose tissues such as CREB, PRDM16, PGC1a, and PPARg (*178*). Moreover, we have uncovered a novel arm of the well-studied β-adrenergic activation of brown adipocytes based on previously unknown mechanical program critical for metabolic flux and uncoupled respiration. Overall, our data suggests that thermogenic adipocytes utilize actomyosin mechanics to provide acute activation of metabolic activity and the coordinated maintenance of their differentiation status.

Actomyosin-mediated mechanotransduction is well known to regulate the differentiation of MSCs through numerous mechanisms (*24, 169, 170, 200, 201*). Previous studies of YAP/TAZ and MSC differentiation have led to the description of YAP/TAZ as anti-adipogenic (Dupont et al.; Hong et al.). However, this conclusion may be convoluted by the culture of MSCs on supraphysiologically stiff (~3 GPa) tissue culture polystyrene (TCPS) surfaces. Adipose tissue depots possess a storage modulus roughly three orders of magnitude softer than that of TCPS, which suggests that the in vitro findings may be due hyperactivation of YAP/TAZ of the stiff TCPS surfaces. Mechnoregulation of MSC differentiation can be controlled by externally-applied or internally-generated physical stresses (*202-205*), making it challenging to decouple extrinsic and intrinsic responses to mechanical stimuli. To date, our study is the first to examine the role of YAP/TAZ in adipose tissue development and function in animal models. Our identification of YAP/TAZ as critical for BAT development certainly prompts further study of YAP/TAZ in WAT development, hypertrophy, and hyperplasia.

Chronic YAP/TAZ activity has been suggested to mediate inflammation of fibrotic adipose tissues due to the altered physical properties ECM, further demonstrating that hyper-activation of this pathway can have undesirable consequences (*206*). In fibrotic white adipose tissues, chronic mechnosensing of the aberrantly composed and crosslinked ECM enhances inflammatory cytokine profiles (*207, 208*), many of the same inflammatory cytokines thought to support the metabolic benefits of thermogenic adipose expansion (*10*). Prevention of chronic activation of YAP/TAZ transcriptional programs is regulated by numerous negative feedback mechanisms YAP/TAZ itself promotes (*209, 210*). YAP/TAZ mediated feedback promotes the expression of proteins and enzymes that regulate specific cofactor associations and YAP/TAZ nuclear exclusion, making it challenging to define the role of YAP/TAZ in long term disease promoting states such as obesity which affects both preadipocyte and mature adipocyte biology.

The cellular mechanobiology of BAT appears to strongly mimic the mechanics found in cardiomyocytes. Specifically, adrenergic simulation increases cAMP levels that activate PKA to activate L-type Ca2+ channels to promote an influx of calcium. The influx of calcium activates MYLKs to phosphorylate myosin hexamers, promoting their association with actin and ATPase activity, in turn generating tension on the actin cytoskeleton. It is surprising that these tensional

responses have such dramatic effects on oxidative phosphorylation and uncoupled respiration. Actin dynamics have only recently been identified to modulate mitochondrial function (*211*) and ER-associated mitochondrial divisions appear to require force generated by the actin cytoskeleton (*212, 213*), which could explain why maximal uncoupling was attenuated by actomyosin inhibition. However, the significance and magnitude of mechanoregulation of mitochondrial function in thermoregulation is clear and requires further study to determine exactly how uncoupled respiration is regulated my myosin-based mechanics.

While our data demonstrates a dynamic and essential role of actomyosin mechanics in thermogenic adipocytes, it remains to be clarified what developmental signals stimulate muscle-like gene expression in preadipocytes. It appears that early in adipogenesis, MSCs destined to express functional levels of UCP1, express muscle-like actomyosin machinery (*214-216*) that are induced by cold exposure (*217*) and IL-33 (*218*). Expression of muscle-like actomyosin and upstream regulators engenders UCP1+ adipocytes with requisite mechanical stimulation to regulate UCP1-expression and generate mechanical tension critical for efficient oxidative metabolism and uncoupled respiration. Pharmacological inhibition of BAT mechanobiology, as with verapamil, may underlie previously unclear clinical side effects such as rapid weight gain and pharmacological activation of actomyosin mechanics in BAT may engender new approaches to address metabolic disease. In summary, actomyosin mechanics provides an essential metabolic function by developing and facilitating the thermogenic activity of adipose.

Figures

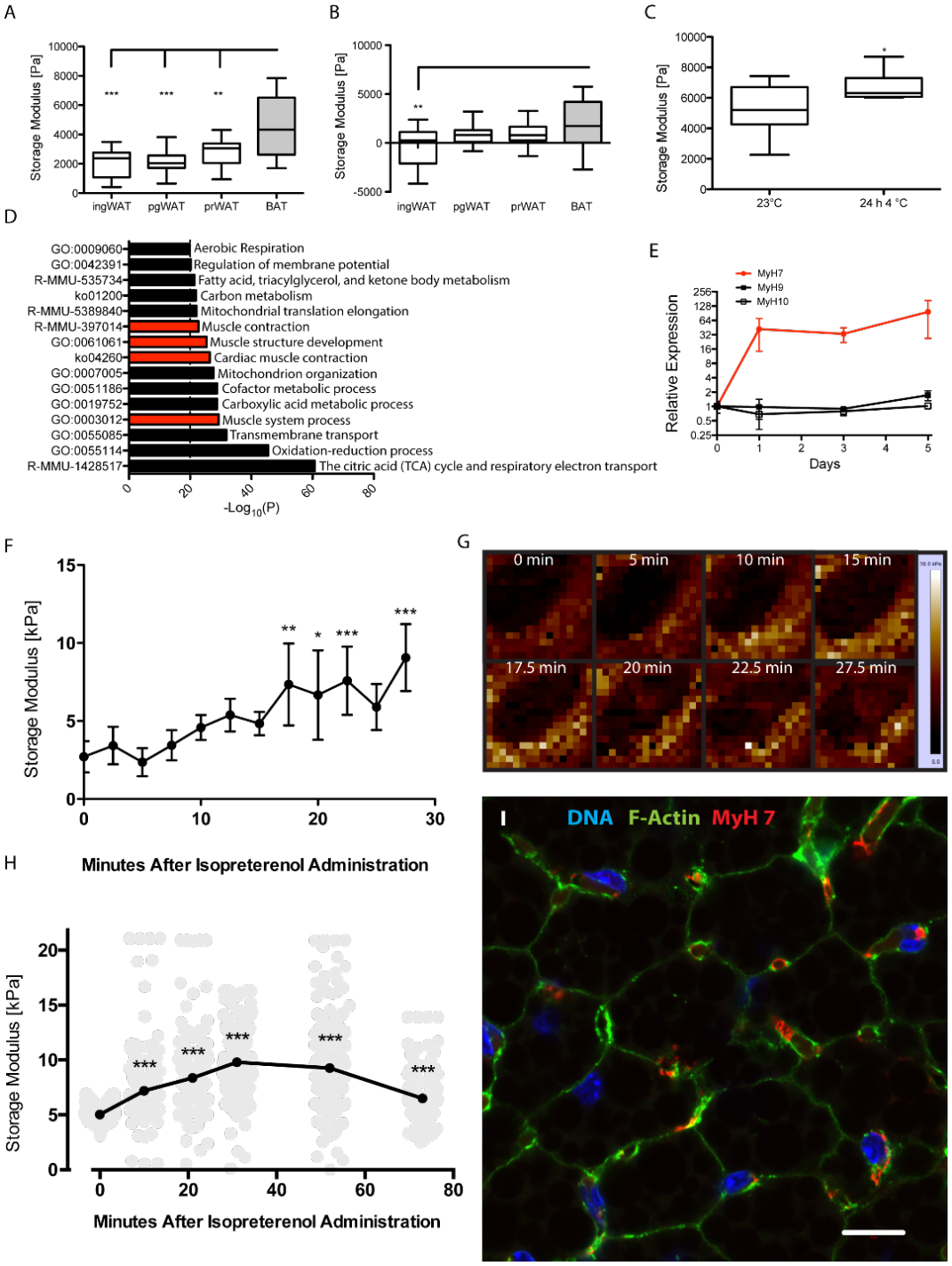


Figure 1: A. Storage modulus of intact adipose tissues from 16 week old FVB/NJ mice, measured with parallel plate rheometry (n=16) [8 males & 8 females]. B. Subtraction of (intact tissue – decellularized tissue), measured with parallel plate rheometry (n=16) [8 males & 8 females]. C. Storage modulus of intact BAT from 16 week old male FVB/NJ mice housed at 23°C or exposed to 24 h of 4°C before measurement, measured with parallel plate rheometry (n=8). D. Metascape gene ontology analysis of BAT and WAT from 22 wk old C57Bl6/J mice fed a high fat diet for 14 weeks (n=4). E. MyH mRNA expression of clonal brown adipocytes during the course of differentiation, normalized to day 0 of differentiation, rtPCR (ΔΔCT, normalized to GAPDH) (n=3). F and G. Isoproterenol induced tension in cultured brown adipocytes, corresponding force map (G) depicting the location of tensional changes in a cell, measured with AFM (n= 6). H. BAT explant response to isoproterenol treatment (100 μM^2, 256 points measured across the tissue explant per timepoint). I. Immunofluorescence of MyH7 in endogenous BAT, MyH7 (red), f-actin (green), DAPI (blue), scale bar 20 μm.

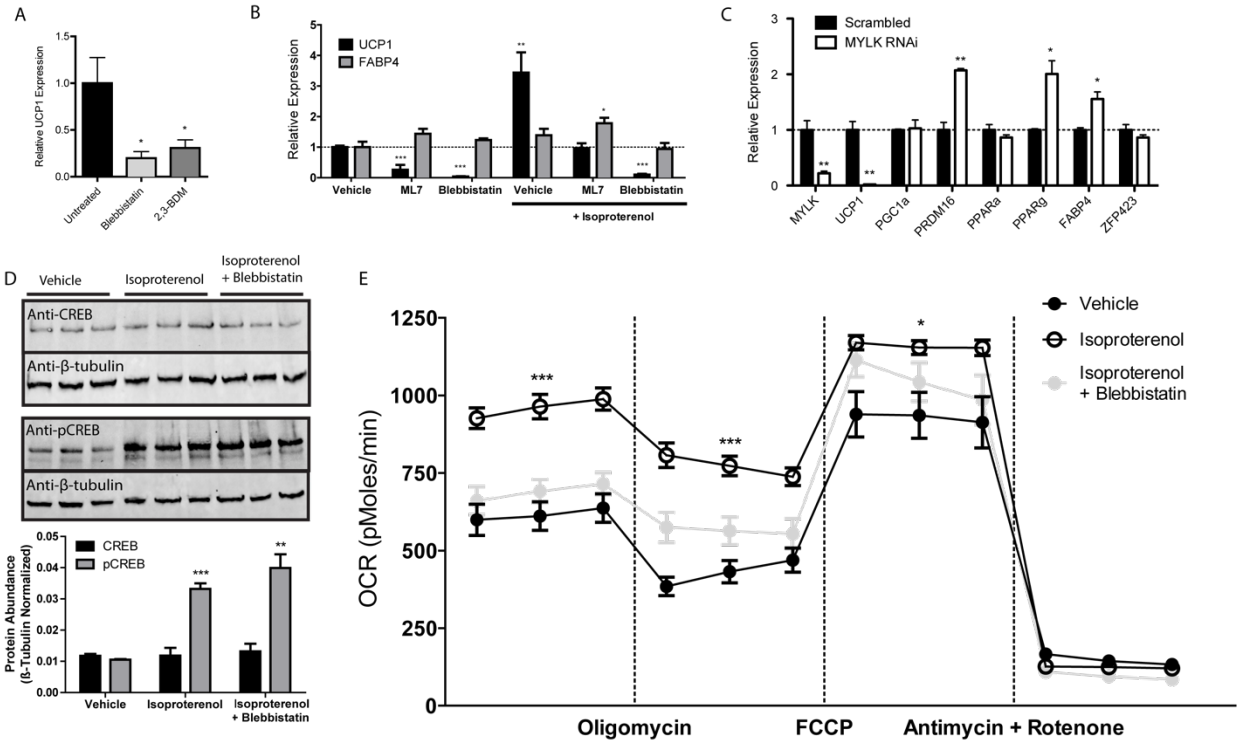


Figure 2: A. UCP1 mRNA expression in BAT explants treated with 100 μM blebbistatin or 1 mM 2,3-BDM for 24 h, rtPCR (ΔΔCT, normalized to GAPDH) (n=10). B. UCP1 and FABP4 mRNA expression in differentiated brown adipocytes treated with +/- 1 μM isoproterenol and/or 10 μM ML-7 or 100 μM blebbistatin, 24 h treatment, rtPCR (ΔΔCT, normalized to PPIA) (n=3). C. Gene expression changes observed in brown adipocytes treated with siRNA during differentiation (day 4 of 8), rtPCR (ΔΔCT, normalized to GAPDH) (n=3). D. Western blot analysis of CREB and pCREB in brown adipocytes treated with +/- 2 h 1 μM isoproterenol with/without prior 22 h of 100 μM blebbistatin treatment, normalized to β-tubulin, LiCor Odyssey (n=3). E. Cellular respirometry brown adipocytes demonstrates that pre-treatment with 100 μM blebbistatin 24 h impairs 1 μM isoproterenol induced metabolic activation, oxygen consumption rate (OCR) measured with Seahorse XF24 (n=5) [statistics reflect Blebbistatin vs Blebbistatin + Isoproternol].

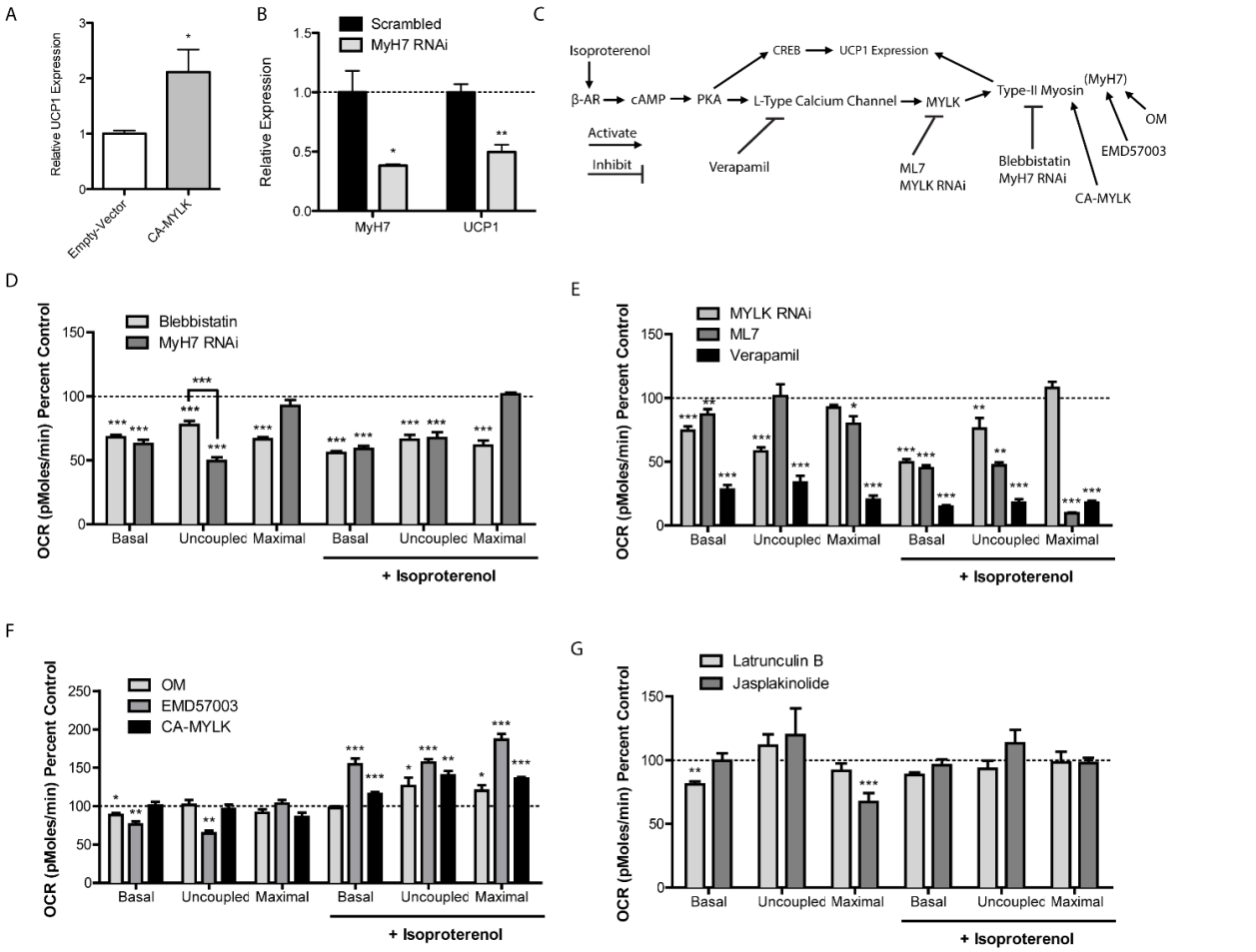


Figure 3: A. UCP1 gene expression of brown adipocytes transfected with lenti-CA-MYLK construct 48 h post transfection compared to empty vector control (n=4). B. Gene expression changes in brown adipocytes treated with MyH7 RNAi or Scrambled RNAi, 48 h post transfection, rtPCR (ΔΔCT, normalized to GAPDH) (n=3). C. Schematic depicting adrenergic activation with the subsequent treatment regime targets identified. D. Cellular respirometry of brown adipocytes treated +/- 1 μM isoproterenol (45 min prior to measurement) +/- 100 μM blebbistatin (45 min prior to measurement) or MyH7 knockdown* (48 h prior to measurement), oxygen consumption rate (OCR) measured with Seahorse XF24 (n=5). E. Cellular respirometry of brown adipocytes treated +/- 1 μM isoproterenol (45 min prior to measurement) +/- 10 μM ML7 (45 min prior to measurement), or 10 μM verapamil (45 min prior to measurement), or MYLK knockdown* (48 h prior to measurement), oxygen consumption rate (OCR) measured with Seahorse XF24 (n=5). F. Cellular respirometry of brown adipocytes treated +/- 1 μM isoproterenol (45 min prior to measurement) +/- 10 μM OM (45 min prior to measurement), or 10 μM EMD57003 (45 min prior to measurement), or CA-MYLK* (48 h prior to measurement), oxygen consumption rate (OCR) measured with Seahorse XF24 (n=5). G. Cellular respirometry of brown adipocytes treated +/- 1 μM isoproterenol (45 min prior to measurement) +/- 20 μM Latrunculin B (45 min prior to measurement) or 1 μM Jasplakinolide (45 min prior to measurement), oxygen consumption rate (OCR) measured with Seahorse XF24 (n=5).
*Indicates reduced UCP1 expression by treatment

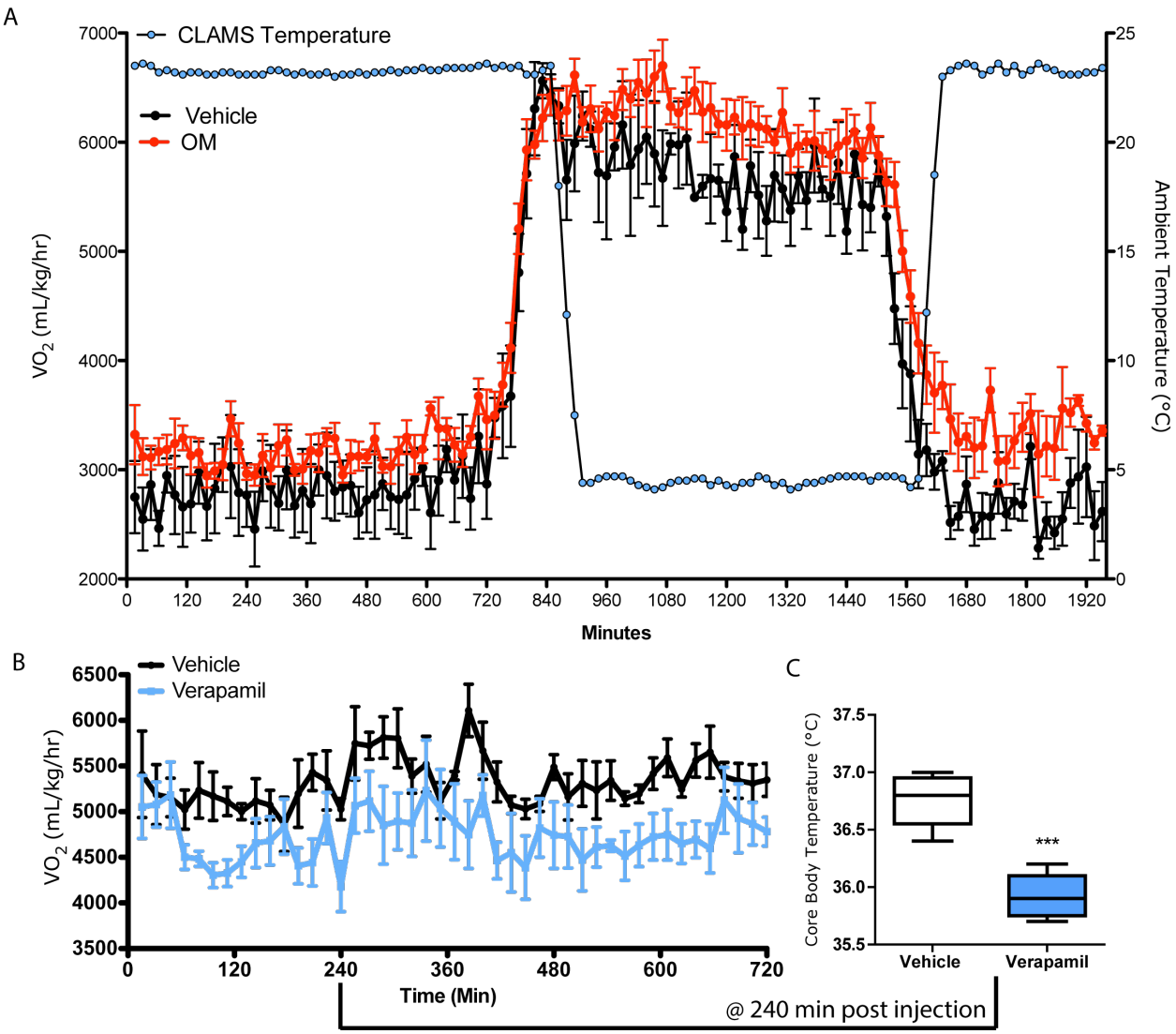


Figure 4: Respiratory rate of 16 wk old FVB/NJ injected directly into the subcutaneous interscapular BAT depot with 100 µL of 1 mM OM or vehicle exposed to ambient temperatures of 4°C and 23°C for 12 h (n=5). VO2 during 12 h interval with no variation in ambulatory parameters observed, measured with temperature controlled Oxymax-CLAMS (Columbus Instruments). Average VO_2 P value = 0.0429* for 1000-1320 min and P value = 0.0233* for 1680-1920 min B. Respiratory rate of 4 wk old male C57bl6/J mice injected directly into the subcutaneous interscapular BAT depot with 5 mg/Kg verapamil (~30 µL) at 23°C for 12 h post injection, Average VO_2 P value = 0.0381* for the 12 h period shown (n=5). C. Core body temperature of 4 wk old male C57bl6/J mice injected directly into the subcutaneous interscapular BAT depot with 5 mg/Kg verapamil (~30 µL) 4 h post injection (n=5).

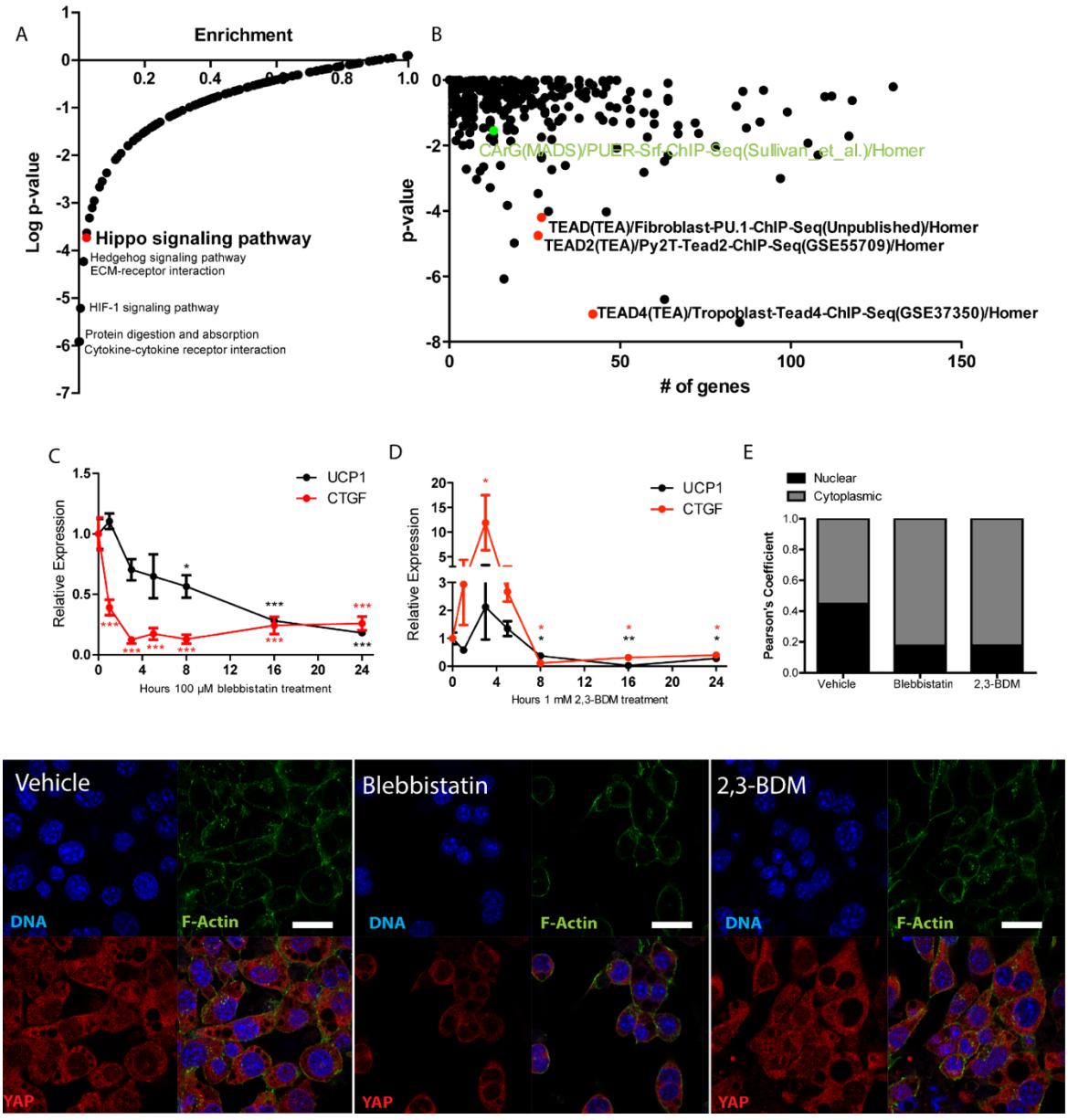


Figure 5 A. KEGG pathway analysis of genes found by RNAseq to be significantly downregulated (log2 <1.5-factor) following treatment of differentiated brown adipocytes with 100 μM blebbistatin for 24 h. B. HOMER de novo motif analysis showing transcription factor binding sites enriched in promoters of genes significantly downregulated by blebbistatin. C. UCP1 and YAP target gene, CTGF, mRNA expression in brown adipocytes treated with 100 μM blebbistatin for 24 h rtPCR (ΔΔCT, normalized to GAPDH) (n=3). D. UCP1 and YAP target gene, CTGF, mRNA expression in brown adipocytes treated with 1 mM 2,3-BDM for 24 h rtPCR (ΔΔCT, normalized to GAPDH) (n=3). E. Pearson's correlation coefficient of DAPI and YAP analyzed with BitPlane Imaris™ software from lower magnification images of the displayed Immunofluorescence depicting YAP localization in of brown adipocytes treated with 100 μM blebbistatin or 1 mM 2,3-BDM for 24 h, YAP (red), f-actin (green), DAPI (blue), scale bar 20 μm.

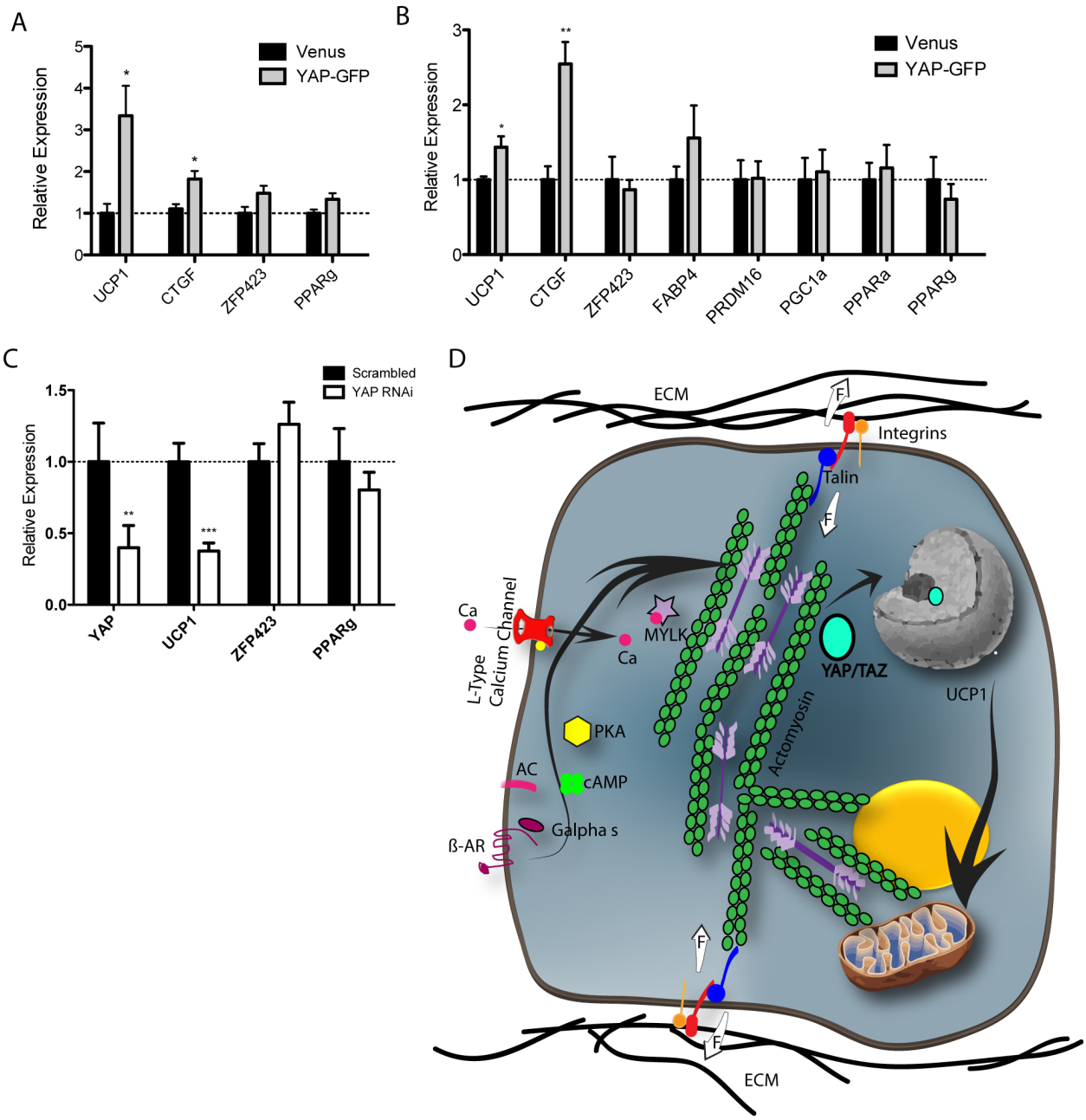


Figure 6: A. Gene expression changes observed in differentiated beige adipocytes 24 h post transfection with YAP-GFP overexpression construct, rtPCR (ΔΔCT, normalized to GAPDH) (n=10). B. Gene expression changes observed in differentiated brown adipocytes 24 h post transfection with YAP-GFP overexpression construct, rtPCR (ΔΔCT, normalized to GAPDH) (n=4). C. Gene expression changes observed in differentiated brown adipocytes 24 h post transfection with YAP RNAi, rtPCR (ΔΔCT, normalized to GAPDH) (n=4). D. Schematic of contractile signaling and YAP/TAZ regulation of UCP1 expression in brown adipocytes.

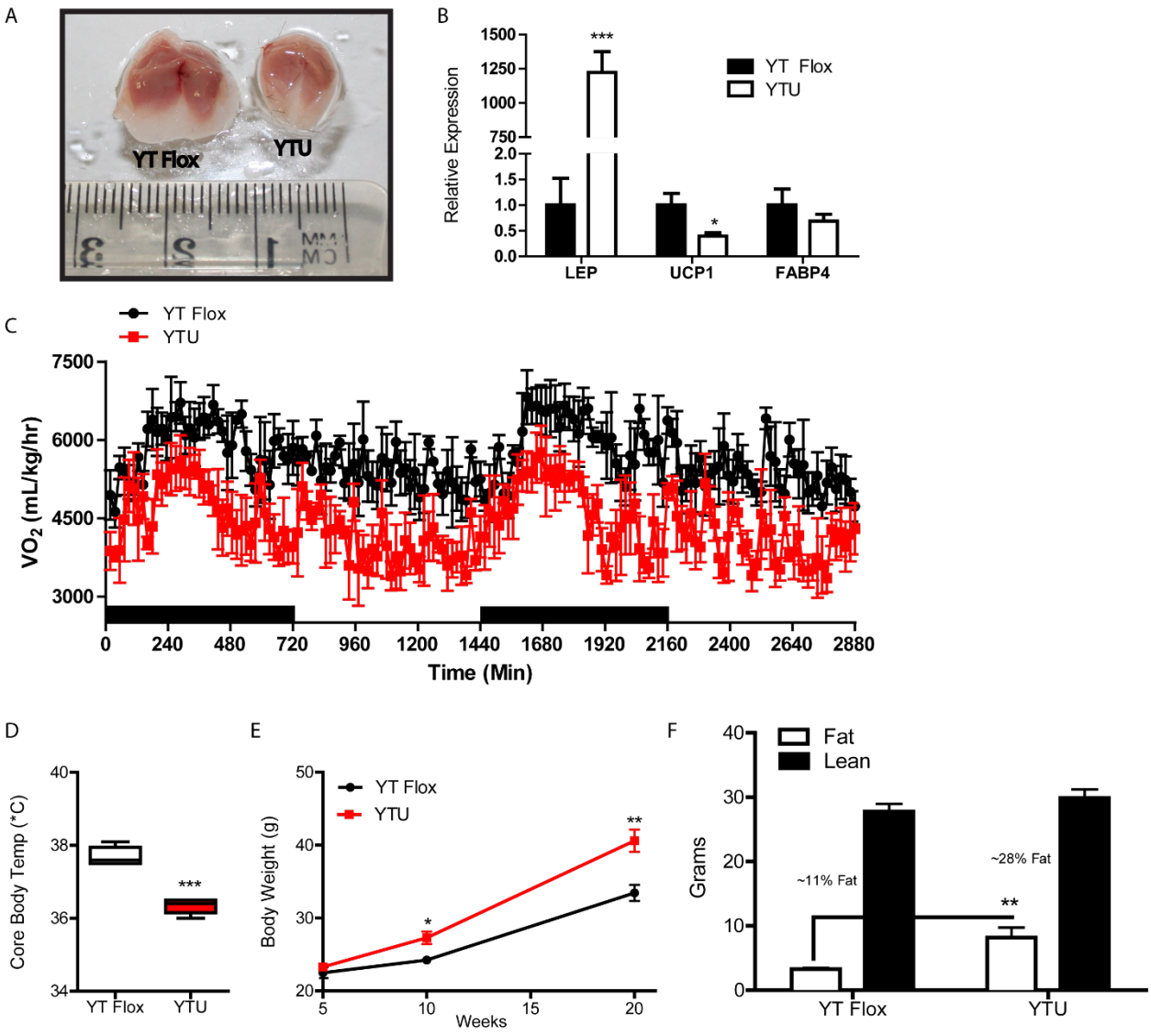


Figure 7: A. Representative photograph of BAT of 4 week old male YTU and YAP/TAZ flox (YT flox) control mice. B. Gene expression observed in 4 week old male YTU mice, rtPCR (ΔΔCT, normalized to GAPDH) (n=4). C. VO_2 of 4 week old female mice at 23°C during 48 h interval with no variation in ambulatory parameters observed, Average VO_2 P value = 0.0444* for 240-720 min (dark) and P value = 0.0294* for 720-1440 min (light), measured with temperature controlled Oxymax-CLAMS (Columbus Instruments) (n=3). D. Core Body temperature of 20 wk old male YTU mice (n=5). E. Body weight of male YTU mice mice fed a normal chow diet (n=5). F. Body mass composition of 20 wk old male YTU mice, assessed with EchoMRI (n=5).

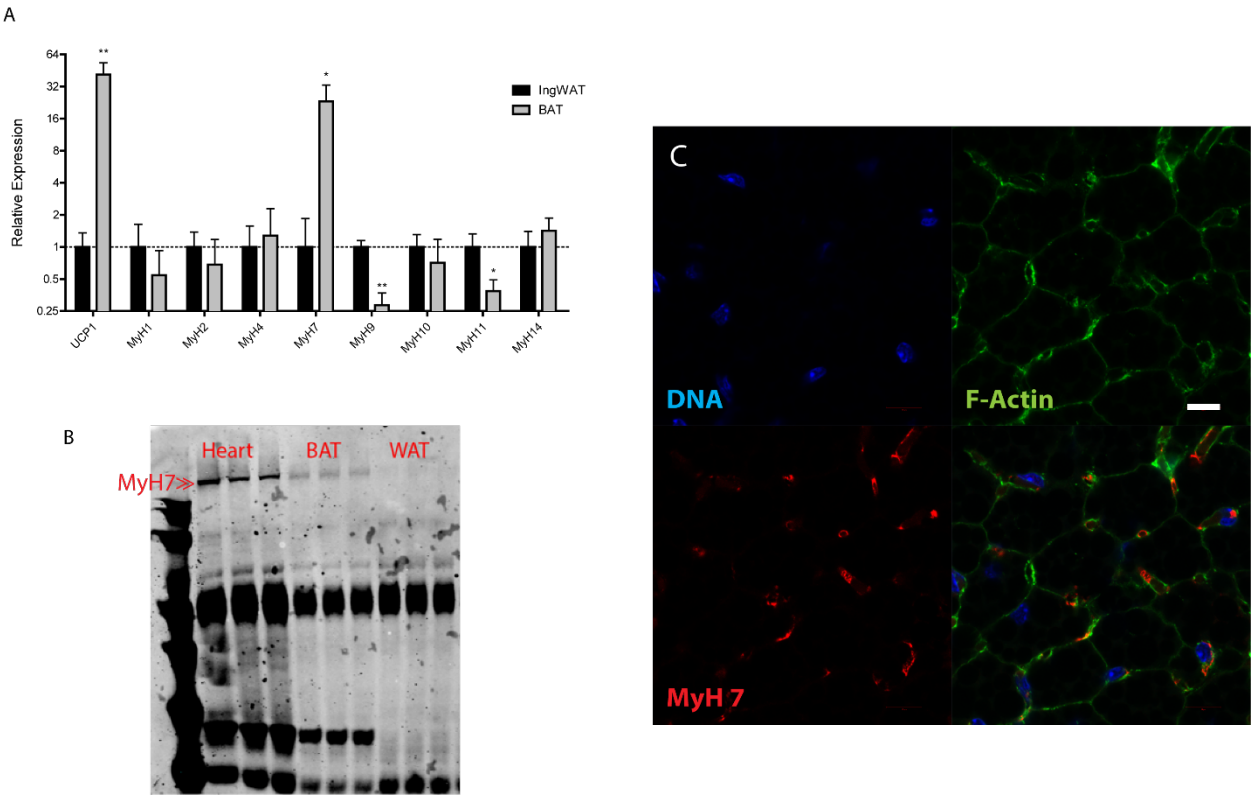


Figure S1. A. Relevant MyH and UCP1 mRNA expression in BAT and inguinal WAT of 8 week old male FVB/NJ mice. B. Western blot of MyH7 expression in heart, BAT, and inguinal WAT of 8 week old male FVB/NJ mice. C. Channel separated immunofluorescence image presented in Figure 1I.

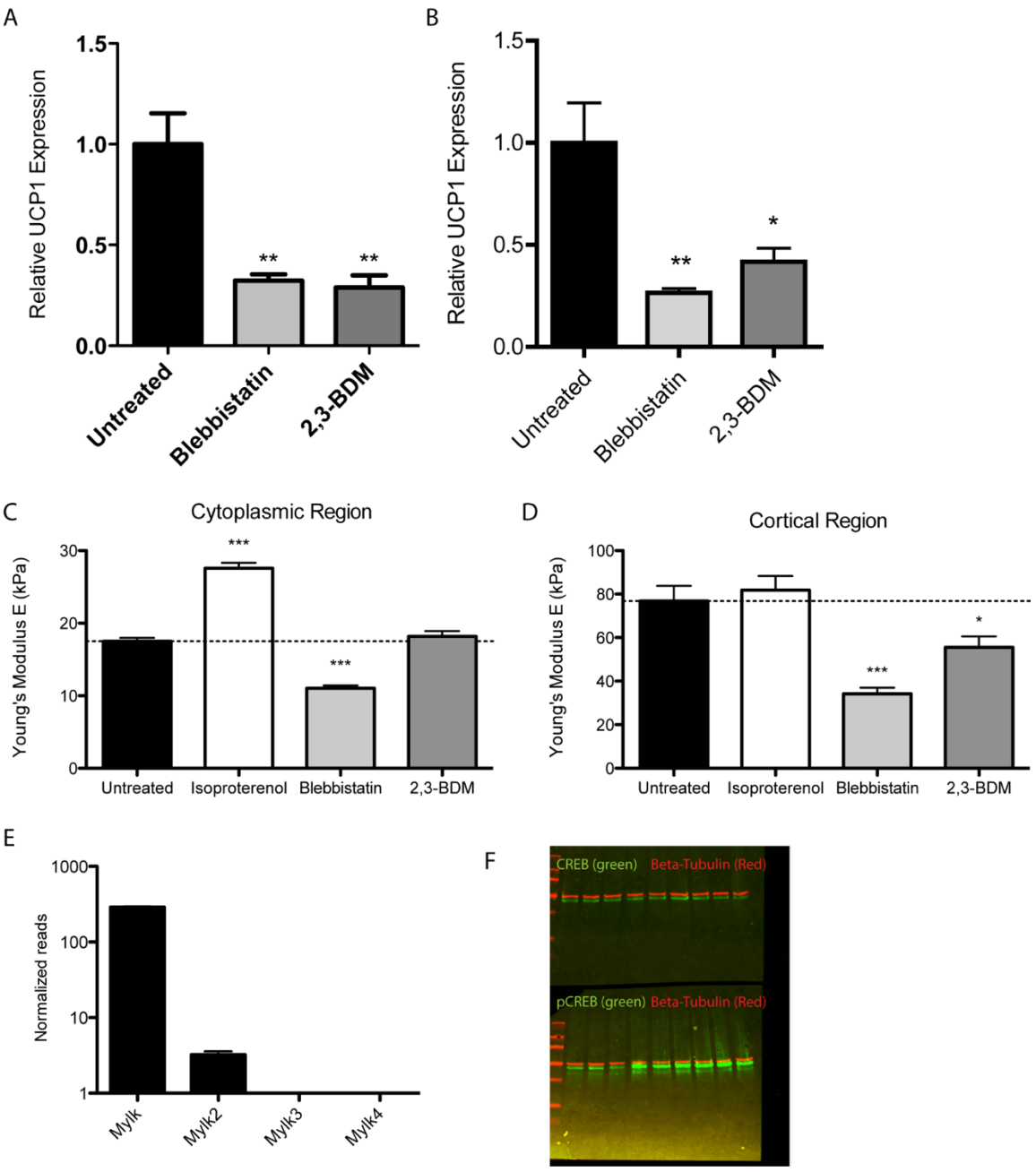


Figure S2: A. UCP1 and FABP4 mRNA expression in differentiated brown adipocytes treated with 100 μM blebbistatin or 1 mM 2,3-BDM for 24 h, rtPCR (ΔΔCT, normalized to GAPDH) (n=6). B. UCP1 mRNA expression in differentiated beige adipocytes treated with 100 μM blebbistatin or 1 mM 2,3-BDM for 24 h, rtPCR (ΔΔCT, normalized to GAPDH) (n=4). C. Elastic modulus of brown adipocytes treated with 1 μM isoproterenol, 100 μM blebbistatin, or 1 mM 2,3-BDM for 24 h, defined as the softest region of the cell, measured with AFM (n=38). D. Elastic modulus in brown adipocytes treated with 1 μM isoproterenol, 100 μM blebbistatin, or 1 mM 2,3-BDM for 24 h, defined as the stiffest region of the cell, measured with AFM (n=38). E. MYLK expression profile of differentiated brown adipocytes, measured by RNAseq RPKM per 10e7 (n=3). F. Multichannel display of full western blots presented in Figure 2D.

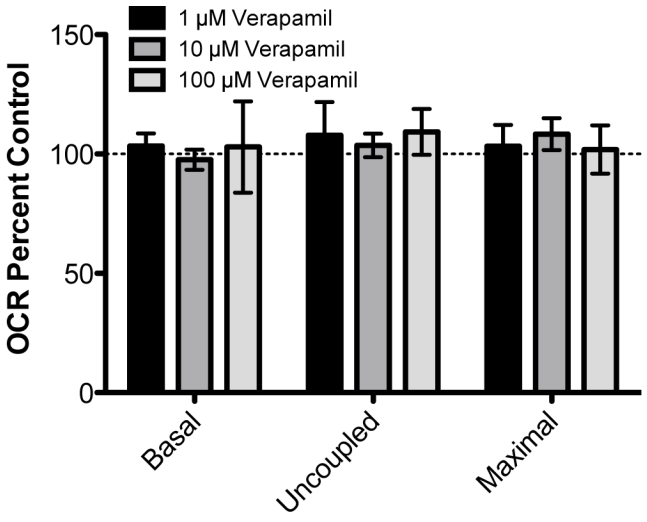


Figure S3 Cellular respirometry of white adipocytes treated with 1, 10, or 100 μM verapamil, oxygen consumption rate (OCR) measured with Seahorse XF24 (n=5).

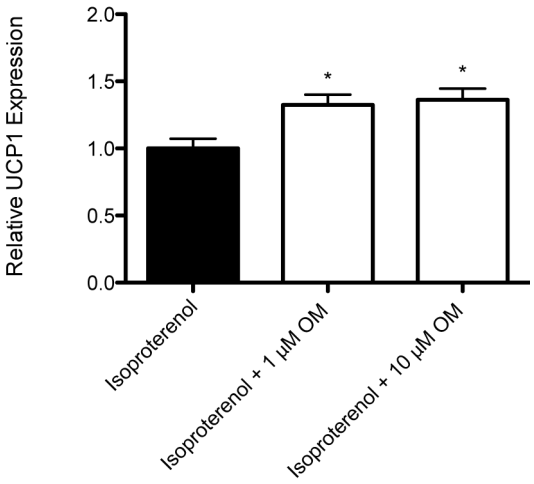


Figure S4: UCP1 mRNA expression in brown adipocytes treated for 24 h of 1 μM isoproterenol along with either 1 or 10 μM OM treatment rtPCR (ΔΔCT, normalized to GAPDH) (n=3).

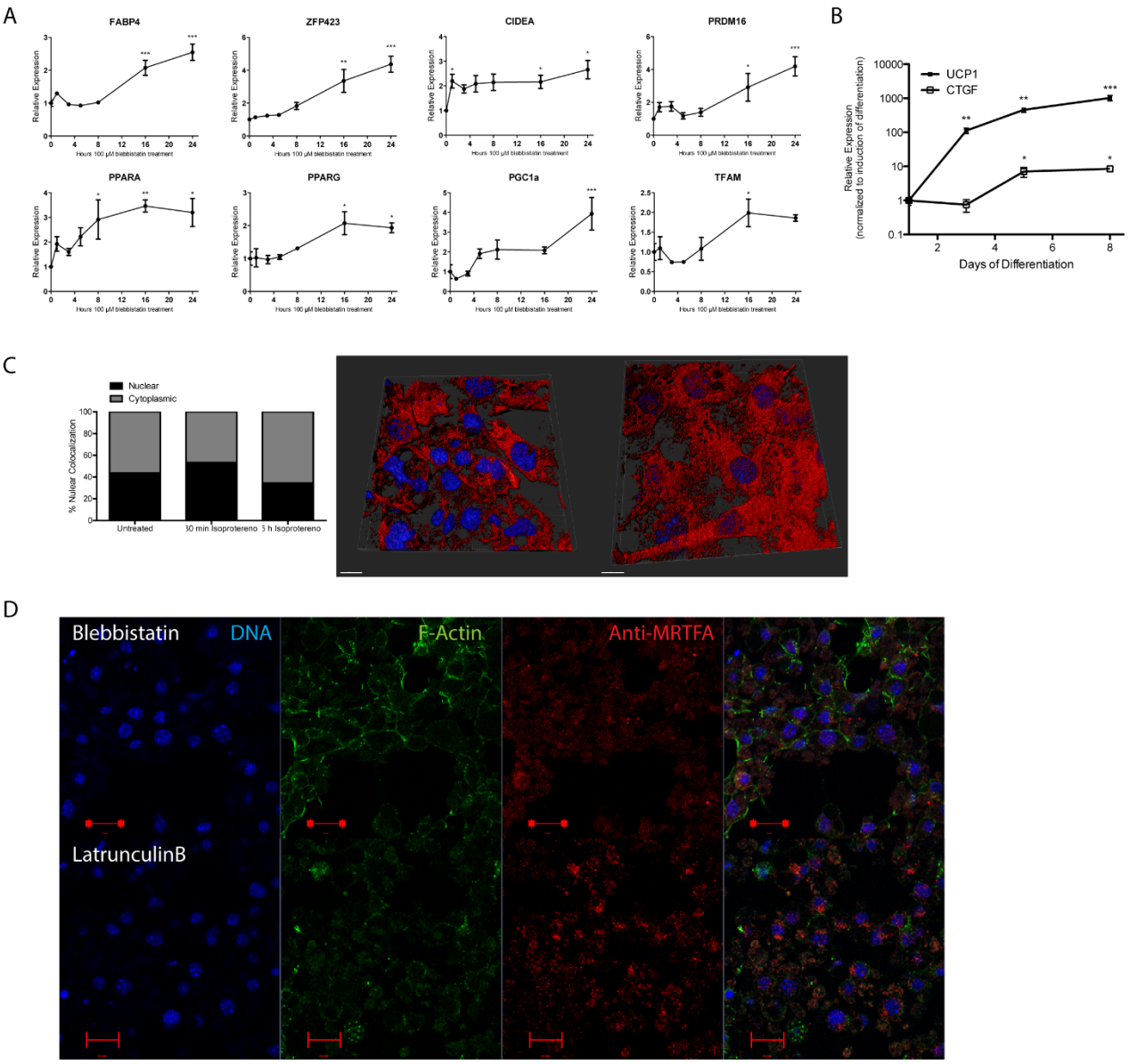


Figure S5: A. Relevant gene expression changes induced by during 24 h of 100 µM blebbistatin, rtPCR (ΔΔCT, normalized to GAPDH) (n=3) UCP1 mRNA expression 24 h post siRNA knockdown, x-axis indicated siRNA targeted genes, (ΔΔCT, normalized to GAPDH) (n=4). B. UCP1 and CTGF mRNA expression during the course of brown adipogenesis, normalized to day 0 of differentiation, rtPCR (ΔΔCT, normalized to GAPDH) (n=3). C. Pearson's correlation coefficient of DAPI and YAP analyzed with BitPlane Imaris™ software and associated 3D reconstruction of YAP localization in brown adipocytes treated with 1 µM isoproterenol for 30 min, YAP (red), DAPI (blue), 20 µm z-stack, 1 µm per slice, generated with BitPlane Imaris™ software. D. Immunofluorescence brown adipocytes treated with of 100 µM blebbistatin or of 20 µM latrunculinB, MRTFA (red), DAPI (blue), scale bar 20 µm.

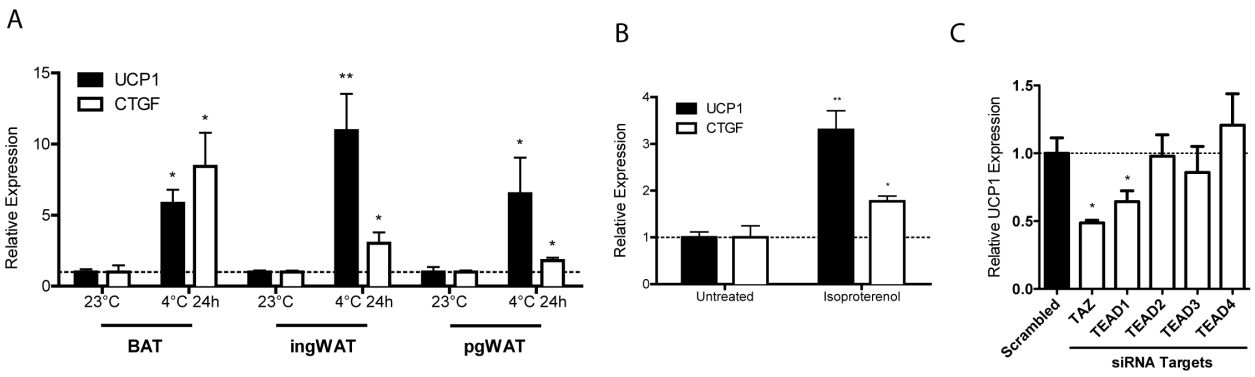


Figure S6: A. UCP1 and CTGF mRNA expression of BAT, subcutaneous inguinal WAT, and perigonadal of 8 wk old male FVB/NJ mice at 23°C or exposed to 24 h cold challenge (4°C), normalized to room temperature (23°C), rtPCR (ΔΔCT, normalized to GAPDH) (n=4). B. UCP1 and CTGF mRNA expression induced in brown adipocytes after 24 h of 1 μM isoproterenol treatment, rtPCR (ΔΔCT, normalized to GAPDH) (n=4). C. UCP1 gene expression changes observed in differentiated brown adipocytes 24 h post transfection with TAZ and TEAD1-4 RNAi, rtPCR (ΔΔCT, normalized to GAPDH) (n=4).

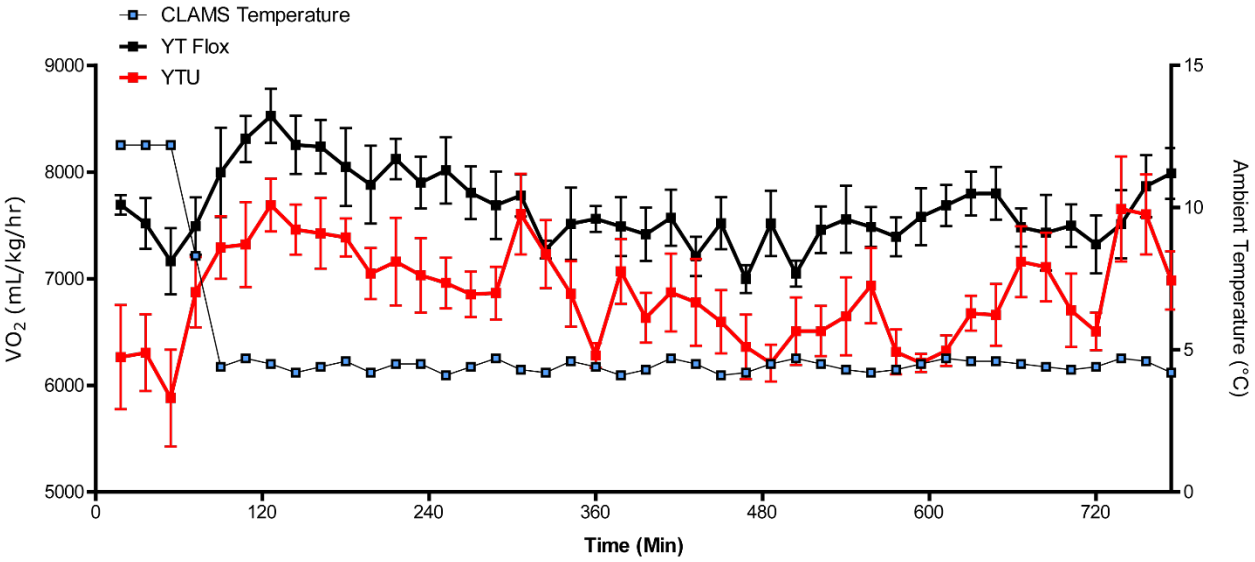


Figure S7: VO_2 of 10 week old male YTU mice at 4°C over 12 h with no variation in ambulatory parameters observed, over 12 h interval the average $V0_2$ P value is 0.0035**, measured with temperature controlled Oxymax-CLAMS (Columbus Instruments) (n=5).

Methods

Brown adipocyte and beige adipocyte cell lines

Cells were maintained in DMEM with 10% serum and 1% penicillin/streptomycin (p/s) (Gibco), and induced to differentiate with the maintenance media fortified with 5 µg/ml Insulin, 1 nM T3, 2 µg/ml Dexamethasone, and 500 µM IBMX (Sigma), and 100nM rosiglitazone (beige cells). After 3 days of differentiation media cells were maintained in DMEM with 10% serum, 1% p/s. Cells were considered fully differentiated on day 6 of differentiation as they stably expressed BAT comparable levels of UCP1, (UCP1-GAPDH with a ΔCT of ~2-3). Experiments assessing effects during differentiation were performed on d4-d6 of differentiation (48 h), specifically MyH7 knockdown, MYLK knockdown, and CA-MYLK expression experiments. Experiments assessing whether or not transient expression or activation effected fully differentiated cells were performed on d7-d8 of differentiation (24 h), specifically YAP/TAZ knockdown, YAP overexpression, and TEAD1-4 knockdown. Transfection/knockdown efficiency was either assessed by rtPCR for target genes or assessment of % GFP-positive cells per field view.

rtPCR

mRNA was isolated from tissues or in vitro cultures with TRIzol reagent (Ambion). Tissue samples were homogenized with a Polytron PT 2100. Assays were carried out on an ABI 7500 RT-PCR system with TaqMan Universal Master Mix II and validated PrimeTime primer probe sets that detect all splice variants (Integrated DNA Technologies). A first-strand cDNA synthesis kit (Fisher) was used to transcribe 5 µg RNA/20 µL. cDNA (100 ng) was used per RT-PCR reaction in triplicates. The ΔΔCT method was used to comparatively assess mRNA quantity.

RNAseq

Libraries were prepared from total RNA isolated with TRIzol reagent (Ambion) (3 biological replicates per condition) using Stranded mRNA-seq Kit (KAPA) and NEXTFlex barcoded adaptors (Bioo Scientific). Multiplexed samples were sequenced on an Illumina HiSeq2500 in Rapid Run mode, and reads were mapped to the mouse genome (mm9 build) using STAR (*219*). DESeq(*220*) was used to identify differentially expressed transcripts, and Metascape or HOMER (*221*) was used for gene ontology and de novo motif finding.

siRNA, YAP-GFP, and CA-MYLK

1 µg or 500n g of siRNA or YAP-GFP (*222*) was diluted in Lipofectamine 3000 and applied per well of differentiated cells on day 7 of differentiation or during differentiation for 48 h on day 4 to day 6 of differentiation (1 µg for 12 well format, 500 ng for seahorse XF24 plates). Sequences: esiRNA SIC001 (Scrambled), Sigma esiRNA EMU088231 (YAP), CUGGUCAGAGAUACUUCUU dTdT (YAP), Sigma esiRNA EMU061601 (MYLK), sc-106222 (MYH7), AGGUACUUCCUCAAUCACA dTdT (TAZ), GGCCGAUUUGUAUACCGAA dTdT (TEAD1), CCUGGUGAAUUUCUUGCACAA dTdT (TEAD2), UACCUUGCUCUCAAUCUGGAG dTdT (TEAD3), and UUUCCUGCACACACGUCUCUU dTdT (TEAD4) (*223*). CA-MYLK tet-off treatment occurred on day 4 to day 6 of differentiation as previously described (*195*).

Immunofluorescence Microscopy

Cells or tissues were fixed in 4% paraformaldehyde for 30 min at room temperature, washed and blocked with a blocking buffer (HBSS fortified with: 10% FBS, 0.1% BSA, 0.05% saponin, and 0.1% Tween20). Primary antibodies [1:100-1:200]: YAP (Santa Cruz Biotech SC-271134 and Abcam EP1674Y), YAP-pSer127(Cell Signaling 4911), MyH7 (Santa Cruz Biotech SC-53089) MyH11 (Santa Cruz Biotech SC-6956). Secondary antibodies [1:1000]: Life Technologies A31573, A31570, A31571, and A11017. ThermoFisher Phalloidin A12379 and A22287. Samples were imaged with a Zeiss 710 confocal microscope and Zeiss Zen software.

In vivo Respirometry
Oxygen consumption was measured with the Oxymax-Comprehensive Laboratory Animal Monitoring System (Columbus Instruments). Measurements were taken over the course of 12, 24, or 48 h periods. Activity was monitored in 1 min intervals of infrared beam breaks in X, Y and Z-axis and found to be not significantly different for any of the groups.

In vitro Respirometry
Oxygen consumption was performed on fully differentiated brown adipocytes (on day 6-8 of differentiation) with the Agilent Seahorse XF24 cellular respirometer. Mitochondrial stress tests were performed on non-permeablized brown adipocytes at 100% confluence per well in XF assay medium with 1 mM pyruvate (Gibco), 2 mM glutamine (Gibco), and 25 mM glucose (Sigma) at pH 7.4. During the mito stress test, sequential additions via injection ports A,B, and C of: Oligomycin [10 μM final], FCCP [10 μM final], and Antimycin A/Rotenone [10 μM final] were applied to the assay wells. All experiments internally controlled and normalized relative to vehicle, scrambled RNAi, or empty vector controls (Figure 3).

Protein Quantification and Western Blotting
Pierce BCA kit, Invitrogen Novex 4-20 tris-glycine gels or Bio-RAD Protean-TGX gels, Invitrogen iBlot transfer system or Bio-Rad Transblot turbo (high MW transfer), and Li-Cor Odyssey with CREB (Cell Signaling 9197), pCreb (Cell Signaling 9198), Anti MyH7 (sc-53089), anti-YAP (Cell Signaling 4912, and SC-271134), anti-TAZ (BD biosciences M2-616), and normalization to anti β-tubulin (e7 clone, DSHB) with IR secondary antibodies (LiCor goat anti-mouse 680 LT, and LiCor goat anti-rabbit 800), signal intensity with LiCor Odyssey software.

Rheology
Viscoelastic properties of tissues were determined using an oscillatory rheometer with parallel-plate geometry (8 mm) and a gap height of 0.2 mm under 10% constant strain and frequency ranging from 0.1 Hz to 10 Hz at 37°C in a humidity-controlled chamber. Tissues were either 1) extracted, placed in PBS, and measured within 2 h of extraction or 2) extracted, decellularized with 1% SDS in PBS for 48 h (*91*), rinsed with fresh PBS and measured.

Atomic Force Microscopy
Indentation measurements were performed with a NanoScope Catalyst (Bruker Corporation, Billerica, MA) atomic force microscope on an inverted optical microscope (Eclipse Ti-E, Nikon Corporation, Chiyoda, Tokyo). Singe cell measurments: PFQNM-LC-A-CAL (Bruker Corporation), with manufacturer measured spring constants between 0.09 - 0.10 N/m and a half-spherical (65 nm radius) tip geometry. Force volumes with indentations of < 1μm were taken in a 30 μm x 30 μm grid with 16 measurements per line at a frequency of 0.3Hz on fully differentiated adipocyte monolayers under basal media conditions or supplemented with 1 μM isoproterenol, 100 μM blebbistatin, or 1 mM 2,3-BDM. Tissue level measurements: Bruker MLCT-BIO - Specs: 35 degree half angle, 20 nm nominal radius, nominal spring constant ~0.01 N/m. Spring constant was calibrated before each experiment by thermal tune (7 kHz resonant freq), braced as previously described (*224*). Force volumes with indentations of < 1 μm were taken in a 100 μm x 100 μm grid under basal media supplemented with 1 μM isoproterenol. For time-lapse experiments, force volumes were acquired continuously for the experimental duration. Data were analyzed using Bruker Nanoscope Analysis v1.7 software. Force curves from cytoplasmic regions of measured cells, defined as the softest zones and verified by brightfield microscopy, and from cortical regions, defined as the stiffest zones, were fitted to the Hertz contact model for a sphere indenting an infinite half-plane. We assumed a nominal Poisson's ratio of 0.3, and fit the model to the extension curve to determine Young's modulus for each force curve.

Mouse Models
YAP-LoxP and TAZ-LoxP mice (*225*) and UCP1-Cre mice (*226, 227*). Data depicts the comparison of age matched YAP/TAZ flox allele control animals relative to UCP1-Cre positive YAP/TAZ heterozygous flox allele mice.

Statistical Analysis
All data are presented as SEM analyzed using Prism (GraphPad). Statistical significance was determined by either one-way ANOVA followed by Tukey posttest or unpaired two-tailed Student t test. Significance presented at $P < 0.05$, $P < 0.01$, and $P < 0.001$.

Conclusion

Due to the immense metabolic therapeutic potential of thermogenic adipose, significant effort has been applied to understand the mechanisms that govern their development and function in the past decade. To determine whether the expansion of thermogenic adipose tissues will truly affect metabolic health, I developed a novel biomaterial scaffold sufficient to support the engraftment of $UCP1^{+}$ adipocytes. This system allowed me to determine that expansion of thermogenic adipose can have a significant effect on core body temperature, energy homeostasis, weight gain, and insulin sensitivity. This preclinical model demonstrated the feasibility of autologous transplantation of thermogenic adipose as an anti-obesity/diabetes therapy.

Subsequently, I sought to clarify how the biomaterial-based signals I defined in chapter I could promote thermogenic gene expression in adipocytes. I identified that thermogenic adipose tissues behave much like muscle in response to adrenergic stimulation, the canonical signal that activates thermogenesis in $UCP1^{+}$ adipose, and utilize actomyosin to generate cellular tension similar to a muscular contraction. Downstream of the stimulation induced tension, mechanosensitive transcription factors are activated to facilitate thermogenic gene expression. Additionally, I identified that the actomyosin mediated tension also plays a direct role in the metabolic program underpinning thermogenesis.

Overall, this dissertation has provided a framework to build clinically applicable thermogenic adipose tissue implants as metabolic therapeutics for humans. The identification of mechanical regulation of differentiation and respiratory capacity of thermogenic adipocytes may also be used therapeutically through actomyosin targeted pharmacology such as Omecamtiv mecarbil or EMD57003. Additionally, since YAP/TAZ is well known to facilitate responses to extracellular contacts, screening for new biomaterials that activate YAP/TAZ may yield greater therapeutic outcomes than what was outlined in chapter I.

Hopefully, the findings presented here will further efforts to promote thermogenic adipose tissue as a metabolic therapy to combat obesity related diseases through tissue engineering or pharmacological means.

References

1. E. D. Rosen, B. M. Spiegelman, What we talk about when we talk about fat. *Cell* **156**, 20-44 (2014); published online EpubJan 16 (10.1016/j.cell.2013.12.012).
2. D. G. Nicholls, R. M. Locke, Thermogenic mechanisms in brown fat. *Physiological reviews* **64**, 1-64 (1984); published online EpubJan (
3. A. Fedorenko, P. V. Lishko, Y. Kirichok, Mechanism of fatty-acid-dependent UCP1 uncoupling in brown fat mitochondria. *Cell* **151**, 400-413 (2012); published online EpubOct 12 (10.1016/j.cell.2012.09.010).
4. B. Cannon, J. Nedergaard, Brown adipose tissue: function and physiological significance. *Physiological reviews* **84**, 277-359 (2004); published online EpubJan (10.1152/physrev.00015.2003).
5. A. M. Cypess, S. Lehman, G. Williams, I. Tal, D. Rodman, A. B. Goldfine, F. C. Kuo, E. L. Palmer, Y. H. Tseng, A. Doria, G. M. Kolodny, C. R. Kahn, Identification and importance of brown adipose tissue in adult humans. *The New England journal of medicine* **360**, 1509-1517 (2009); published online EpubApr 9 (360/15/1509 [pii] 10.1056/NEJMoa0810780).
6. W. D. van Marken Lichtenbelt, J. W. Vanhommerig, N. M. Smulders, J. M. Drossaerts, G. J. Kemerink, N. D. Bouvy, P. Schrauwen, G. J. Teule, Cold-activated brown adipose tissue in healthy men. *The New England journal of medicine* **360**, 1500-1508 (2009); published online EpubApr 9 (360/15/1500 [pii] 10.1056/NEJMoa0808718).
7. S. W. Ma, D. O. Foster, Uptake of glucose and release of fatty acids and glycerol by rat brown adipose tissue in vivo. *Can J Physiol Pharmacol* **64**, 609-614 (1986); published online EpubMay (
8. V. Ouellet, A. Routhier-Labadie, W. Bellemare, L. Lakhal-Chaieb, E. Turcotte, A. C. Carpentier, D. Richard, Outdoor temperature, age, sex, body mass index, and diabetic status determine the prevalence, mass, and glucose-uptake activity of 18F-FDG-detected BAT in humans. *The Journal of clinical endocrinology and metabolism* **96**, 192-199 (2011); published online EpubJan (10.1210/jc.2010-0989).
9. S. C. Gunawardana, D. W. Piston, Reversal of type 1 diabetes in mice by brown adipose tissue transplant. *Diabetes* **61**, 674-682 (2012); published online EpubMar (10.2337/db11-0510).
10. K. I. Stanford, R. J. Middelbeek, K. L. Townsend, D. An, E. B. Nygaard, K. M. Hitchcox, K. R. Markan, K. Nakano, M. F. Hirshman, Y. H. Tseng, L. J. Goodyear, Brown adipose tissue regulates glucose homeostasis and insulin sensitivity. *J Clin Invest* **123**, 215-223 (2013); published online EpubJan (10.1172/JCI62308).
11. H. Ohno, K. Shinoda, B. M. Spiegelman, S. Kajimura, PPARgamma agonists induce a white-to-brown fat conversion through stabilization of PRDM16 protein. *Cell Metab* **15**, 395-404 (2012); published online EpubMar 7 (10.1016/j.cmet.2012.01.019).
12. C. Elabd, C. Chiellini, M. Carmona, J. Galitzky, O. Cochet, R. Petersen, L. Penicaud, K. Kristiansen, A. Bouloumie, L. Casteilla, C. Dani, G. Ailhaud, E. Z. Amri, Human multipotent adipose-derived stem cells differentiate into functional brown adipocytes. *Stem cells* **27**, 2753-2760 (2009); published online EpubNov (10.1002/stem.200).
13. T. J. Schulz, T. L. Huang, T. T. Tran, H. Zhang, K. L. Townsend, J. L. Shadrach, M. Cerletti, L. E. McDougall, N. Giorgadze, T. Tchkonia, D. Schrier, D. Falb, J. L. Kirkland, A. J. Wagers, Y. H. Tseng, Identification of inducible brown adipocyte progenitors residing in skeletal muscle and white fat. *Proc Natl Acad Sci U S A* **108**, 143-148 (2011); published online EpubJan 4 (10.1073/pnas.1010929108).
14. T. Ahfeldt, R. T. Schinzel, Y. K. Lee, D. Hendrickson, A. Kaplan, D. H. Lum, R. Camahort, F. Xia, J. Shay, E. P. Rhee, C. B. Clish, R. C. Deo, T. Shen, F. H. Lau, A.

Cowley, G. Mowrer, H. Al-Siddiqi, M. Nahrendorf, K. Musunuru, R. E. Gerszten, J. L. Rinn, C. A. Cowan, Programming human pluripotent stem cells into white and brown adipocytes. *Nature cell biology* **14**, 209-219 (2012); published online EpubFeb (10.1038/ncb2411).
15. M. S. Rodeheffer, K. Birsoy, J. M. Friedman, Identification of white adipocyte progenitor cells in vivo. *Cell* **135**, 240-249 (2008); published online EpubOct 17 (10.1016/j.cell.2008.09.036).
16. S. Kajimura, P. Seale, K. Kubota, E. Lunsford, J. V. Frangioni, S. P. Gygi, B. M. Spiegelman, Initiation of myoblast to brown fat switch by a PRDM16-C/EBP-beta transcriptional complex. *Nature* **460**, 1154-1158 (2009); published online EpubAug 27 (10.1038/nature08262).
17. M. L. Edelstein, M. R. Abedi, J. Wixon, R. M. Edelstein, Gene therapy clinical trials worldwide 1989-2004-an overview. *The journal of gene medicine* **6**, 597-602 (2004); published online EpubJun (10.1002/jgm.619).
18. S. J. Huang, R. H. Fu, W. C. Shyu, S. P. Liu, G. P. Jong, Y. W. Chiu, H. S. Wu, Y. A. Tsou, C. W. Cheng, S. Z. Lin, Adipose-derived stem cells: isolation, characterization, and differentiation potential. *Cell transplantation* **22**, 701-709 (2013)10.3727/096368912x655127).
19. L. G. Griffith, M. A. Swartz, Capturing complex 3D tissue physiology in vitro. *Nature reviews. Molecular cell biology* **7**, 211-224 (2006); published online EpubMar (10.1038/nrm1858).
20. Y. H. Tseng, E. Kokkotou, T. J. Schulz, T. L. Huang, J. N. Winnay, C. M. Taniguchi, T. T. Tran, R. Suzuki, D. O. Espinoza, Y. Yamamoto, M. J. Ahrens, A. T. Dudley, A. W. Norris, R. N. Kulkarni, C. R. Kahn, New role of bone morphogenetic protein 7 in brown adipogenesis and energy expenditure. *Nature* **454**, 1000-1004 (2008); published online EpubAug 21 (nature07221 [pii]
10.1038/nature07221 [doi]).
21. H. Nakahara, M. Nomizu, S. K. Akiyama, Y. Yamada, Y. Yeh, W. T. Chen, A mechanism for regulation of melanoma invasion. Ligation of alpha6beta1 integrin by laminin G peptides. *J Biol Chem* **271**, 27221-27224 (1996); published online EpubNov 1 (
22. M. Nomizu, W. H. Kim, K. Yamamura, A. Utani, S. Y. Song, A. Otaka, P. P. Roller, H. K. Kleinman, Y. Yamada, Identification of cell binding sites in the laminin alpha 1 chain carboxyl-terminal globular domain by systematic screening of synthetic peptides. *J Biol Chem* **270**, 20583-20590 (1995); published online EpubSep 1 (
23. M. L. Ponce, M. Nomizu, H. K. Kleinman, An angiogenic laminin site and its antagonist bind through the alpha(v)beta3 and alpha5beta1 integrins. *FASEB journal : official publication of the Federation of American Societies for Experimental Biology* **15**, 1389-1397 (2001); published online EpubJun (
24. A. J. Engler, S. Sen, H. L. Sweeney, D. E. Discher, Matrix elasticity directs stem cell lineage specification. *Cell* **126**, 677-689 (2006); published online EpubAug 25 (10.1016/j.cell.2006.06.044).
25. K. Shapira-Schweitzer, D. Seliktar, Matrix stiffness affects spontaneous contraction of cardiomyocytes cultured within a PEGylated fibrinogen biomaterial. *Acta biomaterialia* **3**, 33-41 (2007); published online EpubJan (10.1016/j.actbio.2006.09.003).
26. K. Saha, A. J. Keung, E. F. Irwin, Y. Li, L. Little, D. V. Schaffer, K. E. Healy, Substrate modulus directs neural stem cell behavior. *Biophysical journal* **95**, 4426-4438 (2008); published online EpubNov 1 (10.1529/biophysj.108.132217).
27. A. K. Jha, K. M. Tharp, J. Ye, J. L. Santiago-Ortiz, W. M. Jackson, A. Stahl, D. V. Schaffer, Y. Yeghiazarians, K. E. Healy, Enhanced survival and engraftment of transplanted stem cells using growth factor sequestering hydrogels. *Biomaterials* **47**, 1-

12 (2015); published online Epub4// (http://dx.doi.org/10.1016/j.biomaterials.2014.12.043).
28. S. Kim, E. H. Chung, M. Gilbert, K. E. Healy, Synthetic MMP-13 degradable ECMs based on poly(N-isopropylacrylamide-co-acrylic acid) semi-interpenetrating polymer networks. I. Degradation and cell migration. *Journal of biomedical materials research. Part A* **75**, 73-88 (2005); published online EpubOct 1 (10.1002/jbm.a.30375).
29. E. H. Chung, M. Gilbert, A. S. Virdi, K. Sena, D. R. Sumner, K. E. Healy, Biomimetic artificial ECMs stimulate bone regeneration. *Journal of biomedical materials research. Part A* **79**, 815-826 (2006); published online EpubDec 15 (10.1002/jbm.a.30809).
30. S. T. Wall, C. C. Yeh, R. Y. Tu, M. J. Mann, K. E. Healy, Biomimetic matrices for myocardial stabilization and stem cell transplantation. *Journal of biomedical materials research. Part A* **95**, 1055-1066 (2010); published online EpubDec 15 (10.1002/jbm.a.32904).
31. B. D. Mather, K. Viswanathan, K. M. Miller, T. E. Long, Michael addition reactions in macromolecular design for emerging technologies. *Progress in Polymer Science* **31**, 487-531 (2006)10.1016/j.progpolymsci.2006.03.001).
32. M. P. Lutolf, G. P. Raeber, A. H. Zisch, N. Tirelli, J. A. Hubbell, Cell-responsive synthetic hydrogels. *Advanced materials* **15**, 888-+ (2003); published online EpubJun 5 (10.1002/adma.200304621).
33. K. D. Nguyen, Y. Qiu, X. Cui, Y. P. Goh, J. Mwangi, T. David, L. Mukundan, F. Brombacher, R. M. Locksley, A. Chawla, Alternatively activated macrophages produce catecholamines to sustain adaptive thermogenesis. *Nature* **480**, 104-108 (2011); published online EpubDec 1 (10.1038/nature10653).
34. C. Guerra, R. A. Koza, H. Yamashita, K. Walsh, L. P. Kozak, Emergence of brown adipocytes in white fat in mice is under genetic control. Effects on body weight and adiposity. *J Clin Invest* **102**, 412-420 (1998); published online EpubJul 15 (10.1172/jci3155).
35. F. B. Stillaert, C. Di Bartolo, J. A. Hunt, N. P. Rhodes, E. Tognana, S. Monstrey, P. N. Blondeel, Human clinical experience with adipose precursor cells seeded on hyaluronic acid-based spongy scaffolds. *Biomaterials* **29**, 3953-3959 (2008); published online EpubOct (10.1016/j.biomaterials.2008.06.005).
36. Y. M. Kim, S. H. Oh, J. S. Choi, S. Lee, J. C. Ra, J. H. Lee, J. Y. Lim, Adipose-derived stem cell-containing hyaluronic acid/alginate hydrogel improves vocal fold wound healing. *The Laryngoscope* **124**, E64-72 (2014); published online EpubMar (10.1002/lary.24405).
37. A. H. Henkin, A. S. Cohen, E. A. Dubikovskaya, H. M. Park, G. F. Nikitin, M. G. Auzias, M. Kazantzis, C. R. Bertozzi, A. Stahl, Real time non-invasive imaging of fatty acid uptake in vivo. *ACS Chem Biol*, (2012); published online EpubAug 28 (10.1021/cb300194b).
38. Q. Wu, M. Kazantzis, H. Doege, A. M. Ortegon, B. Tsang, A. Falcon, A. Stahl, Fatty acid transport protein 1 is required for nonshivering thermogenesis in brown adipose tissue. *Diabetes* **55**, 3229-3237 (2006); published online EpubDec (55/12/3229 [pii] 10.2337/db06-0749).
39. A. K. Jha, R. A. Hule, T. Jiao, S. S. Teller, R. J. Clifton, R. L. Duncan, D. J. Pochan, X. Jia, Structural Analysis and Mechanical Characterization of Hyaluronic Acid-Based Doubly Cross-Linked Networks. *Macromolecules* **42**, 537-546 (2009)10.1021/ma8019442).
40. M. W. Lee, J. I. Odegaard, L. Mukundan, Y. Qiu, A. B. Molofsky, J. C. Nussbaum, K. Yun, R. M. Locksley, A. Chawla, Activated type 2 innate lymphoid cells regulate beige fat biogenesis. *Cell* **160**, 74-87 (2015); published online EpubJan 15 (10.1016/j.cell.2014.12.011).

41. Y. Liu, C. H. Vaughan, T. J. Bartness, T. Yoneshiro, S. Aita, M. Matsushita, T. Kayahara, T. Kameya, Y. Kawai, T. Iwanaga, M. Saito, Recruited brown adipose tissue as an antiobesity agent in humans. *The Journal of neuroscience : the official journal of the Society for Neuroscience* **123**, 3404-3408 (2013); published online EpubAug (10.1523/jneurosci.3306-14.2015
10.1172/jci67803).
42. O. Boss, S. R. Farmer, Recruitment of brown adipose tissue as a therapy for obesity-associated diseases. *Frontiers in endocrinology* **3**, 14 (2012)10.3389/fendo.2012.00014).
43. J. Wu, P. Bostrom, L. M. Sparks, L. Ye, J. H. Choi, A. H. Giang, M. Khandekar, K. A. Virtanen, P. Nuutila, G. Schaart, K. Huang, H. Tu, W. D. van Marken Lichtenbelt, J. Hoeks, S. Enerback, P. Schrauwen, B. M. Spiegelman, Beige adipocytes are a distinct type of thermogenic fat cell in mouse and human. *Cell* **150**, 366-376 (2012); published online EpubJul 20 (10.1016/j.cell.2012.05.016).
44. F. S. Celi, Brown adipose tissue--when it pays to be inefficient. *The New England journal of medicine* **360**, 1553-1556 (2009); published online EpubApr 9 (10.1056/NEJMe0900466).
45. G. X. Wang, X. Y. Zhao, J. D. Lin, The brown fat secretome: metabolic functions beyond thermogenesis. *Trends in endocrinology and metabolism: TEM* **26**, 231-237 (2015); published online EpubMay (10.1016/j.tem.2015.03.002).
46. S. C. Gunawardana, D. W. Piston, Insulin-independent reversal of type 1 diabetes in nonobese diabetic mice with brown adipose tissue transplant. *Am J Physiol Endocrinol Metab* **308**, E1043-1055 (2015); published online EpubJun 15 (10.3389/fendo.2012.00014
10.1152/ajpendo.00570.2014).
47. G. X. Wang, X. Y. Zhao, Z. X. Meng, M. Kern, A. Dietrich, Z. Chen, Z. Cozacov, D. Zhou, A. L. Okunade, X. Su, S. Li, M. Bluher, J. D. Lin, The brown fat-enriched secreted factor Nrg4 preserves metabolic homeostasis through attenuation of hepatic lipogenesis. *Nat Med* **20**, 1436-1443 (2014); published online EpubDec (10.1038/nm.3713).
48. M. A. Bredella, C. M. Gill, C. J. Rosen, A. Klibanski, M. Torriani, Positive effects of brown adipose tissue on femoral bone structure. *Bone* **58**, 55-58 (2014); published online EpubJan (10.1016/j.bone.2013.10.007).
49. A. D. Nguyen, N. J. Lee, N. K. Wee, L. Zhang, R. F. Enriquez, E. C. Khor, T. Nie, D. Wu, A. Sainsbury, P. A. Baldock, H. Herzog, Uncoupling protein-1 is protective of bone mass under mild cold stress conditions. *Bone*, (2015); published online EpubJun 6 (10.1016/j.bone.2015.05.037).
50. X. Liu, S. Wang, Y. You, M. Meng, Z. Zheng, M. Dong, J. Lin, Q. Zhao, C. Zhang, X. Yuan, T. Hu, L. Liu, Y. Huang, L. Zhang, D. Wang, J. Zhan, H. Jong Lee, J. R. Speakman, W. Jin, Brown Adipose Tissue Transplantation Reverses Obesity in Ob/Ob Mice. *Endocrinology* **156**, 2461-2469 (2015); published online EpubJul (10.1210/en.2014-1598).
51. M. Komajda, J. J. McMurray, H. Beck-Nielsen, R. Gomis, M. Hanefeld, S. J. Pocock, P. S. Curtis, N. P. Jones, P. D. Home, Heart failure events with rosiglitazone in type 2 diabetes: data from the RECORD clinical trial. *European heart journal* **31**, 824-831 (2010); published online EpubApr (10.1093/eurheartj/ehp604).
52. A. Moisan, Y. K. Lee, J. D. Zhang, C. S. Hudak, C. A. Meyer, M. Prummer, S. Zoffmann, H. H. Truong, M. Ebeling, A. Kiialainen, R. Gerard, F. Xia, R. T. Schinzel, K. E. Amrein, C. A. Cowan, White-to-brown metabolic conversion of human adipocytes by JAK inhibition. *Nature cell biology* **17**, 57-67 (2015); published online EpubJan (10.1038/ncb3075).

53. P. Bostrom, J. Wu, M. P. Jedrychowski, A. Korde, L. Ye, J. C. Lo, K. A. Rasbach, E. A. Bostrom, J. H. Choi, J. Z. Long, S. Kajimura, M. C. Zingaretti, B. F. Vind, H. Tu, S. Cinti, K. Hojlund, S. P. Gygi, B. M. Spiegelman, A PGC1-alpha-dependent myokine that drives brown-fat-like development of white fat and thermogenesis. *Nature* **481**, 463-468 (2012); published online EpubJan 26 (10.1038/nature10777).
54. M. P. Jedrychowski, C. D. Wrann, J. A. Paulo, K. K. Gerber, J. Szpyt, M. M. Robinson, K. S. Nair, S. P. Gygi, B. M. Spiegelman, Detection and Quantitation of Circulating Human Irisin by Tandem Mass Spectrometry. *Cell Metab*, (2015); published online EpubAug 12 (10.1016/j.cmet.2015.08.001).
55. R. R. Rao, J. Z. Long, J. P. White, K. J. Svensson, J. Lou, I. Lokurkar, M. P. Jedrychowski, J. L. Ruas, C. D. Wrann, J. C. Lo, D. M. Camera, J. Lachey, S. Gygi, J. Seehra, J. A. Hawley, B. M. Spiegelman, Meteorin-like is a hormone that regulates immune-adipose interactions to increase beige fat thermogenesis. *Cell* **157**, 1279-1291 (2014); published online EpubJun 5 (10.1016/j.cell.2014.03.065).
56. D. Sellayah, D. Sikder, Orexin restores aging-related brown adipose tissue dysfunction in male mice. *Endocrinology* **155**, 485-501 (2014); published online EpubFeb (10.1210/en.2013-1629).
57. A. Than, H. L. He, S. H. Chua, D. Xu, L. Sun, M. K. Leow, P. Chen, Apelin Enhances Brown Adipogenesis and Browning of White Adipocytes. *J Biol Chem* **290**, 14679-14691 (2015); published online EpubJun 5 (10.1074/jbc.M115.643817).
58. F. M. Fisher, S. Kleiner, N. Douris, E. C. Fox, R. J. Mepani, F. Verdeguer, J. Wu, A. Kharitonenkov, J. S. Flier, E. Maratos-Flier, B. M. Spiegelman, FGF21 regulates PGC-1alpha and browning of white adipose tissues in adaptive thermogenesis. *Genes Dev* **26**, 271-281 (2012); published online EpubFeb 1 (10.1101/gad.177857.111).
59. M. E. McDonald, C. Li, H. Bian, B. D. Smith, M. D. Layne, S. R. Farmer, Myocardin-related transcription factor A regulates conversion of progenitors to beige adipocytes. *Cell* **160**, 105-118 (2015); published online EpubJan 15 (10.1016/j.cell.2014.12.005).
60. Y. Qiu, K. D. Nguyen, J. I. Odegaard, X. Cui, X. Tian, R. M. Locksley, R. D. Palmiter, A. Chawla, Eosinophils and type 2 cytokine signaling in macrophages orchestrate development of functional beige fat. *Cell* **157**, 1292-1308 (2014); published online EpubJun 5 (10.1016/j.cell.2014.03.066).
61. J. R. Brestoff, B. S. Kim, S. A. Saenz, R. R. Stine, L. A. Monticelli, G. F. Sonnenberg, J. J. Thome, D. L. Farber, K. Lutfy, P. Seale, D. Artis, Group 2 innate lymphoid cells promote beiging of white adipose tissue and limit obesity. *Nature* **519**, 242-246 (2015); published online EpubMar 12 (10.1038/nature14115).
62. A. C. Daquinag, C. Tseng, A. Salameh, Y. Zhang, F. Amaya-Manzanares, A. Dadbin, F. Florez, Y. Xu, Q. Tong, M. G. Kolonin, Depletion of white adipocyte progenitors induces beige adipocyte differentiation and suppresses obesity development. *Cell Death Differ* **22**, 351-363 (2015); published online EpubFeb (10.1038/cdd.2014.148).
63. J. Himms-Hagen, J. Cui, E. Danforth, Jr., D. J. Taatjes, S. S. Lang, B. L. Waters, T. H. Claus, Effect of CL-316,243, a thermogenic beta 3-agonist, on energy balance and brown and white adipose tissues in rats. *The American journal of physiology* **266**, R1371-1382 (1994); published online EpubApr (
64. M. L. Bonet, P. Oliver, A. Palou, Pharmacological and nutritional agents promoting browning of white adipose tissue. *Biochim Biophys Acta* **1831**, 969-985 (2013); published online EpubMay (10.1016/j.bbalip.2012.12.002).
65. F. Villarroya, A. Vidal-Puig, Beyond the sympathetic tone: the new brown fat activators. *Cell Metab* **17**, 638-643 (2013); published online EpubMay 7 (10.1016/j.cmet.2013.02.020).
66. A. K. Jha, A. Mathur, F. L. Svedlund, J. Ye, Y. Yeghiazarians, K. E. Healy, Molecular weight and concentration of heparin in hyaluronic acid-based matrices modulates growth

factor retention kinetics and stem cell fate. *J Control Release* **209**, 308-316 (2015); published online EpubJul 10 (10.1016/j.jconrel.2015.04.034).
67. X. Xu, A. K. Jha, R. L. Duncan, X. Jia, Heparin-decorated, hyaluronic acid-based hydrogel particles for the controlled release of bone morphogenetic protein 2. *Acta biomaterialia* **7**, 3050-3059 (2011); published online EpubAug (10.1016/j.actbio.2011.04.018).
68. M. Fan, Y. Ma, Z. Zhang, J. Mao, H. Tan, X. Hu, Biodegradable hyaluronic acid hydrogels to control release of dexamethasone through aqueous Diels-Alder chemistry for adipose tissue engineering. *Materials science & engineering. C, Materials for biological applications* **56**, 311-317 (2015); published online EpubNov 1 (10.1016/j.msec.2015.04.004).
69. G. Bhakta, B. Rai, Z. X. Lim, J. H. Hui, G. S. Stein, A. J. van Wijnen, V. Nurcombe, G. D. Prestwich, S. M. Cool, Hyaluronic acid-based hydrogels functionalized with heparin that support controlled release of bioactive BMP-2. *Biomaterials* **33**, 6113-6122 (2012); published online EpubSep (10.1016/j.biomaterials.2012.05.030).
70. M. Yamamoto, Y. Takahashi, Y. Tabata, Controlled release by biodegradable hydrogels enhances the ectopic bone formation of bone morphogenetic protein. *Biomaterials* **24**, 4375-4383 (2003); published online EpubNov (
71. M. Ishihara, M. Fujita, K. Obara, H. Hattori, S. Nakamura, M. Nambu, T. Kiyosawa, Y. Kanatani, B. Takase, M. Kikuchi, T. Maehara, Controlled releases of FGF-2 and paclitaxel from chitosan hydrogels and their subsequent effects on wound repair, angiogenesis, and tumor growth. *Current drug delivery* **3**, 351-358 (2006); published online EpubOct (
72. G. Tae, J. A. Kornfield, J. A. Hubbell, Sustained release of human growth hormone from in situ forming hydrogels using self-assembly of fluoroalkyl-ended poly(ethylene glycol). *Biomaterials* **26**, 5259-5266 (2005); published online EpubSep (10.1016/j.biomaterials.2005.01.042).
73. T. J. Schulz, P. Huang, T. L. Huang, R. Xue, L. E. McDougall, K. L. Townsend, A. M. Cypess, Y. Mishina, E. Gussoni, Y. H. Tseng, Brown-fat paucity due to impaired BMP signalling induces compensatory browning of white fat. *Nature* **495**, 379-383 (2013); published online EpubMar 21 (10.1038/nature11943).
74. S. Collins, beta-Adrenoceptor Signaling Networks in Adipocytes for Recruiting Stored Fat and Energy Expenditure. *Frontiers in endocrinology* **2**, 102 (2011)10.3389/fendo.2011.00102).
75. V. Ryu, J. T. Garretson, Y. Liu, C. H. Vaughan, T. J. Bartness, Brown adipose tissue has sympathetic-sensory feedback circuits. *The Journal of neuroscience : the official journal of the Society for Neuroscience* **35**, 2181-2190 (2015); published online EpubFeb 4 (10.1523/JNEUROSCI.3306-14.2015).
76. D. Wu, A. B. Molofsky, H. E. Liang, R. R. Ricardo-Gonzalez, H. A. Jouihan, J. K. Bando, A. Chawla, R. M. Locksley, Eosinophils sustain adipose alternatively activated macrophages associated with glucose homeostasis. *Science* **332**, 243-247 (2011); published online EpubApr 8 (10.1126/science.1201475).
77. I. Murano, G. Barbatelli, A. Giordano, S. Cinti, Noradrenergic parenchymal nerve fiber branching after cold acclimatisation correlates with brown adipocyte density in mouse adipose organ. *Journal of anatomy* **214**, 171-178 (2009); published online EpubJan (10.1111/j.1469-7580.2008.01001.x).
78. L. Ye, J. Wu, P. Cohen, L. Kazak, M. J. Khandekar, M. P. Jedrychowski, X. Zeng, S. P. Gygi, B. M. Spiegelman, Fat cells directly sense temperature to activate thermogenesis. *Proc Natl Acad Sci U S A* **110**, 12480-12485 (2013); published online EpubJul 23 (10.1073/pnas.1310261110).

79. M. Watanabe, S. M. Houten, C. Mataki, M. A. Christoffolete, B. W. Kim, H. Sato, N. Messaddeq, J. W. Harney, O. Ezaki, T. Kodama, K. Schoonjans, A. C. Bianco, J. Auwerx, Bile acids induce energy expenditure by promoting intracellular thyroid hormone activation. *Nature* **439**, 484-489 (2006); published online EpubJan 26 (10.1038/nature04330).
80. M. Bordicchia, D. Liu, E. Z. Amri, G. Ailhaud, P. Dessi-Fulgheri, C. Zhang, N. Takahashi, R. Sarzani, S. Collins, Cardiac natriuretic peptides act via p38 MAPK to induce the brown fat thermogenic program in mouse and human adipocytes. *J Clin Invest* **122**, 1022-1036 (2012); published online EpubMar (10.1172/JCI59701).
81. M. J. Obregon, Adipose tissues and thyroid hormones. *Frontiers in physiology* **5**, 479 (2014)10.3389/fphys.2014.00479).
82. D. T. Scadden, The stem-cell niche as an entity of action. *Nature* **441**, 1075-1079 (2006); published online EpubJun 29 (10.1038/nature04957).
83. D. L. Jones, A. J. Wagers, No place like home: anatomy and function of the stem cell niche. *Nature reviews. Molecular cell biology* **9**, 11-21 (2008); published online EpubJan (10.1038/nrm2319).
84. M. J. Bissell, P. A. Kenny, D. C. Radisky, Microenvironmental regulators of tissue structure and function also regulate tumor induction and progression: the role of extracellular matrix and its degrading enzymes. *Cold Spring Harbor symposia on quantitative biology* **70**, 343-356 (2005)10.1101/sqb.2005.70.013).
85. K. Saha, J. F. Pollock, D. V. Schaffer, K. E. Healy, Designing synthetic materials to control stem cell phenotype. *Curr Opin Chem Biol* **11**, 381-387 (2007); published online EpubAug (10.1016/j.cbpa.2007.05.030).
86. M. P. Lutolf, J. A. Hubbell, Synthetic biomaterials as instructive extracellular microenvironments for morphogenesis in tissue engineering. *Nat Biotechnol* **23**, 47-55 (2005); published online EpubJan (10.1038/nbt1055).
87. R. Bhat, M. J. Bissell, Of plasticity and specificity: dialectics of the microenvironment and macroenvironment and the organ phenotype. *Wiley interdisciplinary reviews. Developmental biology* **3**, 147-163 (2014); published online EpubMar-Apr (10.1002/wdev.130).
88. J. K. Mouw, G. Ou, V. M. Weaver, Extracellular matrix assembly: a multiscale deconstruction. *Nature reviews. Molecular cell biology* **15**, 771-785 (2014); published online EpubDec (10.1038/nrm3902).
89. Y. Wang, E. L. Botvinick, Y. Zhao, M. W. Berns, S. Usami, R. Y. Tsien, S. Chien, Visualizing the mechanical activation of Src. *Nature* **434**, 1040-1045 (2005); published online EpubApr 21 (10.1038/nature03469).
90. S. F. Badylak, D. Taylor, K. Uygun, Whole-organ tissue engineering: decellularization and recellularization of three-dimensional matrix scaffolds. *Annual review of biomedical engineering* **13**, 27-53 (2011); published online EpubAug 15 (10.1146/annurev-bioeng-071910-124743).
91. D. A. Young, D. O. Ibrahim, D. Hu, K. L. Christman, Injectable hydrogel scaffold from decellularized human lipoaspirate. *Acta biomaterialia* **7**, 1040-1049 (2011); published online EpubMar (10.1016/j.actbio.2010.09.035).
92. M. W. Tibbitt, K. S. Anseth, Hydrogels as extracellular matrix mimics for 3D cell culture. *Biotechnology and bioengineering* **103**, 655-663 (2009); published online EpubJul 1 (10.1002/bit.22361).
93. M. Kim, J. Y. Lee, C. N. Jones, A. Revzin, G. Tae, Heparin-based hydrogel as a matrix for encapsulation and cultivation of primary hepatocytes. *Biomaterials* **31**, 3596-3603 (2010); published online EpubMay (10.1016/j.biomaterials.2010.01.068).
94. L. M. Weber, K. S. Anseth, Hydrogel encapsulation environments functionalized with extracellular matrix interactions increase islet insulin secretion. *Matrix biology : journal of*

the International Society for Matrix Biology **27**, 667-673 (2008); published online EpubOct (10.1016/j.matbio.2008.08.001).
95. J. C. Friedland, J. N. Lakins, M. G. Kazanietz, J. Chernoff, D. Boettiger, V. M. Weaver, alpha6beta4 integrin activates Rac-dependent p21-activated kinase 1 to drive NF-kappaB-dependent resistance to apoptosis in 3D mammary acini. *J Cell Sci* **120**, 3700-3712 (2007); published online EpubOct 15 (10.1242/jcs.03484).
96. S. T. Lee, J. I. Yun, Y. S. Jo, M. Mochizuki, A. J. van der Vlies, S. Kontos, J. E. Ihm, J. M. Lim, J. A. Hubbell, Engineering integrin signaling for promoting embryonic stem cell self-renewal in a precisely defined niche. *Biomaterials* **31**, 1219-1226 (2010); published online EpubFeb (10.1016/j.biomaterials.2009.10.054).
97. B. M. Spiegelman, C. A. Ginty, Fibronectin modulation of cell shape and lipogenic gene expression in 3T3-adipocytes. *Cell* **35**, 657-666 (1983); published online EpubDec (
98. M. K. Vaicik, J. Thyboll Kortesmaa, S. Moverare-Skrtic, J. Kortesmaa, R. Soininen, G. Bergstrom, C. Ohlsson, L. Y. Chong, B. Rozell, M. Emont, R. N. Cohen, E. M. Brey, K. Tryggvason, Laminin alpha4 deficient mice exhibit decreased capacity for adipose tissue expansion and weight gain. *PLoS One* **9**, e109854 (2014)10.1002/bit.22361 10.1371/journal.pone.0109854).
99. T. Khan, E. S. Muise, P. Iyengar, Z. V. Wang, M. Chandalia, N. Abate, B. B. Zhang, P. Bonaldo, S. Chua, P. E. Scherer, Metabolic dysregulation and adipose tissue fibrosis: role of collagen VI. *Mol Cell Biol* **29**, 1575-1591 (2009); published online EpubMar (10.1371/journal.pone.0109854 10.1128/mcb.01300-08).
100. T. H. Chun, K. B. Hotary, F. Sabeh, A. R. Saltiel, E. D. Allen, S. J. Weiss, A pericellular collagenase directs the 3-dimensional development of white adipose tissue. *Cell* **125**, 577-591 (2006); published online EpubMay 5 (10.1016/j.cell.2006.02.050).
101. J. C. Gerlach, Y. C. Lin, C. A. Brayfield, D. M. Minteer, H. Li, J. P. Rubin, K. G. Marra, Adipogenesis of human adipose-derived stem cells within three-dimensional hollow fiber-based bioreactors. *Tissue engineering. Part C, Methods* **18**, 54-61 (2012); published online EpubJan (10.1089/ten.TEC.2011.0216).
102. M. P. Emont, H. Yu, H. Jun, X. Hong, N. Maganti, J. P. Stegemann, J. Wu, Using a 3D Culture System to Differentiate Visceral Adipocytes In Vitro. *Endocrinology*, en20151567 (2015); published online EpubOct 1 (10.1210/en.2015-1567).
103. A. T. Francisco, R. J. Mancino, R. D. Bowles, J. M. Brunger, D. M. Tainter, Y. T. Chen, W. J. Richardson, F. Guilak, L. A. Setton, Injectable laminin-functionalized hydrogel for nucleus pulposus regeneration. *Biomaterials* **34**, 7381-7388 (2013); published online EpubOct (10.1016/j.biomaterials.2013.06.038).
104. C. Branco da Cunha, D. D. Klumpers, W. A. Li, S. T. Koshy, J. C. Weaver, O. Chaudhuri, P. L. Granja, D. J. Mooney, Influence of the stiffness of three-dimensional alginate/collagen-I interpenetrating networks on fibroblast biology. *Biomaterials* **35**, 8927-8936 (2014); published online EpubOct (10.1016/j.biomaterials.2014.06.047).
105. K. M. Abberton, S. K. Bortolotto, A. A. Woods, M. Findlay, W. A. Morrison, E. W. Thompson, A. Messina, Myogel, a novel, basement membrane-rich, extracellular matrix derived from skeletal muscle, is highly adipogenic in vivo and in vitro. *Cells, tissues, organs* **188**, 347-358 (2008)10.1159/000121575).
106. L. E. Flynn, The use of decellularized adipose tissue to provide an inductive microenvironment for the adipogenic differentiation of human adipose-derived stem cells. *Biomaterials* **31**, 4715-4724 (2010); published online EpubJun (10.1016/j.biomaterials.2010.02.046).
107. R. Xue, M. D. Lynes, J. M. Dreyfuss, F. Shamsi, T. J. Schulz, H. Zhang, T. L. Huang, K. L. Townsend, Y. Li, H. Takahashi, L. S. Weiner, A. P. White, M. S. Lynes, L. L. Rubin, L. J. Goodyear, A. M. Cypess, Y. H. Tseng, Clonal analyses and gene profiling identify

genetic biomarkers of the thermogenic potential of human brown and white preadipocytes. *Nat Med* **21**, 760-768 (2015); published online EpubJul (10.1038/nm.3881).
108. I. Kasza, Y. Suh, D. Wollny, R. J. Clark, A. Roopra, R. J. Colman, O. A. MacDougald, T. A. Shedd, D. W. Nelson, M. I. Yen, C. L. Yen, C. M. Alexander, Syndecan-1 is required to maintain intradermal fat and prevent cold stress. *PLoS genetics* **10**, e1004514 (2014); published online EpubAug (10.1371/journal.pgen.1004514).
109. J. Liu, S. M. DeYoung, M. Zhang, M. Zhang, A. Cheng, A. R. Saltiel, Changes in integrin expression during adipocyte differentiation. *Cell Metab* **2**, 165-177 (2005); published online EpubSep (10.1016/j.cmet.2005.08.006).
110. J. Wu, P. Cohen, B. M. Spiegelman, Adaptive thermogenesis in adipocytes: is beige the new brown? *Genes Dev* **27**, 234-250 (2013); published online EpubFeb 1 (10.1101/gad.211649.112).
111. K. M. Tharp, A. K. Jha, J. Kraiczy, A. Yesian, G. Karateev, R. Sinisi, E. A. Dubikovskaya, K. E. Healy, A. Stahl, Matrix assisted transplantation of functional beige adipose tissue. *Diabetes*, (2015); published online EpubAug 20 (10.2337/db15-0728).
112. A. Khalifeh-Soltani, W. McKleroy, S. Sakuma, Y. Y. Cheung, K. Tharp, Y. Qiu, S. M. Turner, A. Chawla, A. Stahl, K. Atabai, Mfge8 promotes obesity by mediating the uptake of dietary fats and serum fatty acids. *Nat Med* **20**, 175-183 (2014); published online EpubFeb (10.1038/nm.3450).
113. L. F. Tapias, H. C. Ott, Decellularized scaffolds as a platform for bioengineered organs. *Current opinion in organ transplantation* **19**, 145-152 (2014); published online EpubApr (10.1097/MOT.0000000000000051).
114. F. J. Silva, D. J. Holt, V. Vargas, J. Yockman, S. Boudina, D. Atkinson, D. W. Grainger, M. P. Revelo, W. Sherman, D. A. Bull, A. N. Patel, Metabolically active human brown adipose tissue derived stem cells. *Stem cells* **32**, 572-581 (2014); published online EpubFeb (10.1002/stem.1595).
115. L. G. Griffith, Emerging design principles in biomaterials and scaffolds for tissue engineering. *Annals of the New York Academy of Sciences* **961**, 83-95 (2002); published online EpubJun (
116. J. J. Rice, M. M. Martino, L. De Laporte, F. Tortelli, P. S. Briquez, J. A. Hubbell, Engineering the regenerative microenvironment with biomaterials. *Advanced healthcare materials* **2**, 57-71 (2013); published online EpubJan (10.1002/adhm.201200197).
117. A. M. Unser, Y. Tian, Y. Xie, Opportunities and challenges in three-dimensional brown adipogenesis of stem cells. *Biotechnology advances* **33**, 962-979 (2015); published online EpubNov 1 (10.1016/j.biotechadv.2015.07.005).
118. X. Xu, A. K. Jha, D. A. Harrington, M. C. Farach-Carson, X. Jia, Hyaluronic Acid-Based Hydrogels: from a Natural Polysaccharide to Complex Networks. *Soft Matter* **8**, 3280-3294 (2012)10.1039/c2sm06463d).
119. J. A. Burdick, G. D. Prestwich, Hyaluronic acid hydrogels for biomedical applications. *Advanced materials* **23**, H41-56 (2011); published online EpubMar 25 (10.1002/adma.201003963).
120. B. Yang, B. L. Yang, R. C. Savani, E. A. Turley, Identification of a common hyaluronan binding motif in the hyaluronan binding proteins RHAMM, CD44 and link protein. *The EMBO journal* **13**, 286-296 (1994); published online EpubJan 15 (
121. M. S. Piccinno, E. Veronesi, P. Loschi, M. Pignatti, A. Murgia, G. Grisendi, I. Castelli, D. Bernabei, O. Candini, P. Conte, P. Paolucci, E. M. Horwitz, G. De Santis, L. Iughetti, M. Dominici, Adipose stromal/stem cells assist fat transplantation reducing necrosis and increasing graft performance. *Apoptosis : an international journal on programmed cell death* **18**, 1274-1289 (2013); published online EpubOct (10.1007/s10495-013-0878-7).

122. A. Moreno, A. Martinez, S. Olmedillas, S. Bello, F. de Miguel, Hyaluronic acid effect on adipose-derived stem cells. Biological in vitro evaluation. *Revista espanola de cirugia ortopedica y traumatologia* **59**, 215-221 (2015); published online EpubJul-Aug (10.1016/j.recot.2014.10.004).
123. S. H. Huang, Y. N. Lin, S. S. Lee, C. Y. Chai, H. W. Chang, T. M. Lin, C. S. Lai, S. D. Lin, New adipose tissue formation by human adipose-derived stem cells with hyaluronic acid gel in immunodeficient mice. *International journal of medical sciences* **12**, 154-162 (2015)10.7150/ijms.9964).
124. G. D. Prestwich, Engineering a clinically-useful matrix for cell therapy. *Organogenesis* **4**, 42-47 (2008); published online EpubJan (
125. B. De Meyere, S. Mir-Mir, J. Penas, C. C. Camenisch, P. Heden, Stabilized hyaluronic acid gel for volume restoration and contouring of the buttocks: 24-month efficacy and safety. *Aesthetic plastic surgery* **38**, 404-412 (2014); published online EpubApr (10.1007/s00266-013-0251-9).
126. J. Voigt, V. R. Driver, Hyaluronic acid derivatives and their healing effect on burns, epithelial surgical wounds, and chronic wounds: a systematic review and meta-analysis of randomized controlled trials. *Wound Repair Regen* **20**, 317-331 (2012); published online EpubMay-Jun (10.1111/j.1524-475X.2012.00777.x).
127. J. M. Anderson, A. Rodriguez, D. T. Chang, Foreign body reaction to biomaterials. *Seminars in immunology* **20**, 86-100 (2008); published online EpubApr (10.1016/j.smim.2007.11.004).
128. J. A. Burdick, C. Chung, X. Jia, M. A. Randolph, R. Langer, Controlled degradation and mechanical behavior of photopolymerized hyaluronic acid networks. *Biomacromolecules* **6**, 386-391 (2005); published online EpubJan-Feb (10.1021/bm049508a).
129. B. Cousin, S. Cinti, M. Morroni, S. Raimbault, D. Ricquier, L. Penicaud, L. Casteilla, Occurrence of brown adipocytes in rat white adipose tissue: molecular and morphological characterization. *J Cell Sci* **103 (Pt 4)**, 931-942 (1992); published online EpubDec (
130. B. Xue, J. S. Rim, J. C. Hogan, A. A. Coulter, R. A. Koza, L. P. Kozak, Genetic variability affects the development of brown adipocytes in white fat but not in interscapular brown fat. *J Lipid Res* **48**, 41-51 (2007); published online EpubJan (10.1194/jlr.M600287-JLR200).
131. L. P. Kozak, The genetics of brown adipocyte induction in white fat depots. *Frontiers in endocrinology* **2**, 64 (2011)10.3389/fendo.2011.00064).
132. K. Yoshimura, H. Suga, H. Eto, Adipose-derived stem/progenitor cells: roles in adipose tissue remodeling and potential use for soft tissue augmentation. *Regenerative medicine* **4**, 265-273 (2009); published online EpubMar (10.2217/17460751.4.2.265).
133. Y. H. Lee, A. P. Petkova, E. P. Mottillo, J. G. Granneman, In vivo identification of bipotential adipocyte progenitors recruited by beta3-adrenoceptor activation and high-fat feeding. *Cell Metab* **15**, 480-491 (2012); published online EpubApr 4 (10.1016/j.cmet.2012.03.009).
134. S. Ussar, K. Y. Lee, S. N. Dankel, J. Boucher, M. F. Haering, A. Kleinridders, T. Thomou, R. Xue, Y. Macotela, A. M. Cypess, Y. H. Tseng, G. Mellgren, C. R. Kahn, ASC-1, PAT2, and P2RX5 are cell surface markers for white, beige, and brown adipocytes. *Science translational medicine* **6**, 247ra103 (2014); published online EpubJul 30 (10.1126/scitranslmed.3008490).
135. M. Nishio, T. Yoneshiro, M. Nakahara, S. Suzuki, K. Saeki, M. Hasegawa, Y. Kawai, H. Akutsu, A. Umezawa, K. Yasuda, K. Tobe, A. Yuo, K. Kubota, M. Saito, K. Saeki, Production of functional classical brown adipocytes from human pluripotent stem cells using specific hemopoietin cocktail without gene transfer. *Cell Metab* **16**, 394-406 (2012); published online EpubSep 5 (10.1016/j.cmet.2012.08.001).

136. D. Medrikova, T. P. Sijmonsma, K. Sowodniok, D. M. Richards, M. Delacher, C. Sticht, N. Gretz, T. Schafmeier, M. Feuerer, S. Herzig, Brown adipose tissue harbors a distinct sub-population of regulatory T cells. *PLoS One* **10**, e0118534 (2015)10.1371/journal.pone.0118534).
137. W. Tang, D. Zeve, J. M. Suh, D. Bosnakovski, M. Kyba, R. E. Hammer, M. D. Tallquist, J. M. Graff, White fat progenitor cells reside in the adipose vasculature. *Science* **322**, 583-586 (2008); published online EpubOct 24 (10.1126/science.1156232).
138. D. J. Nolan, M. Ginsberg, E. Israely, B. Palikuqi, M. G. Poulos, D. James, B. S. Ding, W. Schachterle, Y. Liu, Z. Rosenwaks, J. M. Butler, J. Xiang, A. Rafii, K. Shido, S. Y. Rabbany, O. Elemento, S. Rafii, Molecular signatures of tissue-specific microvascular endothelial cell heterogeneity in organ maintenance and regeneration. *Developmental cell* **26**, 204-219 (2013); published online EpubJul 29 (10.1016/j.devcel.2013.06.017).
139. J. M. Butler, H. Kobayashi, S. Rafii, Instructive role of the vascular niche in promoting tumour growth and tissue repair by angiocrine factors. *Nature reviews. Cancer* **10**, 138-146 (2010); published online EpubFeb (10.1038/nrc2791).
140. P. Bi, T. Shan, W. Liu, F. Yue, X. Yang, X. R. Liang, J. Wang, J. Li, N. Carlesso, X. Liu, S. Kuang, Inhibition of Notch signaling promotes browning of white adipose tissue and ameliorates obesity. *Nat Med* **20**, 911-918 (2014); published online EpubAug (10.1038/nm.3615).
141. K. Sun, I. Wernstedt Asterholm, C. M. Kusminski, A. C. Bueno, Z. V. Wang, J. W. Pollard, R. A. Brekken, P. E. Scherer, Dichotomous effects of VEGF-A on adipose tissue dysfunction. *Proc Natl Acad Sci U S A* **109**, 5874-5879 (2012); published online EpubApr 10 (10.1073/pnas.1200447109).
142. K. M. Schultz, K. A. Kyburz, K. S. Anseth, Measuring dynamic cell-material interactions and remodeling during 3D human mesenchymal stem cell migration in hydrogels. *Proc Natl Acad Sci U S A* **112**, E3757-3764 (2015); published online EpubJul 21 (10.1073/pnas.1511304112).
143. M. P. Lutolf, J. L. Lauer-Fields, H. G. Schmoekel, A. T. Metters, F. E. Weber, G. B. Fields, J. A. Hubbell, Synthetic matrix metalloproteinase-sensitive hydrogels for the conduction of tissue regeneration: engineering cell-invasion characteristics. *Proc Natl Acad Sci U S A* **100**, 5413-5418 (2003); published online EpubApr 29 (10.1073/pnas.0737381100).
144. M. Guvendiren, J. A. Burdick, Stiffening hydrogels to probe short- and long-term cellular responses to dynamic mechanics. *Nature communications* **3**, 792 (2012)10.1038/ncomms1792).
145. D. A. Young, Y. S. Choi, A. J. Engler, K. L. Christman, Stimulation of adipogenesis of adult adipose-derived stem cells using substrates that mimic the stiffness of adipose tissue. *Biomaterials* **34**, 8581-8588 (2013); published online EpubNov (10.1016/j.biomaterials.2013.07.103).
146. A. Kumar, M. Mazzanti, M. Mistrik, M. Kosar, G. V. Beznoussenko, A. A. Mironov, M. Garre, D. Parazzoli, G. V. Shivashankar, G. Scita, J. Bartek, M. Foiani, ATR mediates a checkpoint at the nuclear envelope in response to mechanical stress. *Cell* **158**, 633-646 (2014); published online EpubJul 31 (10.1128/mcb.01300-08
10.1016/j.cell.2014.05.046).
147. G. V. Shivashankar, Mechanosignaling to the cell nucleus and gene regulation. *Annual review of biophysics* **40**, 361-378 (2011)10.1016/j.cell.2014.05.046
10.1146/annurev-biophys-042910-155319).
148. S. Jakkaraju, X. Zhe, D. Pan, R. Choudhury, L. Schuger, TIPs are tension-responsive proteins involved in myogenic versus adipogenic differentiation. *Developmental cell* **9**, 39-49 (2005); published online EpubJul (10.1016/j.devcel.2005.04.015).

149. M. Hughes-Fulford, Signal transduction and mechanical stress. *Science's STKE : signal transduction knowledge environment* **2004**, RE12 (2004); published online EpubSep 7 (10.1126/stke.2492004re12).
150. R. L. Vinall, S. H. Lo, A. H. Reddi, Regulation of articular chondrocyte phenotype by bone morphogenetic protein 7, interleukin 1, and cellular context is dependent on the cytoskeleton. *Experimental cell research* **272**, 32-44 (2002); published online EpubJan 1 (10.1006/excr.2001.5395).
151. R. Fuchshofer, D. A. Stephan, P. Russell, E. R. Tamm, Gene expression profiling of TGFbeta2- and/or BMP7-treated trabecular meshwork cells: Identification of Smad7 as a critical inhibitor of TGF-beta2 signaling. *Experimental eye research* **88**, 1020-1032 (2009); published online EpubJun (10.1016/j.exer.2009.01.002).
152. G. Konstantinidis, A. Moustakas, C. Stournaras, Regulation of myosin light chain function by BMP signaling controls actin cytoskeleton remodeling. *Cellular physiology and biochemistry : international journal of experimental cellular physiology, biochemistry, and pharmacology* **28**, 1031-1044 (2011)10.1159/000335790).
153. A. Chopra, M. E. Murray, F. J. Byfield, M. G. Mendez, R. Halleluyan, D. J. Restle, D. Raz-Ben Aroush, P. A. Galie, K. Pogoda, R. Bucki, C. Marcinkiewicz, G. D. Prestwich, T. I. Zarembinski, C. S. Chen, E. Pure, J. Y. Kresh, P. A. Janmey, Augmentation of integrin-mediated mechanotransduction by hyaluronic acid. *Biomaterials* **35**, 71-82 (2014); published online EpubJan (10.1016/j.biomaterials.2013.09.066).
154. M. Shachar, O. Tsur-Gang, T. Dvir, J. Leor, S. Cohen, The effect of immobilized RGD peptide in alginate scaffolds on cardiac tissue engineering. *Acta biomaterialia* **7**, 152-162 (2011); published online EpubJan (10.1016/j.actbio.2010.07.034).
155. S. W. Kang, B. H. Cha, H. Park, K. S. Park, K. Y. Lee, S. H. Lee, The effect of conjugating RGD into 3D alginate hydrogels on adipogenic differentiation of human adipose-derived stromal cells. *Macromolecular bioscience* **11**, 673-679 (2011); published online EpubMay 12 (10.1002/mabi.201000479).
156. K. Y. Lee, D. J. Mooney, Hydrogels for tissue engineering. *Chemical reviews* **101**, 1869-1879 (2001); published online EpubJul (
157. M. Mehta, C. M. Madl, S. Lee, G. N. Duda, D. J. Mooney, The collagen I mimetic peptide DGEA enhances an osteogenic phenotype in mesenchymal stem cells when presented from cell-encapsulating hydrogels. *Journal of biomedical materials research. Part A* **103**, 3516-3525 (2015); published online EpubNov (10.1002/jbm.a.35497).
158. M. K. Vaicik, M. Morse, A. Blagajcevic, J. Rios, J. C. Larson, F. Yang, R. N. Cohen, G. Papavasiliou, E. M. Brey, Hydrogel-based engineering of beige adipose tissue. *J. Mater. Chem. B*, (2015)10.1039/c5tb00952a).
159. D. S. Benoit, M. P. Schwartz, A. R. Durney, K. S. Anseth, Small functional groups for controlled differentiation of hydrogel-encapsulated human mesenchymal stem cells. *Nature materials* **7**, 816-823 (2008); published online EpubOct (10.1038/nmat2269).
160. A. Galmozzi, S. B. Sonne, S. Altshuler-Keylin, Y. Hasegawa, K. Shinoda, I. H. Luijten, J. W. Chang, L. Z. Sharp, B. F. Cravatt, E. Saez, S. Kajimura, ThermoMouse: an in vivo model to identify modulators of UCP1 expression in brown adipose tissue. *Cell reports* **9**, 1584-1593 (2014); published online EpubDec 11 (10.1016/j.celrep.2014.10.066).
161. H. Nobusue, N. Onishi, T. Shimizu, E. Sugihara, Y. Oki, Y. Sumikawa, T. Chiyoda, K. Akashi, H. Saya, K. Kano, Regulation of MKL1 via actin cytoskeleton dynamics drives adipocyte differentiation. *Nature communications* **5**, 3368 (2014)10.1038/ncomms4368).
162. A. Bartelt, J. Heeren, Adipose tissue browning and metabolic health. *Nat Rev Endocrinol* **10**, 24-36 (2014); published online EpubJan (10.1038/nrendo.2013.204).
163. M. Harms, P. Seale, Brown and beige fat: development, function and therapeutic potential. *Nat Med* **19**, 1252-1263 (2013); published online EpubOct (10.1038/nm.3361).

164. S. Kajimura, B. M. Spiegelman, P. Seale, Brown and Beige Fat: Physiological Roles beyond Heat Generation. *Cell Metab* **22**, 546-559 (2015); published online EpubOct 06 (10.1016/j.cmet.2015.09.007).
165. F. M. Gregoire, C. M. Smas, H. S. Sul, Understanding adipocyte differentiation. *Physiological reviews* **78**, 783-809 (1998); published online EpubJul (
166. F. Miralles, G. Posern, A. I. Zaromytidou, R. Treisman, Actin dynamics control SRF activity by regulation of its coactivator MAL. *Cell* **113**, 329-342 (2003); published online EpubMay 2 (
167. G. Posern, R. Treisman, Actin' together: serum response factor, its cofactors and the link to signal transduction. *Trends in cell biology* **16**, 588-596 (2006); published online EpubNov (10.1016/j.tcb.2006.09.008).
168. E. N. Olson, A. Nordheim, Linking actin dynamics and gene transcription to drive cellular motile functions. *Nature reviews. Molecular cell biology* **11**, 353-365 (2010); published online EpubMay (10.1038/nrm2890).
169. R. Sordella, W. Jiang, G. C. Chen, M. Curto, J. Settleman, Modulation of Rho GTPase signaling regulates a switch between adipogenesis and myogenesis. *Cell* **113**, 147-158 (2003); published online EpubApr 18 (
170. R. McBeath, D. M. Pirone, C. M. Nelson, K. Bhadriraju, C. S. Chen, Cell shape, cytoskeletal tension, and RhoA regulate stem cell lineage commitment. *Developmental cell* **6**, 483-495 (2004); published online EpubApr (
171. C. G. Hansen, T. Moroishi, K. L. Guan, YAP and TAZ: a nexus for Hippo signaling and beyond. *Trends in cell biology* **25**, 499-513 (2015); published online EpubSep (10.1016/j.tcb.2015.05.002).
172. G. Halder, S. Dupont, S. Piccolo, Transduction of mechanical and cytoskeletal cues by YAP and TAZ. *Nature reviews. Molecular cell biology* **13**, 591-600 (2012); published online EpubSep (10.1038/nrm3416).
173. T. Moroishi, C. G. Hansen, K. L. Guan, The emerging roles of YAP and TAZ in cancer. *Nature reviews. Cancer* **15**, 73-79 (2015); published online EpubFeb (10.1038/nrc3876).
174. S. Dupont, L. Morsut, M. Aragona, E. Enzo, S. Giulitti, M. Cordenonsi, F. Zanconato, J. Le Digabel, M. Forcato, S. Bicciato, N. Elvassore, S. Piccolo, Role of YAP/TAZ in mechanotransduction. *Nature* **474**, 179-183 (2011); published online EpubJun 9 (10.1038/nature10137).
175. J. H. Hong, E. S. Hwang, M. T. McManus, A. Amsterdam, Y. Tian, R. Kalmukova, E. Mueller, T. Benjamin, B. M. Spiegelman, P. A. Sharp, N. Hopkins, M. B. Yaffe, TAZ, a transcriptional modulator of mesenchymal stem cell differentiation. *Science* **309**, 1074-1078 (2005); published online EpubAug 12 (10.1126/science.1110955).
176. K. M. Tharp, A. Stahl, Bioengineering Beige Adipose Tissue Therapeutics. *Frontiers in endocrinology* **6**, 164 (2015)10.3389/fendo.2015.00164).
177. D. M. Bers, Cardiac excitation-contraction coupling. *Nature* **415**, 198-205 (2002); published online EpubJan 10 (10.1038/415198a).
178. T. Inagaki, J. Sakai, S. Kajimura, Transcriptional and epigenetic control of brown and beige adipose cell fate and function. *Nature reviews. Molecular cell biology* **17**, 480-495 (2016); published online EpubAug (10.1038/nrm.2016.62).
179. W. Cao, A. V. Medvedev, K. W. Daniel, S. Collins, beta-Adrenergic activation of p38 MAP kinase in adipocytes: cAMP induction of the uncoupling protein 1 (UCP1) gene requires p38 MAP kinase. *J Biol Chem* **276**, 27077-27082 (2001); published online EpubJul 20 (10.1074/jbc.M101049200).
180. K. Hattori, I. Naguro, K. Okabe, T. Funatsu, S. Furutani, K. Takeda, H. Ichijo, ASK1 signalling regulates brown and beige adipocyte function. *Nature communications* **7**, 11158 (2016)10.1038/ncomms11158).

181. B. G. Hill, Insights into an adipocyte whitening program. *Adipocyte* **4**, 75-80 (2015); published online EpubJan-Mar (10.4161/21623945.2014.960351).
182. J. Limouze, A. F. Straight, T. Mitchison, J. R. Sellers, Specificity of blebbistatin, an inhibitor of myosin II. *Journal of muscle research and cell motility* **25**, 337-341 (2004)10.1007/s10974-004-6060-7).
183. A. F. Straight, A. Cheung, J. Limouze, I. Chen, N. J. Westwood, J. R. Sellers, T. J. Mitchison, Dissecting temporal and spatial control of cytokinesis with a myosin II Inhibitor. *Science* **299**, 1743-1747 (2003); published online EpubMar 14 (10.1126/science.1081412).
184. Z. A. Schiller, N. R. Schiele, J. K. Sims, K. Lee, C. K. Kuo, Adipogenesis of adipose-derived stem cells may be regulated via the cytoskeleton at physiological oxygen levels in vitro. *Stem cell research & therapy* **4**, 79 (2013)10.1186/scrt230).
185. E. M. Ostap, 2,3-Butanedione monoxime (BDM) as a myosin inhibitor. *Journal of Muscle Research & Cell Motility* **23**, 305-308 (2002)10.1023/a:1022047102064).
186. P. H. Backx, W. D. Gao, M. D. Azan-Backx, E. Marban, Mechanism of force inhibition by 2,3-butanedione monoxime in rat cardiac muscle: roles of [Ca2+]i and cross-bridge kinetics. *The Journal of physiology* **476**, 487-500 (1994); published online EpubMay 1 (
187. M. Kovacs, J. Toth, C. Hetenyi, A. Malnasi-Csizmadia, J. R. Sellers, Mechanism of blebbistatin inhibition of myosin II. *J Biol Chem* **279**, 35557-35563 (2004); published online EpubAug 20 (10.1074/jbc.M405319200).
188. A. R. Hall, D. J. Hausenloy, Mitochondrial respiratory inhibition by 2,3-butanedione monoxime (BDM): implications for culturing isolated mouse ventricular cardiomyocytes. *Physiological reports* **4**, (2016); published online EpubJan (10.14814/phy2.12606).
189. K. E. Kamm, J. T. Stull, The function of myosin and myosin light chain kinase phosphorylation in smooth muscle. *Annual review of pharmacology and toxicology* **25**, 593-620 (1985)10.1146/annurev.pa.25.040185.003113).
190. L. P. Dolgacheva, B. B. Abzhalelov, S. J. Zhang, V. P. Zinchenko, G. E. Bronnikov, Norepinephrine induces slow calcium signalling in murine brown preadipocytes through the beta-adrenoceptor/cAMP/protein kinase A pathway. *Cellular signalling* **15**, 209-216 (2003); published online EpubFeb (
191. E. V. Leaver, P. A. Pappone, Beta-adrenergic potentiation of endoplasmic reticulum Ca(2+) release in brown fat cells. *American journal of physiology. Cell physiology* **282**, C1016-1024 (2002); published online EpubMay (10.1152/ajpcell.00204.2001).
192. W. Cao, K. W. Daniel, J. Robidoux, P. Puigserver, A. V. Medvedev, X. Bai, L. M. Floering, B. M. Spiegelman, S. Collins, p38 mitogen-activated protein kinase is the central regulator of cyclic AMP-dependent transcription of the brown fat uncoupling protein 1 gene. *Mol Cell Biol* **24**, 3057-3067 (2004); published online EpubApr (
193. S. G. Pfisterer, G. Gateva, P. Horvath, J. Pirhonen, V. T. Salo, L. Karhinen, M. Varjosalo, S. J. Ryhanen, P. Lappalainen, E. Ikonen, Role for formin-like 1-dependent acto-myosin assembly in lipid droplet dynamics and lipid storage. *Nature communications* **8**, 14858 (2017); published online EpubMar 31 (10.1038/ncomms14858).
194. P. M. Hwang, B. D. Sykes, Targeting the sarcomere to correct muscle function. *Nature reviews. Drug discovery* **14**, 313-328 (2015); published online EpubMay (10.1038/nrd4554).
195. S. Y. Wong, T. A. Ulrich, L. P. Deleyrolle, J. L. MacKay, J. M. Lin, R. T. Martuscello, M. A. Jundi, B. A. Reynolds, S. Kumar, Constitutive activation of myosin-dependent contractility sensitizes glioma tumor-initiating cells to mechanical inputs and reduces tissue invasion. *Cancer research* **75**, 1113-1122 (2015); published online EpubMar 15 (10.1158/0008-5472.can-13-3426).

196. Y. T. Shen, F. I. Malik, X. Zhao, C. Depre, S. K. Dhar, P. Abarzua, D. J. Morgans, S. F. Vatner, Improvement of cardiac function by a cardiac Myosin activator in conscious dogs with systolic heart failure. *Circulation. Heart failure* **3**, 522-527 (2010); published online EpubJul (10.1161/circheartfailure.109.930321).
197. F. I. Malik, J. J. Hartman, K. A. Elias, B. P. Morgan, H. Rodriguez, K. Brejc, R. L. Anderson, S. H. Sueoka, K. H. Lee, J. T. Finer, R. Sakowicz, R. Baliga, D. R. Cox, M. Garard, G. Godinez, R. Kawas, E. Kraynack, D. Lenzi, P. P. Lu, A. Muci, C. Niu, X. Qian, D. W. Pierce, M. Pokrovskii, I. Suehiro, S. Sylvester, T. Tochimoto, C. Valdez, W. Wang, T. Katori, D. A. Kass, Y. T. Shen, S. F. Vatner, D. J. Morgans, Cardiac myosin activation: a potential therapeutic approach for systolic heart failure. *Science* **331**, 1439-1443 (2011); published online EpubMar 18 (10.1126/science.1200113).
198. D. A. Winkelmann, E. Forgacs, M. T. Miller, A. M. Stock, Structural basis for drug-induced allosteric changes to human beta-cardiac myosin motor activity. *Nature communications* **6**, 7974 (2015); published online EpubAug 06 (10.1038/ncomms8974).
199. M. B. Radke, M. H. Taft, B. Stapel, D. Hilfiker-Kleiner, M. Preller, D. J. Manstein, Small molecule-mediated refolding and activation of myosin motor function. *eLife* **3**, e01603 (2014); published online EpubFeb 11 (10.7554/eLife.01603).
200. H. Lv, L. Li, M. Sun, Y. Zhang, L. Chen, Y. Rong, Y. Li, Mechanism of regulation of stem cell differentiation by matrix stiffness. *Stem cell research & therapy* **6**, 103 (2015)10.1186/s13287-015-0083-4).
201. A. L. Zajac, D. E. Discher, Cell differentiation through tissue elasticity-coupled, myosin-driven remodeling. *Curr Opin Cell Biol* **20**, 609-615 (2008); published online EpubDec (10.1016/j.ceb.2008.09.006).
202. D. E. Discher, P. Janmey, Y. L. Wang, Tissue cells feel and respond to the stiffness of their substrate. *Science* **310**, 1139-1143 (2005); published online EpubNov 18 (10.1126/science.1116995).
203. D. N. Robinson, Molecular Mechanisms of Contractility-Based Cellular Mechanosensing. *Biophysical journal* **108**, 4a-5a (2015)10.1016/j.bpj.2014.11.041).
204. M. A. Schwartz, Integrins and extracellular matrix in mechanotransduction. *Cold Spring Harbor perspectives in biology* **2**, a005066 (2010); published online EpubDec (10.1101/cshperspect.a005066).
205. V. Vogel, M. Sheetz, Local force and geometry sensing regulate cell functions. *Nature reviews. Molecular cell biology* **7**, 265-275 (2006); published online EpubApr (10.1038/nrm1890).
206. F. Zanconato, M. Cordenonsi, S. Piccolo, YAP/TAZ at the Roots of Cancer. *Cancer cell* **29**, 783-803 (2016); published online EpubJun 13 (10.1016/j.ccell.2016.05.005).
207. V. Pellegrinelli, J. Heuvingh, O. du Roure, C. Rouault, A. Devulder, C. Klein, M. Lacasa, E. Clement, D. Lacasa, K. Clement, Human adipocyte function is impacted by mechanical cues. *The Journal of pathology* **233**, 183-195 (2014); published online EpubJun (10.1002/path.4347).
208. K. Sun, J. Park, O. T. Gupta, W. L. Holland, P. Auerbach, N. Zhang, R. Goncalves Marangoni, S. M. Nicoloro, M. P. Czech, J. Varga, T. Ploug, Z. An, P. E. Scherer, Endotrophin triggers adipose tissue fibrosis and metabolic dysfunction. *Nature communications* **5**, 3485 (2014); published online EpubMar 19 (10.1038/ncomms4485).
209. S. Moleirinho, W. Guerrant, J. L. Kissil, The Angiomotins--from discovery to function. *FEBS letters* **588**, 2693-2703 (2014); published online EpubAug 19 (10.1016/j.febslet.2014.02.006).
210. T. Moroishi, H. W. Park, B. Qin, Q. Chen, Z. Meng, S. W. Plouffe, K. Taniguchi, F. X. Yu, M. Karin, D. Pan, K. L. Guan, A YAP/TAZ-induced feedback mechanism regulates Hippo pathway homeostasis. *Genes Dev* **29**, 1271-1284 (2015); published online EpubJun 15 (10.1101/gad.262816.115).

211. H. Beck, K. Flynn, K. S. Lindenberg, H. Schwarz, F. Bradke, S. Di Giovanni, B. Knoll, Serum Response Factor (SRF)-cofilin-actin signaling axis modulates mitochondrial dynamics. *Proc Natl Acad Sci U S A* **109**, E2523-2532 (2012); published online EpubSep 18 (10.1073/pnas.1208141109).
212. A. L. Hatch, P. S. Gurel, H. N. Higgs, Novel roles for actin in mitochondrial fission. *J Cell Sci* **127**, 4549-4560 (2014); published online EpubNov 1 (10.1242/jcs.153791).
213. F. Korobova, V. Ramabhadran, H. N. Higgs, An actin-dependent step in mitochondrial fission mediated by the ER-associated formin INF2. *Science* **339**, 464-467 (2013); published online EpubJan 25 (10.1126/science.1228360).
214. S. R. Farmer, Brown fat and skeletal muscle: unlikely cousins? *Cell* **134**, 726-727 (2008); published online EpubSep 5 (10.1016/j.cell.2008.08.018).
215. J. A. Timmons, K. Wennmalm, O. Larsson, T. B. Walden, T. Lassmann, N. Petrovic, D. L. Hamilton, R. E. Gimeno, C. Wahlestedt, K. Baar, J. Nedergaard, B. Cannon, Myogenic gene expression signature establishes that brown and white adipocytes originate from distinct cell lineages. *Proc Natl Acad Sci U S A* **104**, 4401-4406 (2007); published online EpubMar 13 (10.1073/pnas.0610615104).
216. J. Z. Long, K. J. Svensson, L. Tsai, X. Zeng, H. C. Roh, X. Kong, R. R. Rao, J. Lou, I. Lokurkar, W. Baur, J. J. Castellot, Jr., E. D. Rosen, B. M. Spiegelman, A smooth muscle-like origin for beige adipocytes. *Cell Metab* **19**, 810-820 (2014); published online EpubMay 6 (10.1016/j.cmet.2014.03.025).
217. M. Rosell, M. Kaforou, A. Frontini, A. Okolo, Y. W. Chan, E. Nikolopoulou, S. Millership, M. E. Fenech, D. MacIntyre, J. O. Turner, J. D. Moore, E. Blackburn, W. J. Gullick, S. Cinti, G. Montana, M. G. Parker, M. Christian, Brown and white adipose tissues: intrinsic differences in gene expression and response to cold exposure in mice. *Am J Physiol Endocrinol Metab* **306**, E945-964 (2014); published online EpubApr 15 (10.1152/ajpendo.00473.2013).
218. J. I. Odegaard, M. W. Lee, Y. Sogawa, A. M. Bertholet, R. M. Locksley, D. E. Weinberg, Y. Kirichok, R. C. Deo, A. Chawla, Perinatal Licensing of Thermogenesis by IL-33 and ST2. *Cell* **166**, 841-854 (2016); published online EpubAug 11 (10.1016/j.cell.2016.06.040).
219. A. Dobin, C. A. Davis, F. Schlesinger, J. Drenkow, C. Zaleski, S. Jha, P. Batut, M. Chaisson, T. R. Gingeras, STAR: ultrafast universal RNA-seq aligner. *Bioinformatics (Oxford, England)* **29**, 15-21 (2013); published online EpubJan 1 (10.1093/bioinformatics/bts635).
220. S. Anders, W. Huber, Differential expression analysis for sequence count data. *Genome biology* **11**, R106 (2010)10.1186/gb-2010-11-10-r106).
221. S. Heinz, C. Benner, N. Spann, E. Bertolino, Y. C. Lin, P. Laslo, J. X. Cheng, C. Murre, H. Singh, C. K. Glass, Simple combinations of lineage-determining transcription factors prime cis-regulatory elements required for macrophage and B cell identities. *Mol Cell* **38**, 576-589 (2010); published online EpubMay 28 (10.1016/j.molcel.2010.05.004).
222. S. Rammensee, M. S. Kang, K. Georgiou, S. Kumar, D. V. Schaffer, Dynamics of Mechanosensitive Neural Stem Cell Differentiation. *Stem cells*, (2016); published online EpubAug 30 (10.1002/stem.2489).
223. F. Zanconato, M. Forcato, G. Battilana, L. Azzolin, E. Quaranta, B. Bodega, A. Rosato, S. Bicciato, M. Cordenonsi, S. Piccolo, Genome-wide association between YAP/TAZ/TEAD and AP-1 at enhancers drives oncogenic growth. *Nature cell biology* **17**, 1218-1227 (2015); published online EpubSep (10.1038/ncb3216).
224. T. Luque, M. S. Kang, Microelastic mapping of the rat dentate gyrus. **3**, 150702 (2016); published online EpubApr (10.1098/rsos.150702).
225. M. Xin, Y. Kim, L. B. Sutherland, M. Murakami, X. Qi, J. McAnally, E. R. Porrello, A. I. Mahmoud, W. Tan, J. M. Shelton, J. A. Richardson, H. A. Sadek, R. Bassel-Duby, E. N.

Olson, Hippo pathway effector Yap promotes cardiac regeneration. *Proc Natl Acad Sci U S A* **110**, 13839-13844 (2013); published online EpubAug 20 (10.1073/pnas.1313192110).
226. J. Dempersmier, A. Sambeat, O. Gulyaeva, S. M. Paul, C. S. Hudak, H. F. Raposo, H. Y. Kwan, C. Kang, R. H. Wong, H. S. Sul, Cold-inducible Zfp516 activates UCP1 transcription to promote browning of white fat and development of brown fat. *Mol Cell* **57**, 235-246 (2015); published online EpubJan 22 (10.1016/j.molcel.2014.12.005).
227. A. Sambeat, O. Gulyaeva, J. Dempersmier, K. M. Tharp, A. Stahl, S. M. Paul, H. S. Sul, LSD1 Interacts with Zfp516 to Promote UCP1 Transcription and Brown Fat Program. *Cell reports* **15**, 2536-2549 (2016); published online EpubJun 14 (10.1016/j.celrep.2016.05.019).